UNDERSTANDING INTERMOLECULAR FORCES:
DFT–SAPT STUDIES ON GRAPHITE-LIKE ACENES
INTERACTING WITH WATER

by

Glen R. Jenness

B.S. Chemistry, Northland College, 2005

Submitted to the Graduate Faculty of

the Department of Chemistry in partial fulfillment

of the requirements for the degree of

Doctor of Philosophy

University of Pittsburgh

2011

UNIVERSITY OF PITTSBURGH

DEPARTMENT OF CHEMISTRY

This dissertation was presented

by

Glen R. Jenness

It was defended on

May 27, 2011

and approved by

Kenneth D. Jordan, Distinguished Professor of Chemistry

David Pratt, Professor of Chemistry

Geoffrey Hutchison, Assistant Professor of Chemistry

J. Karl Johnson, Professor of Chemical and Petroleum Engineering

Dissertation Director: Kenneth D. Jordan, Distinguished Professor of Chemistry

UNDERSTANDING INTERMOLECULAR FORCES: DFT–SAPT STUDIES ON GRAPHITE-LIKE ACENES INTERACTING WITH WATER

Glen R. Jenness, PhD

University of Pittsburgh, 2011

The interaction of water with graphene has been a quintessential example of hydrophobic interactions for many years. However, no reliable experimental or theoretical value exists for the water–graphene interaction energy. In the current document, the water–graphene interaction energy is explored using high-level *ab initio* methods. In addition, the water–graphene interaction energy is decomposed into its physical components in order to give further physical insight into the water–graphene interaction.

Water is found in a variety of environments, ranging from small clusters to the bulk. Because of this, the development of accurate models capable of describing water in a wide range of environments has been an active area of research. In the second part of this document, the nature of the water–water interaction is explored and a new polarizable water model is presented.

TABLE OF CONTENTS

LIST OF TABLES

LIST OF FIGURES

1.0 INTRODUCTION

The focus of this document is to give a better physical insight into the intermolecular interactions for two important systems: a single water molecule interacting with a graphene surface, and the interaction between water molecules in a variety of environments.

In Chapter 2, the cluster model of Feller and Jordan[1] is used along side the density functional theory (DFT) based symmetry-adapted perturbation theory (SAPT) method of Heßelmann et al[2–4] for studying the interaction energy of a single water molecule with a graphene surface. The cluster model for graphene takes small sub-units of graphene (*i.e.* acenes) interacting with a single water molecule, and by analyzing how the interaction energy and its physical components evolve with the size of the acene, the extrapolation to the graphene limit is possible. For this study, the acenes benzene (C_6H_6), anthracene ($C_{14}H_{10}$), coronene ($C_{24}H_{12}$), pentacene ($C_{22}H_{14}$), and dodecabenzocoronene ($C_{54}H_{18}$, also referred to as DBC or circumcoronene) were chosen. In addition to the DFT–SAPT analysis, a comparison is carried out between the extrapolated DFT–SAPT interaction energy and the interaction energy from several popular force fields used in water–graphene and water–carbon nanotube (CNT) simulations in order to assess their accuracy for the water–graphene system.

Chapter 3 extends on the previous chapter by employing a more realistic geometry for the water–acene system, in addition to employing a basis set on the acenes that is more appropriate for capturing the long-range dispersion interactions commonly found in graphene. In this chapter, benzene, coronene, and DBC are again considered, in addition to hexabenzo[bc,ef,hi,kl,no,qr]coronene, or HBC ($C_{48}H_{18}$). Several methods for including long-range correlation (*i.e.* van der Waals or dispersion) interactions into density functional theory (DFT) are also investigated, using the

DFT–SAPT results as a benchmark.

Chapter 4 focuses on a single water molecule interacting with a series of "linear" acenes — benzene (C_6H_6), anthracene ($C_{14}H_{10}$), pentacene ($C_{22}H_{14}$), heptacene ($C_{30}H_{18}$), and nonacene ($C_{38}H_{22}$). As in Chapter 3, several methods for including dispersion within the DFT framework are assessed, using the DFT–SAPT results as a benchmark. In addition, several wavefunction based methods, along with several variants of the random phase approximation (RPA)[5–7] are also explored.

In Appendix B, the Hartree–Fock based SAPT [SAPT(HF)] method is used in conjunction with two energy decomposition analysis' — LMO–EDA[8] and ALMO–EDA[9] — are used to examine how well various density functionals recover the various interaction energy terms, including both charge-transfer and dispersion, in the four low-lying minima of the $(H_2O)_6$ clusters.

Appendix C presents a reparameterization of the distributed point polarizable (DPP) water model of DeFusco *et al.*,[10] utilizing the Hartree–Fock based SAPT [SAPT(HF)] method with fully correlated intramolecular terms,[11–13] and three-body CCSD(T) interaction energies. The new water model is used to calculate the many-body interaction energies, geometries, and radial distribution functions, which are then compared to high-level results from both theory and experiment.

Finally, Appendix E explores both the SAPT(HF) and DFT–SAPT methods, and presents the basic equations and physical meanings behind them.

2.0 DF–DFT–SAPT INVESTIGATION OF THE INTERACTION OF A WATER MOLECULE TO CORONENE AND DODECABENZOCORONENE: IMPLICATIONS FOR THE WATER–GRAPHITE INTERACTION

2.1 ABSTRACT

In the present study we revisit the problem of the interaction of a water molecule with a single graphite sheet. The density fitting–density functional theory–symmetry-adapted perturbation theory (DF–DFT–SAPT; J. Chem. Phys. **2005**, *122*, 014103) method is used to calculate the individual contributions arising from the interaction of a water molecule with various acenes, including benzene, coronene, and dodecabenzocoronene. These results are combined with calculations of the electrostatic interactions with water and a $C_{216}H_{36}$ acene to extrapolate to the limit of an infinite graphite sheet, giving a interaction energy of -2.2 kcal mol^{-1} for the water-graphite system, with the assumed geometrical structure with one hydrogen atom pointed down toward the ring system. The structure with two hydrogens pointed down is predicted to be more stable, with a net interaction energy of -2.7 kcal mol^{-1}.

2.2 INTRODUCTION

The interaction of water with graphite and with carbon nanotube (CNT) surfaces has been a topic of considerable interest. Much of the recent interest in this area has been motivated by the findings that water can fill carbon nanotubes[14] and that water confined in small diameter nanotubes can have properties very different from those of bulk water.[15–24] Although there have been several experimental studies of water inside carbon nanotubes and on graphite,[14,19–23,25–28] most of the work in this area is theoretical.[1,15–18,24,27,29–48] Specifically, numerous Monte Carlo and molecular dynamics simulations of water on graphitic surfaces or in carbon nanotubes have appeared. Nearly all of these simulations have employed relatively simple force fields, in general, neglecting induction and using the same parameters for water–nanotube interactions potential as employed in the water–graphite simulations, in spite of the fact that graphitic systems are highly polarizable with the polarizability per atom depending on the curvature and on whether the system is metallic or semiconducting.[49]

A major limitation for developing accurate force fields for water interacting with graphite or CNT surfaces is the uncertainty in the values of the interaction energies of a single water molecule interacting with a graphite sheet or with the interior or exterior surfaces of CNTs. For the water monomer-graphite system various force fields give interaction energies ranging from -1.5 to -5.8 kcal mol^{-1}.[35] In principal, this is a problem that can be addressed using electronic structure methods. Due to its computational efficiency, density functional theory (DFT) would seem to be an ideal method for addressing this problem. Indeed, several DFT studies of water on a single layer of graphite and inside carbon nanotubes have appeared.[46–48] However, DFT calculations using standard functionals are expected to underestimate the magnitude of the interaction between water and graphite due to their neglect of long-range dispersion interactions,[50–55] which are important for water–graphite and water–CNT systems. Although there are several strategies for correcting DFT for dispersion,[50–52,56–62] the reliability of these approaches for the interaction of molecules with graphite or CNTs has not been established.

Probably the most ambitious attempt to use electronic structure methods to estimate the water–

graphite interaction energy is that of Feller and Jordan[1] who carried out second-order Möller–Plesset perturbation theory (MP2) calculations on the water–benzene, water–coronene, and water–dodecabenzocoronene (DBC or circumcoronene) sequence of cluster models, together with a series of increasingly flexible basis sets in an attempt to estimate the interaction energy for water–graphene at the MP2 level in the complete basis set (CBS) limit (coronene and DBC are depicted in Figure 2.1). However, the counterpoise corrections for basis set superposition error (BSSE)[63] were comparable to the net interaction energy, and it is now clear that truncation of the basis sets used for the larger clusters introduced a sizable error in the extrapolated interaction energy.[30–32] Moreover, the MP2 method can overestimate the magnitude of interaction energies as evidenced by the benzene dimer,[64–69] and its suitability for describing a water molecule interacting with large acenes has not been established.

Recently, Sudiarta and Geldart used this cluster model approach, considering both hydrogen- and fluorine-terminated structures, in an attempt to understand edge effects on the interaction energy.[70] However, these authors used a small basis set (6–31G(d=0.25)), which does not adequately describe polarization and dispersion interactions[71] and has a large BSSE.[30,70] Thus, their final estimate (-2.32 kcal mol^{-1}) of the interaction energy of a water molecule with a graphite sheet has a sizable uncertainty.

Wehling *et al.*[47] and Leenaerts *et al.*[48] used DFT with periodic boundary conditions and a plane-wave basis set to calculate the interaction energy of water–graphite. Their calculations gave interaction energies between -0.83 and -0.92 kcal mol^{-1}, which are appreciably smaller in magnitude than most current estimates of this quantity.[30] Here the problem is the above-mentioned neglect of long-range dispersion interactions in the DFT functional employed.

In the present study, we revisit the problem of the interaction energy between a water molecule and a single-sheet model of graphite (graphene). Earlier studies have shown that the interaction energy between water and graphite is reasonably well described in employing a single sheet of graphite,[1,30–32,40] and in this paper all references to graphite actually refer to the single sheet. To make the problem tractable, we use the cluster models employed by Feller and Jordan but employ the density functional theory–symmetry-adapted perturbation theory (DFT–SAPT)[2–4,72] method

rather than supermolecular MP2 calculations. The DFT–SAPT approach has several advantages over the supermolecular approach. First, DFT–SAPT calculations generally give more accurate interaction energies than supermolecule MP2 calculations,[2–4] including challenging cases such as the benzene dimer.[69] Second, SAPT calculations are free of BSSE. Third, the SAPT procedure provides a decomposition of the net interaction energy into electrostatic, exchange (repulsion), induction (polarization), and dispersion contributions[11,12] that can be exploited in developing model potentials.

2.3   THEORETICAL METHODOLOGY

The calculations were carried out using the DFT–SAPT program[2–4,72] with density fitting (hereafter referred to as DF–DFT–SAPT) as implemented in the MOLPRO2006.1[73] package. The calculations on water–benzene and on water–coronene were carried out using a modified version of the aug-cc-pVTZ[74] basis set, with the exponents of the most diffuse functions of each angular momentum type multiplied by 2.3 to minimize problems associated with near-linear dependency. Test calculations on water–benzene using the standard aug-cc-pVTZ basis set show that this scaling of the exponents has only a very small effect on the net interaction energy. For water–coronene and water–DBC, the modified aug-cc-pVTZ basis set, hereafter referred to as basis set A, contains 1472 and 2990 contracted Gaussian functions, respectively. Even with density fitting, DFT–SAPT calculations on water–DBC would be computationally prohibitive using basis set A. For this reason we also considered a smaller basis set, B, which employs the modified aug-cc-pVTZ basis set on water and $5s4p2d$ and $4s2p$ basis sets on the ring carbon and hydrogen atoms, respectively. The carbon $5s4p2d$ basis set was formed by combining the s and p functions from the modified aug-cc-pVTZ basis set and the d functions from the aug-cc-pVDZ[74] basis set. The $4s2p$ hydrogen basis set was similarly formed by combining the s functions from the modified aug-cc-pVTZ basis set and the p functions from the aug-cc-pVDZ basis set. DF–DFT–SAPT calculations on water–coronene using basis set B give a interaction energy only 0.07 kcal mol^{-1} smaller in magnitude than that

(a) Anthracene

(b) Pentacene

(c) Coronene

(d) DBC
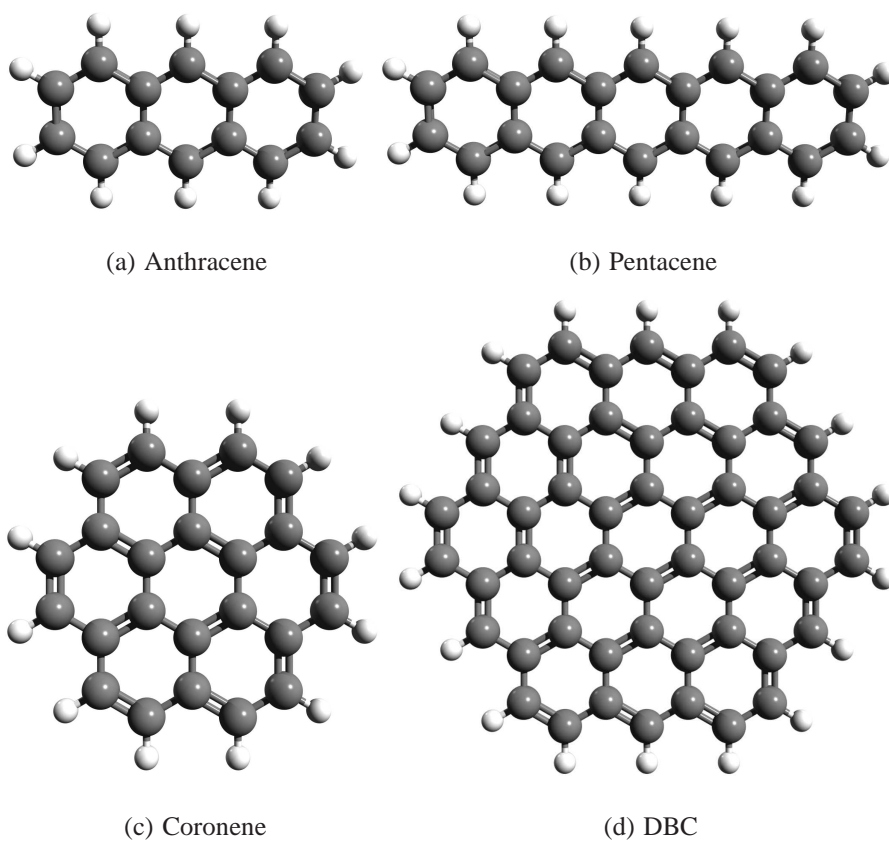
Figure 2.1: Acenes used in the current study.
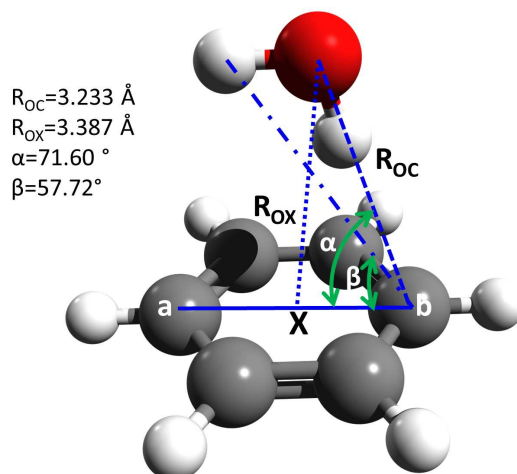
Figure 2.2: Geometry used in the current study, illustrated in the case of water–benzene.

obtained with the larger basis set A. We then proceeded to carry out DF–DFT–SAPT calculations on water–DBC using basis set B, which employs 1782 contracted basis functions. We anticipate that the error introduced in the water–DBC interaction energy due the adoption of the smaller basis set is on the order of 0.1 kcal mol^{-1}.

The use of a DFT description of the monomers avoids the costly intramonomer correlation corrections of traditional Hartree–Fock based SAPT.[75] In the present study, the hybrid PBE0[76] functional as recommended by Heßelmann *et al.*[2–4] and by Misquitta *et al.*[77–79] is employed. The asymptotic behavior of the PBE0 functional is corrected by adding in a fraction of the LB94 functional[80] using the GRAC connection scheme of Grüning *et al.*[81] (hereafter called PBE0AC[4]). For this approach, the first vertical ionization potentials are needed for each monomer.[81] Experimental ionization potentials of 9.24, 7.44, 6.63, and 7.29 eV were used for benzene, anthracene, pentacene, and coronene, respectively.[82] For DBC we used an ionization potential of 6.2 eV, which is close to the experimental value of 6.3 eV.[83]

Since DFT with functionals such as PBE0 does not accurately represent energy differences between filled and unoccupied orbitals, a sum-over-states approach would not give reliable dis-

person energies.[3,72,75,77–79,84–86] To avoid this problem, frequency-dependent density suscepti-bilities (FDDSs) from time-dependent DFT are used in the Casimir–Polder formula[4,72,78,84–86] to calculate the dispersion and exchange-dispersion contributions.

To make the calculations on the larger systems tractable, density fitting[87] was employed. Weigends cc-pVQZ JK-fitting basis set[88] was used for both first-order and induction contribu-tions, and the aug-cc-pVTZ MP2-fitting basis set of Weigend and co-workers[89] was used for the dispersion and exchange-dispersion contributions. Following the recommendation of Reference 72, a modified version of PBE0AC (called LPBE0AC), which uses the localized Hartree–Fock (LHF) density functional of Sala and Görling[90] in the exchange part of the PBE0AC functional, was used in the density fitting calculations.

For the acenes the experimental CC bond lengths (1.420 Å) and CCC angles (120°) appropriate for graphite were employed.[91] The CH bond lengths and the CCH angles were chosen to be 1.09 Å and 120°, respectively. The water monomer was taken to be rigid, with OH bond lengths (0.9572 Å) and HOH bond angle (104.52°) equal to the experimental values for the gas-phase monomer.[92] For each dimer, the water monomer was located above the central aromatic ring with the distance and orientation determined from the MP2 optimization of water–triphenylene in Reference 1. Fig-ure 2.2 specifies the key geometrical parameters. In Section 2.6, we consider the consequences of relaxing the geometry from that optimized for water–triphenylene.

2.4   ANALYSIS OF ACENE–WATER INTERACTIONS

Table 2.1 reports the individual contributions and net interaction energies for the water–benzene, water–coronene, and water–DBC complexes as well as for the water–anthracene and water–pentacene complexes. Values are reported for the electrostatic, exchange, induction, exchange-induction, dispersion, exchange-dispersion, and δ(HF) contributions. The δ(HF) cor-rections are determined by calculating the $E_{elst}^{(10)}$, $E_{exch}^{(10)}$, $E_{ind}^{(20)}$, and $E_{ex-ind}^{(20)}$ SAPT contributions at the Hartree–Fock level and subtracting their sum from the net Hartree–Fock interaction energy[11,12]

9

Table 2.1: Interaction energies (kcal mol^{-1}) for water–acene complexes from DF–DFT–SAPT calculations.

Term	Benzene	Anthracene	Pentacene	Coronene	DBC[a]
Electrostatics	−3.74	−2.63	−2.49	−1.96	−1.68
Exchange–repulsion	5.72	5.26	5.22	5.07	5.13
Induction	−2.41	−2.42	−2.43	−2.40	−2.47
Exchange–induction	1.59	1.55	1.55	1.53	1.58
δ(HF)	−0.59	−0.57	−0.57	−0.46	−0.47
Net induction	−1.40	−1.44	−1.46	−1.32	−1.35
Dispersion	−4.40	−4.73	−4.80	−4.97	(−5.22)
Exchange–dispersion	0.69	0.66	0.65	0.64	(0.64)
Net dispersion	−3.72	−4.07	−4.15	−4.33	(−4.57)
Total interaction energy	−3.14	−2.88	−2.88	−2.54	(−2.48)

[a] The SAPT calculations of the dispersion and exchange-dispersion energies of water–DBC did not converge, and the values reported in parentheses were estimated by combining the results for coronene with those for anthracene and pentacene, allowing for the differences in the number of carbon atoms.
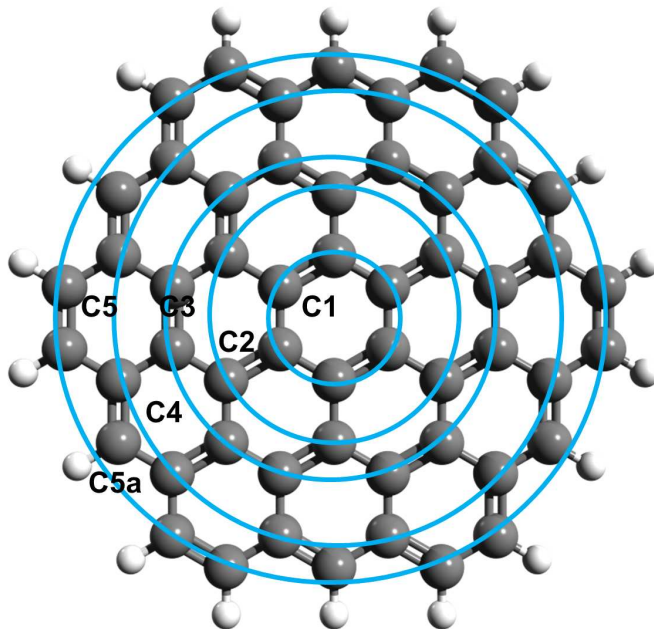
Figure 2.3: Labels for the carbon atoms used in Tables 2.2 and 3.4.

(the numbers in parentheses indicate the orders of the contributions). In addition, we report net induction and net dispersion contributions, defined as

$$E_{ind} = E_{ind}^{(2)} + E_{ex-ind}^{(2)} + \delta(HF) \tag{2.1}$$

$$E_{disp} = E_{disp}^{(2)} + E_{ex-disp}^{(2)} \tag{2.2}$$

In Equation 2.1 it is assumed that the $\delta(HF)$ term is dominated by third and higher-order induction and exchange-induction contributions.

For water–benzene the DF–DFT–SAPT calculations give an interaction energy of -3.14 kcal mol^{-1}, which is close to the values of the interaction energy obtained from large basis set CCSD(T)[95] calculations (-3.37 kcal mol^{-1})[96] and from quantum Monte Carlo calculations (-3.4 ± 0.2 kcal mol^{-1}).[97] In fact, most of the discrepancy in the DF–DFT–SAPT value of the interaction energy from the CCSD(T) and DMC values is due to the use of geometrical parameters

Table 2.2: Multipole moments[a] (a.u.) for the various carbon and hydrogen atoms in benzene, coronene, and DBC[b].

Atom Type[c]	q			$|\mu|$			Q_{20}			$|Q_{22c} + Q_{22s}|$		
	C_6H_6	$C_{24}H_{12}$	$C_{54}H_{18}$	C_6H_6	$C_{24}H_{12}$	$C_{54}H_{18}$	C_6H_6	$C_{24}H_{12}$	$C_{54}H_{18}$	C_6H_6	$C_{24}H_{12}$	$C_{54}H_{18}$
C1	-0.09	-0.01	0.00	0.11	0.01	0.00	-1.14	-1.28	-1.28	0.09	0.00	0.00
C2		-0.04	0.00		0.11	0.01		-1.22	-1.28		0.09	0.01
C3		-0.07	-0.01		0.16	0.01		-1.17	-1.28		0.02	0.01
C4			-0.04			0.12			-1.22			0.10
C5			-0.07			0.16			-1.16			0.02
C5a			-0.06			0.16			-1.18			0.12
H	0.09	0.10	0.11	0.14	0.14	0.15	-0.13	-0.13	-0.13	0.11	0.08	0.06

[a] The spherical tensor representation of the quadrupole is employed. For conversion into Cartesian representation: $\Theta_{XX} = -\frac{1}{2}Q_{20} + \frac{1}{2}\sqrt{3}Q_{22c}$; $\Theta_{YY} = -\frac{1}{2}Q_{20} - \frac{1}{2}\sqrt{3}Q_{22c}$; $\Theta_{XY} = \frac{1}{2}\sqrt{3}Q_{22s}$; $\Theta_{ZZ} = Q_{20}$.[93] The z-axis is perpendicular to the plane of the molecule.

[b] Benzene, C_6H_6; Coronene, $C_{24}H_{12}$; DBC, $C_{54}H_{18}$

[c] The various carbon atoms are defined in Figure 2.4. DBC has two types of H atoms, with very similar moments, so only the average values are reported in the table.

Table 2.3: Interaction energies (kcal mol^{-1}) between the acene[a] multipoles and the three point charges of the water monomer as described by the Dang–Chang model.[94]

Atom Type[c]	charge-charge			charge-dipole			charge-Q_{20}			charge-$(|Q_{22c}+Q_{22s}|)$			Total		
	C_6H_6	$C_{24}H_{12}$	$C_{54}H_{18}$	C_6H_6	$C_{24}H_{12}$	$C_{54}H_{18}$	C_6H_6	$C_{24}H_{12}$	$C_{54}H_{18}$	C_6H_6	$C_{24}H_{12}$	$C_{54}H_{18}$	C_6H_6	$C_{24}H_{12}$	$C_{54}H_{18}$
C1	−4.70	−0.55	−0.13	1.38	0.18	0.03	−2.78	−3.09	−3.12	0.10	−0.01	0.00	−6.00	−3.47	−3.22
C2		−1.18	−0.11		0.84	0.05		0.45	0.48		−0.10	−0.01		0.01	0.41
C3		−2.30	−0.28		1.43	0.11		0.91	1.00		0.01	−0.01		0.05	0.82
C4			−0.72			0.46			0.49			−0.04			0.19
C5			−0.73			0.38			0.25			0.00			−0.10
C5a			−0.39			0.24			0.17			−0.02			0.00
H	2.76	1.91	1.17	1.27	0.70	0.33	0.16	0.06	0.03	0.13	0.04	0.01	4.32	2.71	1.52
Total	−1.95	−2.12	−1.18	2.64	3.16	1.59	−2.62	−1.67	−0.70	0.23	−0.06	−0.09	−1.68	−0.70	−0.38

[a] Benzene, C_6H_6; Coronene, $C_{24}H_{12}$; DBC, $C_{54}H_{18}$

optimized for water–triphenylene. Indeed DF–DFT–SAPT calculations on water–benzene using the geometry of the complex optimized at the MP2/aug-cc-pVTZ level[98] with rigid monomers (also optimized at the MP2/aug-cc-pVTZ level) give an interaction energy of -3.40 kcal mol^{-1}, in excellent agreement with the best current estimates of this quantity (-3.44 ± 0.09 kcal mol^{-1}).[98, 99]

From Table 2.1 it is seen that the electrostatic contribution to the interaction energy drops off in magnitude by 1.78 kcal mol^{-1} in going from water–benzene to water–coronene and by a much smaller amount (0.28 kcal mol^{-1}) in going from water–coronene to water–DBC. One might antic-ipate that the large attractive electrostatic interaction energy for water–benzene is the result of the carbon atoms of benzene carrying an appreciable negative charge. To examine this issue, we have carried out a distributed multipole analysis (DMA)[100–103] of benzene, coronene, and DBC using the MP2/cc-pVDZ charge densities from Gaussian03[104] and Stone's GDMA2 program.[103] For ben-zene nearly the same atomic multipoles are obtained using the cc-pVDZ and cc-pVQZ basis sets, leading us to expect that the former basis set is adequate for calculating the distributed multipole moments of the larger acenes as well. The resulting atomic charges, dipoles, and quadrupole mo-ments are summarized in Table 2.2. The GDMA analysis gives charges (in atomic units) on the C atoms in benzene of -0.093, with the corresponding charges on the central six carbon atoms of coronene and DBC being only -0.010 and -0.002, respectively. Although these results ap-pear to confirm the conjecture that the negative charges on the C atoms of benzene are responsible for the large attractive electrostatic contribution between water and benzene, the situation is more complicated than this as the atomic dipoles and quadrupoles are also sizable. The dipole moments associated with the carbon atoms of benzene are 0.11 a.u. in magnitude, with the dipole moments on the inner carbon atoms rapidly decreasing along the sequence benzene to coronene to DBC. The values of the Q_{20} (Θ_{ZZ}) component of the quadrupole moments on the C atoms are nearly the same on all carbon atoms and are relatively independent of the ring size. The Q_{22c} and Q_{22s} components[93] of the atomic quadrupole moments are much smaller than the Q_{20} components, and, as expected, vanish on the inner carbon atoms with increasing ring size.

The electrostatic interactions between the water molecule and the benzene, coronene, and DBC molecules were decomposed into contributions from the various atomic moments on differ-

ent groups of acene atoms. In calculating these contributions, the charge distribution on the water monomer was modeled using the Dang–Chang model.[94] In the case of water–coronene the electrostatic contributions were also calculated using distributed multipole analysis through quadrupoles on the water monomer. The resulting contributions to the electrostatic energy agree to within a few percent of those obtained using Dang–Chang charges alone on the water monomer, thereby justifying the use of this model in analyzing the electrostatic contributions due to the interaction of water with the various multipole moments on the atoms of the acenes. We also examined the contributions of higher-order atomic multipoles (octopoles and hexadecapoles) on coronene and found that together they contribute only about 0.02 kcal mol^{-1} to the net interaction energy with the water monomer.

From Table 2.3 it is seen that the electrostatic interactions of the water molecule with the atomic dipoles and quadrupoles of benzene are larger in magnitude than the interactions with the atomic charges. However, the electrostatic interactions of the water monomer with the atomic dipoles and quadrupoles of benzene are of opposite sign and largely cancel. Although the net electrostatic interactions of the water molecules with the atomic charges and dipoles associated with the carbon atoms of the central ring drop off rapidly along the benzene, coronene, DBC sequence, even for DBC the electrostatic interactions between the water monomer and the charges and dipoles on the noncentral C and H atoms of the acene are sizable. Most noteworthy, the net electrostatic interaction of the water molecule with the atomic quadrupole (Q_{20}) moments of the acenes are -2.62, -1.67, and -0.70 kcal mol^{-1} for benzene, coronene, and DBC, respectively, while the corresponding values allowing for the interactions with all three moments charges, dipoles, and quadrupoles on the acene atoms are -1.68, -0.70, and -0.38 kcal mol^{-1}, respectively, indicating that one needs to employ still larger acenes to converge the net electrostatic interaction energy to the graphite limit. The fall off of the net electrostatic interaction between the water monomer and the atomic quadrupoles of the acene with the increasing size of the ring system is a consequence of the interaction being repulsive beyond the central six carbon atoms. It is reassuring, however, that the magnitudes of the atomic charges and dipole moments on the inner carbon atoms decrease rapidly with increasing size of the acene, as this indicates that the charge distributions around these

15

central atoms are close to those in graphite, which justifies the use of the cluster model calculations with the SAPT procedure for designing a water–graphite potential.

Comparison of the results in Tables 2.1 and 2.3 reveals that the DFT–SAPT calculations give an electrostatic interaction between water and benzene that is 2.06 kcal mol^{-1} more attractive than obtained from the interactions between the atomic multipoles of the two molecules. For water–coronene and water–DBC, the DFT–SAPT calculations give an electrostatic interaction about 1.3 kcal mol^{-1} more attractive than that obtained from the interactions of the distributed moments. The differences between the two sets of electrostatic energies is due primarily to charge-penetration,[93, 105] which is present in the DFT–SAPT calculations but is absent in the values calculated using the multipole moments. The greater importance of charge-penetration for water–benzene than for water–coronene or water–DBC is consistent with there being greater electron density in the vicinity of the carbon atoms of benzene than in the vicinity of the central carbon atoms of coronene or DBC.

The exchange contribution to the water–acene interaction energy drops off by 0.61 kcal mol^{-1} in going from benzene to coronene but is nearly the same for DBC as for coronene. The larger value of the exchange for the interaction of the water monomer with benzene than with the larger acenes is again consistent with the carbon atoms of benzene carrying excess negative charge. The net induction interaction is approximately the same for all systems considered, while the dispersion interaction grows slowly in magnitude with the increasing size of the ring system (*e.g.* being 0.61 kcal mol^{-1} greater in magnitude for water–coronene than for water–benzene). It is not immediately clear why the dispersion and induction contributions behave differently with increasing ring size.

Table 2.4: Water–graphite interaction energies (kcal mol^{-1}) for various models[a].

| Reference | Model | Interaction energy | | | | |
		Electrostatics	Exchange	Induction	Dispersion	Total
[17]	Hummer *et al.*		1.39		−3.14	−1.76
[37]	Gordillo–Martí		2.87		−4.24	−1.37
[40]	Werder *et al.*		0.93		−2.46	−1.54
[32]	Pertsin–Grunze	0.00	1.16		−3.10	−1.94
[30]	Karapetian–Jordan	0.00	1.42	−0.85	−2.99	−2.42
[33]	Zhao–Johnson	−0.36	1.02	−0.46	−2.26	−2.05
[106]	Dang–Feller	0.00	6.45	−0.45	−6.44	−0.44
[107]	AMOEBA	−0.01	3.75	−0.82	−4.55	−1.63
This study	SAPT extrapolated	−1.30	5.13	−1.35	−4.68	−2.20

[a] These calculations were performed with the acene geometries employed in the current study (all CC bonds set to 1.420 Å and water placement described in Section 2.3). As such, the resulting interaction energies are expected to be slightly different from those published.

[b] Using the 1SΘ model of Reference [32], which employs a single Lennard–Jones site on water together with a term accounting for the interaction of the water atomic charges from the TIP4P water model[108] with the Whitehouse–Buckingham[109] value of the quadrupole moments on the C atoms.

[c] The Dang–Feller and AMOEBA models were actually developed for water–benzene. In applying these models to water–graphite, we replaced the moments on the C atoms in the original models with the atomic quadrupole moment as obtained from the GDMA analysis of DBC ($Q_{20} = -1.28$ a.u.).

2.5   INTERACTION OF WATER MOLECULE WITH A SINGLE SHEET OF GRAPHITE

From Table 2.1 it is seen that for the assumed geometry the net interaction energy for both water–coronene and water–DBC is about -2.5 kcal mol^{-1}. The exchange, induction, and charge-penetration contributions to the interaction energy for the water–graphite system should be essentially identical to the corresponding contributions for water–DBC (Table 2.1). On the other hand, we expect the electrostatic interaction to be less attractive and the dispersion contribution to more attractive than for water–DBC. To estimate the former quantity for water–graphite, we combine the charge-penetration contribution for water–DBC with the electrostatic interaction between water, modeled by the Dang–Chang point charges,[94] and the quadrupole moments on the C atoms of $C_{216}H_{36}$, which has two more shells of benzene rings than does DBC. For the acene only the Q_{20} components were used, with the numerical value being chosen to be that of the inner carbon atoms of DBC (-1.28 a.u.) as determined from the GDMA analysis. The electrostatic interaction energy of the Dang–Chang water monomer with this array of quadrupole moments is only -0.005 kcal mol^{-1}. Thus, for our assumed geometry, as one approaches the graphite limit, the net interaction between the atomic multipoles on water with the atomic quadrupole moments on the C atoms tends to zero, leaving only the charge-penetration contribution to electrostatics. Since charge-penetration falls off exponentially with distance[93, 105] it should contribute nearly the same amount (-1.30 kcal mol^{-1}) for water–graphite as for water–DBC. Although charge-penetration has not been accounted for explicitly in existing water–graphite model potentials, in some cases it has been included implicitly through a weakening of the repulsion term in the potential.

Similarly, we have fit DFT–SAPT dispersion energies between water–coronene for a range of distances between the water and coronene molecules. Application of the resulting potential to water–$C_{216}H_{36}$ gives a dispersion energy of -4.68 kcal mol^{-1} (again assuming that the water is positioned relative to the ring as determined for water–triphenylene), compared to the -4.33 kcal mol^{-1} DFT–SAPT value for water–coronene, and our -4.57 kcal mol^{-1} estimate for water–DBC. Combining the various contributions gives a net interaction energy of -2.20 kcal mol^{-1} for

water–graphite at our standard geometry.

Our results for water–graphite are summarized in Table 2.4 along with the results from six water–graphite potentials, as well as from modified Dang–Feller[106] and AMOEBA[107] models. For the later two models, the CC bond lengths were adjusted to match the values used in the SAPT calculations, and the multipoles on the C atoms in the original models were replaced with the -1.28 a.u. value of Q_{20} obtained from the GDMA analysis of DBC. The energies for the Karapetian–Jordan,[30] Dang–Feller, and AMOEBA models were calculated using the `Tinker` molecular modeling package;[110] the energies for the other models were obtained using our own codes.

The models of Hummer *et al.*,[17] Gordillo–Martí,[37] and Werder *et al.*[40] all employ Lennard–Jones potentials between the water molecule and the carbon atoms of graphite and do not account explicitly for either electrostatics or induction. The Pertsin–Grunze model[32] employs a Lennard–Jones potential together with electrostatic interactions between three point charges on the water and quadrupole moments on the C atoms, with the value of the moment being taken from Whitehouse and Buckingham.[109] The Karapetian–Jordan,[30] Zhao–Johnson,[33] Dang–Feller,[106] and AMOEBA[107] models all include electrostatics and induction interactions as well as terms to account for dispersion and short-ranged repulsion. With the exception of the Zhao–Johnson model, all of the models reported in Table 2.4 are atomistic. The Zhao–Johnson[33] model was obtained by integrating the atomic interactions over the x and y (in-plane) directions.

Only the Zhao–Johnson and Karapetian–Jordan models gives net interaction energies within 10% of the value obtained by extrapolating the DFT–SAPT results to the infinite graphite sheet. We note also that the Gordillo–Martí and AMOEBA models give dispersion energies close to that deduced from the SAPT calculations, and only the AMOEBA model gives an electrostatic plus exchange contribution close to the value derived in the present study. Interestingly the value of the induction contribution to the water–graphite interaction deduced from the SAPT calculations is appreciably larger in magnitude than those obtained from any of the model potentials. We believe that this is due to charge-transfer interactions which are included in the SAPT calculations but are absent in any of the model potentials. An EDA analysis[9] of water–benzene reveals that electron transfer from water→benzene contributes about -0.6 kcal mol^{-1} (calculated at the HF/aug-cc-

19

pVDZ level with QChem3.2[111]) to the interaction energy of this system.

2.6 CONCLUSION

DFT–SAPT calculations have been used to analyze the interaction between a water molecule with benzene, anthracene, pentacene, coronene, and dodecabenzocoronene. These results have been combined with calculations of the electrostatic interaction between water and a $C_{216}H_{36}$ acene, employing atomic quadrupoles from a GDMA analysis of DBC to estimate that the interaction energy of a water molecule to a single graphite sheet, obtaining a value of -2.20 kcal mol^{-1}. This value is appreciably larger in magnitude than the values of the interaction energies obtained from the force fields commonly applied to study water on graphite surfaces.

The largest single source of error in our approach for estimating the water–graphite interaction energy is the use of the MP2 geometry of water–triphenylene for positioning the water monomer relative to the larger acenes. To estimate the magnitude of the error due to this restriction, we carried out two potential energy surface scans for water–coronene using the SAPT procedure, varying the distance from the ring system. In one scan we retained the orientation of the water found in the water–triphenylene system. In the other we considered a structure with water positioned above the center of the central ring, with both H atoms pointed down. The first scan revealed that the energy decreases by 0.15 kcal mol^{-1} for the one H atom down structure, when the water is moved about 0.1 Å further from the ring system than in the case of water–triphenylene. The second scan revealed that the water–coronene complex with both H atoms pointed toward the ring is about 0.35 kcal mol^{-1} more stable than the one H atom down structure. This is largely a consequence of the more favorable electrostatic interaction between water and coronene for the structure with both H atoms down. Indeed, calculations of the electrostatics between atomic multipole moments of water and $C_{216}H_{36}$, with the water positioned above the center of the central ring (R_{OX} 3.36 Å, from Reference 112) with both H atoms down, give an electrostatic energy of -0.29 kcal mol^{-1} as compared to the -0.005 kcal mol^{-1} contribution for the complex with the structure shown in Fig-

ure 2.2. On the basis of these results, we estimate that the interaction energy of a water molecule with a single graphite sheet is about -2.7 kcal mol^{-1} for the minimum energy structure.

It is also noteworthy that our GDMA analysis of acenes as large as DBC gives a value of the carbon quadrupole moment nearly twice as large in magnitude as that reported by Whitehouse and Buckingham.[109] This leads us to question whether the quadrupole moment deduced by these authors is indeed correct for the case of a single graphite sheet. However, the electrostatic and induction contributions due to the interaction of the water molecule with the carbon quadrupole moments are quite small at the minimum energy structure, and our estimate of the water–graphite interaction energy would be reduced in magnitude by only about 0.1 kcal mol^{-1}, were we to assume that the Whitehouse–Buckingham value of the quadrupole moment of graphite is correct.

While we were preparing this paper, we learned of unpublished work of Bludský and co-workers[112] who used their DFT/CC[62] approach to estimate the interaction energy between water and a single graphite sheet. These authors obtain a interaction energy of -2.8 kcal mol^{-1} for a structure with the water positioned above the ring with both H atoms down, in excellent agreement with our estimate of this value.

2.7 ACKNOWLEDGEMENTS

21

3.0   BENCHMARK CALCULATIONS OF WATER-ACENE INTERACTION ENERGIES: EXTRAPOLATION TO THE WATER-GRAPHENE LIMIT AND ASSESSMENT OF DISPERSION-CORRECTED DFT METHODS

3.1   ABSTRACT

In a previous study (*J. Phys. Chem. C*, 2009, **113**, 10242–10248) we used density functional theory based symmetry-adapted perturbation theory (DFT–SAPT) calculations of water interacting with benzene (C_6H_6), coronene $(C_{24}H_{12})$, and circumcoronene $(C_{54}H_{18})$ to estimate the interaction energy between a water molecule and a graphene sheet. The present study extends this earlier work by use of a more realistic geometry with the water molecule oriented perpendicular to the acene with both hydrogen atoms pointing down. We also include results for an intermediate $C_{48}H_{18}$ acene. Extrapolation of the water–acene results gives a value of -3.0 ± 0.15 kcal mol^{-1} for the binding of a water molecule to graphene. Several popular dispersion-corrected DFT methods are applied to the water–acene systems and the resulting interacting energies are compared to results of the DFT–SAPT calculations in order to assess their performance.

3.2 INTRODUCTION

The physisorption of atoms and molecules on surfaces is of fundamental importance in a wide range of processes. In recent years, there has been considerable interest in the interaction of water with carbon nanotube and graphitic surfaces, in part motivated by the discovery that water can fill carbon nanotubes.[14] Computer simulations of these systems requires the availability of accurate force fields and this, in turn, has generated considerable interest in the characterization of the water–graphene potential using electronic structure methods.[1,47,48,112,113]

Density functional theory (DFT) has evolved into the method of choice for much theoretical work on the adsorption of molecules on surfaces. However, due to the failure of the local density approximation (LDA) and generalized gradient approximations (GGA) to account for long-range correlation (hereafter referred to as dispersion or van der Waals) interactions, density functional methods are expected to considerably underestimate the interaction energies for molecules on graphitic surfaces. In recent years, several strategies have been introduced for "correcting" DFT for dispersion interactions. These range from adding a pair-wise $C_6^{ij} R_{ij}^{-6}$ interactions,[114–117] to fitting parameters in functionals so that they better describe long-range dispersion,[118–121] to accounting explicitly for long-range non-locality, *e.g.*, with the vdW–DF functional.[122] Although these approaches have been quite successful for describing dispersion interactions between molecules, it remains to be seen whether they can accurately describe the interactions of water and other molecules with carbon nanotubes or with graphene, given the tendency of DFT methods to overestimate charge-transfer interactions[123] and to overestimate polarization in extended conjugated systems.[124] Thus, even if dispersion interactions were properly accounted for, it is not clear how well DFT methods would perform at describing the interaction of polar molecules with extended acenes and graphene.

Second-order Möller–Plesset perturbation theory (MP2) does recover long-range two-body dispersion interactions and has been used in calculating the interaction energies of water with acenes as large as $C_{96}H_{24}$.[1] However, MP2 calculations can appreciably overestimate two-body dispersion energies.[125,126] This realization has led to the development of spin-scaled MP2 (SCS–

MP2),[127, 128] empirically-corrected MP2,[129] and "coupled" MP2 (MP2C)[130] methods for better describing van der Waals interactions. However, it is not clear that even these variants of the MP2 method would give quantitatively accurate interaction energies for water or other molecules adsorbed on large acenes since the HOMO–LUMO energy gap decreases with the size of the acene. In addition to these issues, the MP2 method is inadequate for systems with large three-body dispersion contributions to the interaction energies.[131]

Given the issues and challenges described above, we have employed the DFT-based symmetry-adapted perturbation theory (DFT–SAPT) method of Heßelmann *et al.*[72] to calculate the interaction energies between a water molecule and benzene, coronene, hexabenzo[bc,ef,hi,kl,no,qr]-coronene (referred to as hexabenzocoronene or HBC), and circumcoronene (also referred to as dodecabenzocoronene or DBC). As will be discussed below, the DFT–SAPT approach has major advantages over both traditional DFT and MP2 methods. The DFT–SAPT method also provides a dissection of the net interaction energies into electrostatic, exchange-repulsion, induction, and dispersion contributions, which is valuable for the development of classical force fields and facilitates the extrapolation of the results for the clusters to the water–graphene limit. In the current paper, we extend our earlier study[113] of water–acene systems to include more realistic geometrical structures. The DFT–SAPT results are also used to assess various methods for including dispersion effects in DFT calculations.

(a) Coronene   (b) Hexabenzocoronene (HBC)   (c) Dodecabenzocoronene (DBC)
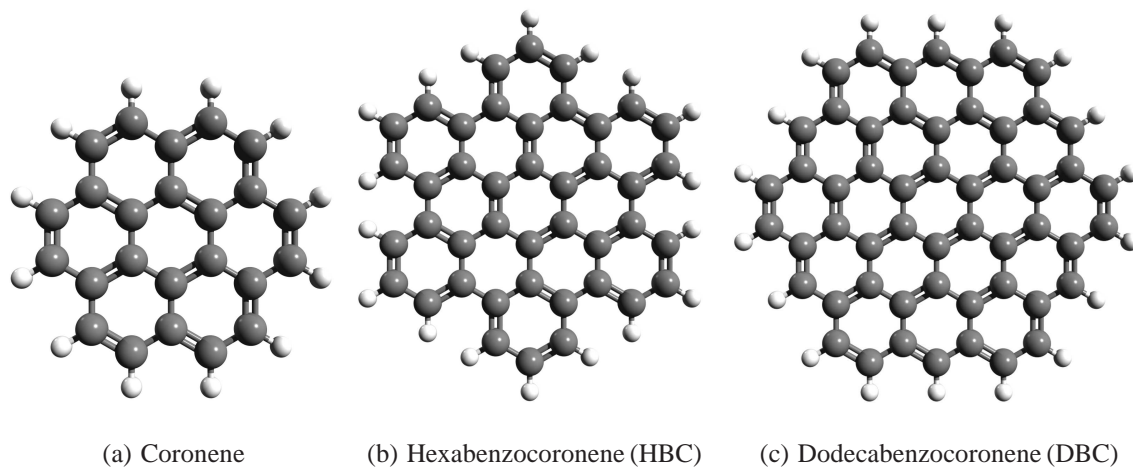
Figure 3.1: Acenes used in the current study.
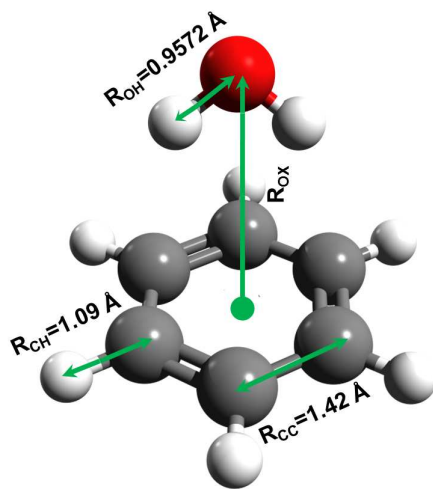
Figure 3.2: Geometry used in the current study, illustrated in the case of water–benzene.

3.3 THEORETICAL METHODS

The coronene, HBC, and DBC acenes used in this study are depicted in Figure 3.1. For each of the acenes, including benzene, all CC bond lengths and CCC angles (1.420 Å and 120°, respectively) were taken to match the experimental values for graphite.[91] The dangling bonds were capped with hydrogen atoms with CH bond lengths and CCH angles of 1.09 Å and 120°, respectively. This facilitates extrapolation of the interaction energies to the limit of a water molecule interacting with graphene. The geometry of the water monomer was constrained to the experimental gas phase geometry (OH bond length of 0.9572 Å and HOH angle of 104.52°).[92] The water molecule was placed above the middle of the central ring, with both hydrogens pointing towards the acene. Note that this is a different water orientation than used for most of the calculations reported in Reference 113[‡]. The orientation and distance of the water molecule relative to the ring system were obtained from a series of single-point DFT–SAPT calculations on water–coronene. These calculations give a minimum energy structure with the water dipole oriented perpendicular to the acene ring system, and an oxygen-ring distance of 3.36 Å, which is close to that obtained in prior theoretical studies of water–coronene.[70, 112, 135–137] However, the potential energy surface is quite flat (our calculations give an energy difference of only 0.02 kcal mol^{-1} between $R_{OX} = 3.26$ Å and 3.36 Å), and thus small geometry differences are relatively unimportant.

The DFT–SAPT method, and the closely related SAPT(DFT) method of Szalewicz and co-workers,[79] evaluate the electrostatic and exchange-repulsion contributions using integrals involving the Coulomb operator and the Kohn–Sham orbitals, and are thus free of the problems inherent in evaluating the exchange-repulsion contributions using common density functionals. The induction and dispersion contributions are calculated using response functions from time-dependent DFT. In the present study, the calculations made use of the LPBE0AC functional,[72] which replaces the 25% exact Hartree–Fock exchange of the PBE0 functional[76] with the localized Hartree–Fock exchange functional of Sala and Görling[90] and includes an asymptotic correction. In general, DFT–SAPT calculations give interaction energies close to those obtained from CCSD(T) calcula-

---

[‡]Chapter 2

Table 3.1: Methods and programs used in the current study.

Method	Scheme	Program
DFT–SAPT[72]	Uses linear response functions from TD-DFT to calculate dispersion energies *via* the Casimir–Polder integral	MOLPRO[73]
DFT+D[114, 115]	Adds empirical $C_6^{ij}R_{ij}^{-6}$ corrections to DFT energies	GAMESS[132]
DCACP[118–120]	Uses pseudopotential terms to recover dispersion	CPMD[133]
C_6/Hirshfeld[116]	Adds to DFT energies $C_6^{ij}R_{ij}^{-6}$ corrections determined using Hirshfeld partitioning	FHI-AIMS[134]

tions.[138, 139] For more details, we refer the reader to Reference 139.

The DFT–SAPT calculations were carried out with a modified aug-cc-pVTZ basis set in which the exponents of the diffuse functions were scaled by 2.0 to minimize convergence problems due to near linear dependency in the basis set. In addition, for the carbon atoms the *f* functions were removed and the three *d* functions were replaced with the two *d* functions from the aug-cc-pVDZ basis set. Similarly, for the acene hydrogen atoms the *d* functions were removed and the three *p* functions were replaced with the two *p* functions from the aug-cc-pVDZ basis set. The full aug-cc-pVTZ basis set with the diffuse functions scaled by the same amount as the acene carbon and hydrogen atoms was employed for the water molecule. For water–benzene, the DFT–SAPT calculations with the modified basis set give an interaction energy only 0.05 kcal mol^{-1} smaller in magnitude than that obtained with the full, unscaled, aug-cc-pVTZ basis set. Density fitting (DF) using Weigend's cc-pVQZ JK-fitting basis set[88] was employed for the first order and the induction and exchange-induction contributions. For the dispersion and exchange-dispersion contributions, Weigend and co-worker's aug-cc-pVTZ MP2-fitting basis set[89] was used. The DF–DFT–SAPT

calculations were carried out with the MOLPRO *ab initio* package.[73]

We also examined several approaches for correcting density functional calculations for dispersion, including the dispersion-corrected atom-centered potential (DCACP) method of Roethlisberger,[118–120] the DFT+dispersion (DFT+D) method of Grimme,[114,115] and the C_6/Hirshfeld partitioning scheme of Tkatchenko and Scheffler.[116] The DCACP procedure uses modified Göedecker pseudopotentials[140] to incorporate dispersion effects. These calculations were carried out using the CPMD program,[133] utilizing a planewave basis set and periodic boundary conditions. These calculations employed a planewave cutoff of 4082 eV and box sizes of $42 \times 42 \times 28$ a.u. for water–benzene and water–coronene, and $46 \times 46 \times 28$ a.u. for water–HBC and water–DBC to minimize interactions between unit cells.

The DFT+D method adds damped empirical $C_6^{ij}R_{ij}^{-6}$ atom-atom corrections[114,115] to the "uncorrected" DFT energies. The DFT+D calculations were performed with the same Gaussian-type-orbital basis sets as used in the DFT–SAPT calculations and were carried out using the GAMESS *ab initio* package[132] (using the implementation of Peverati and Baldridge[141]). The dispersion corrections were added to the interaction energies calculated using the PBE,[142] BLYP,[143,144] and B97–D[115] GGA functionals. The B97-D functional is Grimme's reparameterization of Becke's B97 functional[145] for use with dispersion corrections.

The calculations involving the C_6/Hirshfeld method of Tkatchenko and Scheffler[116] were performed with the FHI-AIMS package.[134] The C_6/Hirshfeld method, like the DFT+D method, incorporates dispersion *via* atom-atom $C_6^{ij}R_{ij}^{-6}$ terms. However, unlike the DFT+D method, the C_6/Hirshfeld scheme calculates the C_6^{ij} coefficients using frequency-dependent polarizabilities for the free atoms, scaling these values by ratios of the effective and free volumes, with the former being obtained from Hirshfeld partitioning[146] of the DFT charge density. This procedure results in dispersion corrections that are sensitive to the chemical bonding environments. The tier 4 numerical atom-centered basis sets[147] native to FHI-AIMS were employed. These basis sets provide a $6s5p4d3f2g$ description of the carbon and oxygen atoms, and a $5s3p2d1f$ description of the hydrogen atoms. A summary of the theoretical methods employed is given in Table 3.1.

3.4 RESULTS

3.4.1 DFT–SAPT calculations

The DFT–SAPT results for the water–acene systems are summarized in Table 3.2. The net interaction energies along the water–benzene, water–coronene, water–HBC, and water–DBC sequence obtained using the DFT–SAPT procedure are -3.16, -3.05, -3.01, -2.93 kcal mol^{-1}, respectively. The interaction energies and R_{OX} values from recent studies of water–coronene summarized in Table 3.3. These earlier studies give interaction energies of water–coronene ranging from -2.56 to -3.54 kcal mol^{-1}.

From Table 3.2, it is seen that the electrostatic interaction energy decreases in magnitude, the dispersion energies increase in magnitude, and the induction energies are relatively constant along the benzene–coronene–HBC–DBC sequence. The exchange-repulsion interaction energy is 3.24 kcal mol^{-1} for water–benzene but only about 2.8 kcal mol^{-1} for the interaction of water with the larger acenes. This reflects the fact that the charge distribution in the vicinity of the carbon atoms is appreciably different for benzene than for the central carbon atoms in the larger acenes. Perhaps the most surprising result of the SAPT calculations is the near constancy of the induction contributions with increasing size of the acene ring system. This is not the case for models employing point inducible dipoles on the carbon atoms, and we expect that it is a consequence of charge-flow polarization,[148, 149] which is not recovered in such an approach.

In classical simulations of water interacting with graphitic surfaces the dominant electrostatic contributions are generally described by interactions of the water dipoles (or atomic point charges) with atomic quadrupoles on the carbon atoms, as the quadrupole is the leading moment in an atom-centered distributed multipole representation of graphene. However for finite acenes there are also atomic charges and dipoles associated with the carbon atoms as well as with the edge H atoms. In addition, the electrostatic interaction energies obtained from the SAPT calculations include the effect of charge-penetration, which is a consequence of overlap of the charge densities of the water and acene molecules. It is useful, therefore, to decompose the net electrostatic interaction energies into contributions from charge-penetration and from interactions between the atom-centered mul-

Table 3.2: Contributions to the DF–DFT–SAPT water–acene interaction energies (kcal mol^{-1}).

Term	Benzene	Coronene	HBC	DBC
Electrostatics	-2.85	-1.73	-1.54	-1.39
Exchange-repulsion	3.24	2.79	2.85	2.85
Induction	-1.28	-1.29	-1.36	-1.37
Exchange-induction	0.82	0.80	0.83	0.84
δ(HF)	-0.26	-0.20	-0.23	-0.23
Net induction	-0.71	-0.69	-0.75	-0.75
Dispersion	-3.28	-3.83	-4.00	$(-4.07)^a$
Exchange-dispersion	0.44	0.42	0.43	(0.43)
Net dispersion	-2.84	-3.42	-3.57	$(-3.64)^a$
Total interaction energy	-3.16	-3.05	-3.01	$(-2.93)^b$

[a] Estimated using E_{disp}(water–DBC)=E_{disp}(water–HBC) + $\sum C_6^{ij} R_{ij}^{-6}$, where the $C_6^{ij} R_{ij}^{-6}$ terms account for the dispersion interactions of the water molecule with the twelve additional C atoms of DBC. The C_6 coefficients were determined by fitting the DFT–SAPT water–coronene results.

[b] Total energy calculated using the estimated dispersion energy, described in footnote *a*.

Table 3.3: Interaction energies (kcal mol^{-1}) and R$_{OX}$ values (Å) for water–coronene from various theoretical studies.

	R$_{OX}$	E$_{int}$	Approach
Rubeš et al.[112]	3.27	−3.54	DFT/CC//aug-cc-pVQZ
Sudiarta and Geldart[70]	3.39	−2.81	MP2//6-31G(d=0.25)
Huff and Pulay[137]	3.40	−2.85	MP2//6-311++G**[a]
Reyes et al.[135]	3.33	−2.56	LMP2//aug-cc-pVTZ(-f)
Cabaleiro–Lago et al.[136]	3.35	−3.15	SCS–MP2//cc-pVTZ
Current study	3.36	−3.05	DFT–SAPT//modified aug-cc-pVTZ(-f)[b]

[a] Diffuse functions were used on every other carbon atom.

[b] Modified as described in the text.

tipole moments.

For each of the acenes studied we used Stone's Gaussian distributed multipole analysis (GDMA) program[103] to calculate atomic charges, dipoles and quadrupoles on the acene atoms. Moments higher than the quadrupole make a negligible contribution to the interaction energies and thus were neglected from the multipole analysis. Table 3.4 summarizes the GDMA moments for the acenes obtained from MP2/cc-pVDZ charge densities (the MP2 calculations were carried out using Gaussian03[104]). As expected, the values of the charges and dipoles on the inner carbons decrease in magnitude as the size of the acene increases. For coronene the atomic charges and dipoles are near zero for the central six C atoms, whereas for DBC the atomic charges and dipoles are near zero for the inner three rings of carbon atoms. In order to estimate the interaction energies in the absence of charge-penetration, the three point charges from the Dang–Chang model[94] of the water monomer were allowed to interact with the multipole moments on the atoms of the acenes (the use of higher multipoles on the hydrogen and oxygen atoms of the water molecule does not

Table 3.4: Multipole moments[a] (in atomic units) for the carbon and hydrogen atoms in benzene, coronene, HBC and DBC[b].

Atom Type	q				$|\mu|$				Q_{20}				$|Q_{22c}+Q_{22s}|$			
	C_6H_6	$C_{24}H_{12}$	$C_{42}H_{18}$	$C_{54}H_{18}$	C_6H_6	$C_{24}H_{12}$	$C_{42}H_{18}$	$C_{54}H_{18}$	C_6H_6	$C_{24}H_{12}$	$C_{42}H_{18}$	$C_{54}H_{18}$	C_6H_6	$C_{24}H_{12}$	$C_{42}H_{18}$	$C_{54}H_{18}$
C1	−0.09	−0.01	−0.01	0.00	0.11	0.01	0.00	0.00	−1.14	−1.28	−1.29	−1.28	0.09	0.00	0.00	0.00
C2		−0.04	−0.01	0.00		0.11	0.02	0.01		−1.22	−1.28	−1.28		0.09	0.01	0.01
C3		−0.07	−0.03	−0.01		0.16	0.08	0.01		−1.17	−1.25	−1.28		0.02	0.08	0.01
C4			−0.08	−0.04			0.16	0.12			−1.18	−1.22			0.04	0.10
C5			−0.07	−0.07			0.13	0.16			−1.13	−1.16			0.08	0.02
C5a				−0.06				0.16				−1.18				0.12
Ha[c]			0.10				0.14				−0.15				0.09	
Hb[d]	0.09	0.10	0.09	0.11	0.14	0.14	0.14	0.15	−0.13	−0.13	−0.13	−0.13	0.11	0.08	0.10	0.06

[a] Spherical tensor notation is employed here. To convert into a Cartesian representation: $\Theta_{XX} = -\frac{1}{2}Q_{20} + \frac{1}{2}\sqrt{3}Q_{22c}$; $\Theta_{YY} = -\frac{1}{2}Q_{20} - \frac{1}{2}\sqrt{3}Q_{22c}$; $\Theta_{XY} = -\frac{1}{2}\sqrt{3}Q_{22s}$; $\Theta_{ZZ} = Q_{20}$;

[b] Benzene: C_6H_6; Coronene: $C_{24}H_{12}$; HBC: $C_{42}H_{18}$; DBC: $C_{54}H_{18}$;

[c] Ha hydrogen atoms are connected to C4 carbon atoms.

[d] Hb hydrogen atoms are connected to C1 carbons in benzene, to C3 carbons in coronene, and to C5 carbons in HBC and DBC.

Table 3.5: Electrostatic interaction energies (kcal mol^{-1}) between atomic charges on water and the atomic multipoles of the acenes.

Term	Benzene	Coronene	HBC	DBC	Graphene[a]
Charge-Charge	−1.36	−2.18	−1.89	−1.57	0.00
Charge-Dipole	1.86	3.20	2.53	2.01	0.00
Charge-Quadrupole	−2.30	−2.13	−1.55	−1.22	−0.65[b]
Total multipole	−1.80	−1.11	−0.91	−0.77	−0.65
Charge-penetration	−1.05	−0.62	−0.62	−0.62	−0.62[c]
DFT–SAPT	−2.85	−1.73	−1.54	−1.39	(−1.27)[d]

[a] Modeled by $C_{216}H_{36}$ as described in the text.

[b] Calculated by using atomic quadrupoles of $Q_{20} = −1.28$ a.u. on each carbon atom.

[c] The charge-penetration in the electrostatic interaction between water–graphene is assumed to be the same as between water and DBC.

[d] Taken to be the sum of the charge-penetration (from water–DBC) and charge-quadrupole interactions for the water–$C_{216}H_{36}$ model.

Table 3.6: Net interaction energies (kcal mol^{-1}) for water–acene systems.

Method	Benzene	Coronene	HBC	DBC	MAE[a]
DF–DFT–SAPT	−3.17	−3.05	−3.00	(−2.94)[b]	
B97-D	−3.24	−3.62	−3.70	−3.61	0.50
PBE+D	−3.69	−3.61	−3.61	−3.49	0.56
BLYP+D	−3.12	−3.37	−3.48	−3.39	0.32
DCACP-BLYP	−3.08	−3.24	−3.08	−3.10	0.13
C_6/Hirshfeld-BLYP	−2.50	−3.04	−3.11	−3.06	0.22
C_6/Hirshfeld-PBE	−3.77	−4.09	−4.16	−4.07	0.98

[a] Mean absolute error (MAE) relative to DFT–SAPT results.

[b] Calculated using the estimated dispersion term from Table 3.2.

significantly impact the electrostatic interactions between water and the acenes). The results for the various water–acene systems for $R_{OX} = 3.36$ Å are summarized in Table 3.5[§]. The charge-charge, charge-dipole and charge-quadrupole interactions are large in magnitude (≥ 1.2 kcal mol^{-1}) for all acenes considered, with the charge-charge and charge-quadrupole contributions being attractive and the charge-dipole contributions being repulsive. Interestingly, the charge-dipole and charge-quadrupole contributions roughly cancel for water–HBC and water–DBC. The charge-quadrupole contribution decreases in magnitude with increasing size of the acene. This is a consequence of the fact that the short-range electrostatic interactions with the carbon quadrupole moments are attractive while long-range interactions with the carbon quadrupoles are repulsive. The differences of the SAPT and GDMA electrostatic energies provide estimates of the charge-penetration contributions which are found to be −0.62 kcal mol^{-1} for water–coronene, water–HBC, and water–DBC

[§]Due to a small conversion error, the actual electrostatic interactions for water-DBC in Table 3.5 differ from those published in Reference 150. These values should be replaced with the following (in kcal mol^{-1}): charge-charge=−1.44; charge-dipole=1.97; charge-quadrupole=−1.24; Total multipole=−0.71

for $R_{OX} = 3.36$ Å.

3.4.2 Dispersion-corrected DFT calculations

The interaction energies of the water–acene complexes (at $R_{OX} = 3.36$ Å) obtained using the various dispersion-corrected DFT methods are reported in Table 3.6. Of the dispersion-corrected DFT methods investigated, the DCACP method is the most successful at reproducing the DFT–SAPT values of the interaction energies at $R_{OX} = 3.36$ Å. For water–coronene, water–HBC, and water–DBC the interaction energies obtained with the C_6/Hirshfeld method combined with the BLYP functional are also in good agreement with the DFT–SAPT values, although this approach underestimates the magnitude of the interaction energy for water–benzene by about 0.7 kcal mol^{-1}. Interestingly, with the exception of the PBE+D approach, all the dispersion-corrected DFT methods predict a larger in magnitude interaction energy for water–coronene than for water–benzene, opposite from the results of the DFT–SAPT calculations. This could be due to the overestimation of charge-transfer in the DFT methods, with the overestimation being greater for water–coronene. Figure 3.4.2 reports the potential energy curves for the water–coronene and water–HBC systems calculated with the various dispersion-corrected DFT methods. From Figures 3(a) and 3(b) it is seen that the DFT+D methods and C_6/Hirshfeld methods both tend to overbind the complexes. The DFT+D methods with all three functionals considered and the C_6/Hirshfeld calculations using the BLYP functional locate the potential energy minimum at much smaller R_{OX} values than found in the DFT–SAPT calculations. It is also seen that the potential energy curves calculated using the DCACP procedure differ significantly from the DFT–SAPT potential for $R_{OX} \geq 4.2$ Å. This is on account of the fact that the dispersion corrections in the DCACP method fall off much more abruptly than R^{-6} at large R. It appears that part of the success of the DCACP method is actually due to the pseudopotential terms improving the description of the exchange-repulsion contribution to the interaction energies.
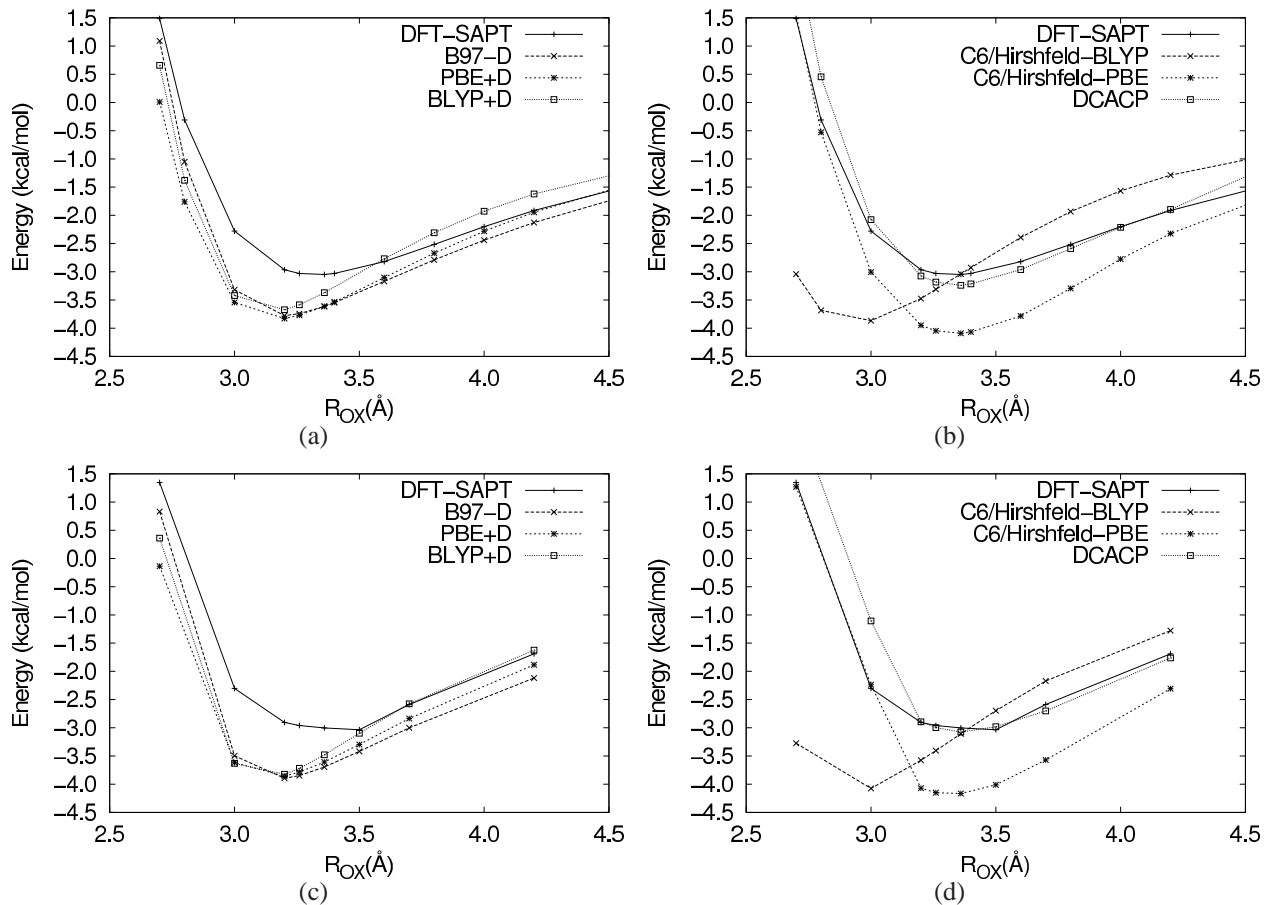
Figure 3.3: Potential energy curves for approach of a water molecule to (a,b) coronene and (c,d) HBC. The water molecule is oriented with both of the H atoms pointed towards the acene, with the water dipole moment perpendicular to the plane of the ring systems.

3.4.3 Extrapolation to the DFT–SAPT results to water–graphene

The exchange-repulsion, induction, exchange-dispersion, and charge-penetration contributions between water and an acene are already well converged, with respect to the size of the acene, by water–DBC. The contributions that have not converged by water–DBC are the non-charge-penetration portion of the electrostatics and the dispersion (although the latter is nearly converged). The non-charge-penetration contribution to the electrostatic energy for water–graphene was estimated by calculating the electrostatic energy of water–$C_{216}H_{36}$ using only atomic quadrupoles on the carbon atoms of the acene. The carbon quadrupole moments were taken to be $Q_{20} = -1.28$ a.u., the value calculated for the innermost six carbon atoms of DBC. We note that this value is about twice as large in magnitude as that generally assumed for graphene.[109] This gives an estimate of -0.65 kcal mol^{-1} for the non-charge-penetration contribution to the electrostatic energy between a water monomer and graphene.

Finally we estimate, using atomistic $C_6^{ij}R_{ij}^{-6}$ correction terms, that the dispersion energy is about 0.05 kcal mol^{-1} larger in magnitude in water–graphene then for water–DBC. Adding the various contributions we obtain a net interaction energy of -2.85 kcal mol^{-1} for water–graphene assuming our standard geometry with $R_{OX} = 3.36$ Å. Rubeš *et al.*, extrapolating results obtained using their DFT/CC method, predicted an interaction energy of -3.17 kcal mol^{-1} for water–graphene. Interestingly, while Rubeš *et al.* conclude the R_{OX} is essentially the same for water–coronene, water–DBC, and water–graphene, our DFT–SAPT calculations indicate that R_{OX} increases by about 0.15 Å in going from water–coronene to water–HBC, with an energy lowering of about 0.05 kcal mol^{-1} accompanying this increase of R_{OX} for water–HBC. We further estimate, based on calculations on water–benzene, that due to the basis set truncation errors, the DFT–SAPT energies could be underestimated by as much as 0.1 kcal mol^{-1}. Thus, we estimate that the "true" interaction energy for water–graphene at the optimal geometry is -3.0 ± 0.15 kcal mol^{-1}, consistent with the result of Rubeš *et al.*[112]

3.5 CONCLUSIONS

In this study, we have used the DFT–SAPT procedure to provide benchmark results for the interaction of a water molecule with a sequence of acenes up to $C_{54}H_{18}$ in size. All results are for structures with the water molecule positioned above the central ring, with both hydrogen atoms down, and with the water–acene separation obtained from geometry optimization of water–coronene. The magnitude of the interaction energy is found to fall off gradually along the benzene–coronene–HBC–DBC sequence. This is on account of the fact that the electrostatic contribution falls off more slowly with increasing ring size than the dispersion energy grows. We combine the DFT–SAPT results with long-range electrostatic contributions calculated using distributed multipoles and long-range dispersion interactions calculated using $C_6^{ij}R_{ij}^{-6}$ terms to obtain an estimate of the water–graphene interaction energy. This gives a net interaction energy of -2.85 kcal mol^{-1} for water–graphene assuming our standard geometry. We estimate that in the limit of an infinite basis set and with geometry reoptimization, a value of -3.0 ± 0.15 kcal mol^{-1} would result for the binding of a water molecule to a graphene sheet.

We also examined several procedures for correcting DFT calculations for dispersion. Of the methods examined, the BLYP/DCACP approach gives interaction energies that are in the best agreement with the results from the DFT–SAPT calculations. In an earlier work, it was shown that the BLYP functional overestimates exchange-repulsion contributions,[123] leading us to conclude that the pseudopotential terms added in the DCACP procedure must also be correcting the exchange-repulsion contributions.

Although the focus of this work has been on the interaction of a water molecule with a series of acenes, the strategy employed is applicable for characterizing the interaction potentials of other species with acenes and for extrapolating to the graphene limit. Although there is a large number of theoretical papers addressing the interactions of various molecules with benzene, relatively little work using accurate electronic structure methods has been carried out on molecules other than water interacting with larger acenes.

38

3.6 ACKNOWLEDGEMENTS

4.0 EVALUATION OF THEORETICAL APPROACHES FOR DESCRIBING THE INTERACTION OF WATER WITH LINEAR ACENES

4.1 ABSTRACT

The interaction of a water monomer with a series of linear acenes (benzene, anthracene, pentacene, heptacene, and nonacene) is investigated using a wide range of electronic structure methods, including several "dispersion"-corrected density functional theory (DFT) methods, several variants of the random-phase approximation (RPA), DFT based symmetry-adapted perturbation theory with density fitting (DF–DFT–SAPT), with MP2, and coupled-cluster methods. The DF–DFT–SAPT calculations are used to monitor the evolution of the electrostatics, exchange-repulsion, induction and dispersion contributions to the interaction energies with increasing acene size, and also provide the benchmark data against which the other methods are assessed.

---

[*]G. R. J. contributed the wavefunction, DF–DFT–SAPT, DFT+D2, DFT+D3, and DFT/CC numerical data. O. K contributed the vdW–TS, DCACP, and RPA numerical data. W. A. S. contributed the vdW–DF1 and vdW–DF2 numerical data. G. R. J., O. K., and K. D. J. contributed to the discussion. W. A. S. also gave useful suggestions to the manuscript.

4.2 INTRODUCTION

Graphene and graphite are prototypical hydrophobic systems.[151] Interest in water interacting with graphitic systems has also been motivated by the discovery that water can fill carbon nanotubes.[14] One of the challenges in modeling such systems is that experimental data for characterizing classical force fields are lacking. Even the most basic quantity for testing force fields, the binding energy of a single water molecule to a graphene or graphite surface, is not known experimentally. Several studies have appeared using electronic structure calculations to help fill this void.[1,47,48,70,112,113,136,137,150,152–154] However, this is a very challenging problem since most DFT methods rely on either local or semi-local density functionals that fail to appropriately describe long-range dispersion interactions, which are the dominant attractive term in the interaction energies between a water molecule and graphene (or the acenes often used to model graphene).

In a recent study we applied the DF–DFT–SAPT procedure[72] to a water molecule interacting with a series of "circular" acenes (benzene, coronene, hexabenzo[bc,ef,hi,kl,no,qr]coronene, and circumcoronene)[150]†. These results were used to extrapolate to the binding energy of a water molecule interacting with the graphene surface and also proved valuable as benchmarks for testing other more approximate methods. Water–circumcoronene is essentially the limit of the size system that can be currently be studied using the DF–DFT–SAPT method together with sufficiently flexible basis sets to give nearly converged interaction energies. In the present study we consider a water molecule interacting with a series of "linear" acenes, specifically, benzene, anthracene, pentacene, heptacene, and nonacene, which allows us to explore longer-range interactions than in the water–circumcoronene case and also explore in more detail the applicability of various theoretical methods with decreasing HOMO/LUMO gap of the acenes. The theoretical methods considered include DF–DFT–SAPT, several methods for correcting density functional theory for dispersion, including the DFT–D2 and DFT–D3 schemes of Grimme and co-workers,[115,155] vdW–TS scheme of Tkatchenko and Scheffler,[116] the van der Waals density functional (vdW–DF) functionals of Lundqvist, Langreth and co-workers,[156,157] and the dispersion-corrected atom-centered pseudopo-

---

†Chapter 3

tential (DCACP) method of Rothlisberger and co-workers.[118, 120] Due to computational costs, only a subset of these methods were applied to water–nonacene.

The results of these methods are compared to those from several wavefunction based methods, including second-order Möller–Plesset perturbation theory (MP2),[158] coupled-cluster with singles, doubles and perturbative triples [CCSD(T)],[95, 159, 160] spin-component-scaled MP2 (SCS–MP2),[127] "coupled" MP2 (MP2C),[130] and several variants of the random phase approximation (RPA).[5–7] For comparative purposes, we also report interaction energies calculated using the recently introduced DFT/CC method,[112, 161] which combines DFT interaction energies with atom-atom corrections based on coupled-cluster calculations on water–benzene.

4.3   THEORETICAL METHODS

The base DFT calculations for the DFT–D2 and DFT–D3 procedures and the CCSD(T), various MP2, and DFT–SAPT calculations were performed with the MOLPRO[73] *ab initio* package (version 2009.1). The DFT/CC corrections were calculated using a locally modified version of MOLPRO. The dispersion corrections for the DFT–D2 and DFT–D3 procedures[115, 155] were calculated using the DFT-D3 program[155] of Grimme and co-workers. The DCACP calculations were performed with the CPMD[133] code (version 3.11.1). The vdW–DF energies were computed non-self-consistently using an in-house implementation of the Román–Pérez and Soler[166] methodology and employing densities from plane-wave DFT calculations carried out using the VASP code.[162–165] The RPA and vdW–TS calculations, including the base DFT (or Hartree–Fock) calculations required for both methods, were carried out with the FHI-AIMS[134] program (version 010110). The calculations with MOLPRO used Gaussian-type orbital basis sets, those with FHI-AIMS employed numerical atom-centered basis sets,[147] and those with CPMD and VASP used plane-wave basis sets. Details about the basis sets used are provided in Sections 4.3.2–4.3.5.

42

(a) Anthracene ($C_{14}H_{10}$)

(b) Pentacene ($C_{22}H_{14}$)

(c) Heptacene ($C_{30}H_{18}$)

(d) Nonacene ($C_{38}H_{22}$)
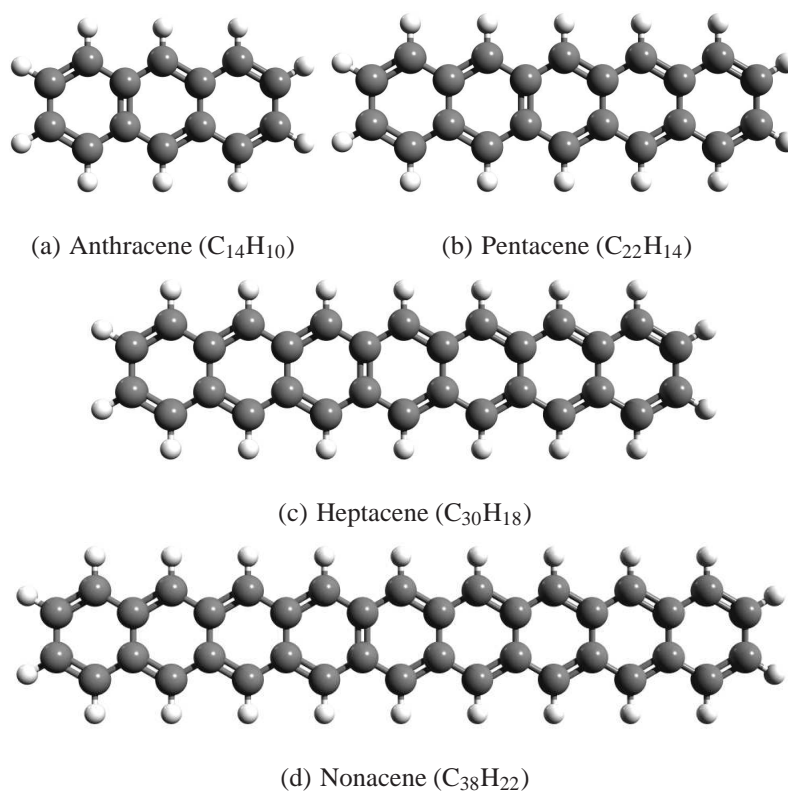
Figure 4.1: Acenes studied.
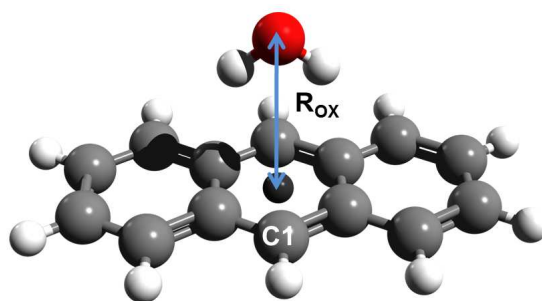
Figure 4.2: Placement of the water molecule relative to the acene, illustrated in the case of water–anthracene. The position of atom type C1 used in Figure 4.3 is labeled. R_{OX}, the distance between the oxygen atom and the center of the acene is taken to be 3.36 Å.
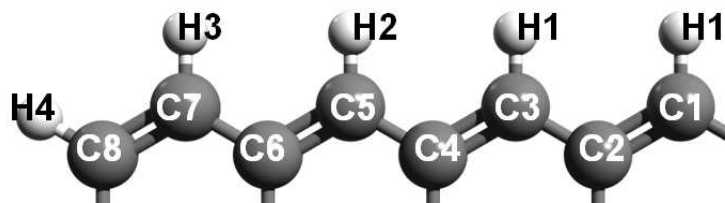
Figure 4.3: Labeling scheme of the carbon and hydrogen atoms. The C1 and H1 atoms are associated with the central ring as shown in Figure 4.2.

4.3.1 Geometries

For the acenes, the same geometrical parameters were employed as in our earlier study of a water molecule interacting with circular acenes,[150] *i.e.*, the CC and CH bond lengths were fixed at 1.42 Å and 1.09 Å, respectively, and the CCC and CCH bond angles were fixed at 120°. Obviously, the linear acenes in their equilibrium geometries have a range of CC bond lengths and CCC bond angles; the fixed values given above were used as it facilitates comparison with our results for the circular acenes. The experimental gas-phase geometry was used for the water monomer (OH bond length of 0.9572 Å and HOH angle of 104.52°).[92] The water monomer was positioned above the central ring so that the water C_2 rotation axis is perpendicular to the plane of the acene and the oxygen atom is directly above the acene center-of-mass at a distance of 3.36 Å (obtained from our earlier optimization of water–coronene). Figure 4.2 depicts the orientation of the water monomer relative to the acene, illustrated for the water–anthracene case. For water–anthracene, we also carried out a full geometry optimization at the MP2/aug-cc-pVDZ level to determine the sensitivity of the interaction energy to geometry relaxation. These calculations reveal that the net interaction energy is altered by less than 5% in going from our standard geometry to the fully relaxed geometry.

Table 4.1: Summary of methods and programs used in the current study.

Method	Scheme	Program
DFT–SAPT[72]	Dispersion energies calculated *via* the Casimir–Polder integral using TDDFT response functions	MOLPRO[73]
MP2C[130]	Replaces uncoupled Hartree–Fock dispersion terms in MP2 with coupled Kohn–Sham dispersion terms	MOLPRO
DFT–D2[115]	Adds damped atom-atom $C_6^{ij}R_{ij}^{-6}$ corrections to DFT energies	DFT-D3[155]
DFT–D3[155]	Adds damped atom-atom $C_6^{ij}R_{ij}^{-6} + C_8^{ij}R_{ij}^{-8}$ corrections to the DFT energies	DFT-D3
vdW–TS[116]	Adds damped atom-atom $C_6^{ij}R_{ij}^{-6}$ corrections, with C_6^{ij} coefficients determined from Hirshfeld partitioning of the DFT charge densities	FHI-AIMS[134]
DFT/CC[112, 161]	Applies distance-dependent atom-atom corrections from CCSD(T) calculations on model systems to standard DFT energies	MOLPRO[a]
DCACP[118–120]	Adds atom-centered pseudopotential terms to correct ft DFT energies	CPMD[133]
vdW–DF1,[156] vdW–DF2[157]	Incorporates dispersion interactions *via* an integral over a product of a non-local kernel $\Phi(\mathbf{r}, \mathbf{r}')$ and the densities $n(\mathbf{r})$ and $n(\mathbf{r}')$ at two points	In-house code using densities from VASP[162–165]
RPA	Calculates interaction energies using the random phase approximation	FHI--AIMS

[a] Denotes a locally modified version.

4.3.2 Wavefunction-based methods

The majority of the calculations using Gaussian-type orbitals were carried out using the aug-cc-pVTZ (AVTZ) basis set,[74, 167] although for a subset of systems and methods, the aug-cc-pVQZ (AVQZ) basis set[74, 167] and the explicitly correlated F12 methods[168–170] were used to investigate the convergence of the interaction energies with respect to the size of the basis set.

The various MP2 calculations were carried out with density fitting (DF) for both the Hartree–Fock and MP2 contributions (referred to as DF–HF and DF–MP2, respectively). The calculations involving the aug-cc-pVxZ (AVxZ, where x=T or Q) basis sets utilized the corresponding AVxZ JK- and MP2-fitting sets of Weigend and co-workers[88, 89] for the DF–HF and DF–MP2 calculations, respectively.

As has been noted numerous times in the literature, the MP2 method frequently overestimates dispersion interactions.[171] Cybulski and Lytle,[125] and Pitoňák and Heßelmann[130, 172] have suggested simple (and closely related) solutions to this problem. Here we explore the MP2C method of the latter authors where the uncoupled Hartree–Fock (UCHF) dispersion contribution (calculated *via* a sum-over-states expression) is replaced with the coupled Kohn–Sham (CKS) dispersion contribution from a time-dependent DFT (TDDFT) calculation (we include this method under wavefunction-based methods even though it uses the TDDFT procedure in evaluating the dispersion contribution). The 1s orbitals on the carbon and oxygen atoms were frozen in the evaluation of the response functions required for the dispersion calculations. The MP2C method generally gives interaction energies of near CCSD(T) quality, but with the computational cost scaling as $O(\mathcal{N}^4)$ (where $\mathcal{N}$ is the number of basis functions) rather than as $O(\mathcal{N}^7)$ as required for CCSD(T).[130] For water–benzene, water–anthracene, and water–pentacene, DF–MP2 and DF–MP2C calculations were also carried out with the explicitly-correlated F12 method,[168, 173] for the first two cases in conjunction with the AVTZ and AVQZ basis sets, and for water–pentacene, with the AVTZ basis set only.

CCSD calculations were carried out for water–benzene, water–anthracene and water–pentacene. CCSD(T) calculations, which include triple excitations in a non-iterative manner, were carried out for water–benzene and water–anthracene. To reduce the computational cost, the water–

pentacene CCSD calculations were performed with the truncated AVTZ basis set described in Reference 150[‡] (and hereafter referred to as Tr-AVTZ). We then estimated the full CCSD/AVTZ interaction energy for water–pentacene *via*

$$E_{int}^{CCSD/AVTZ} = E_{int}^{CCSD/Tr-AVTZ} + \left(E_{int}^{MP2/AVTZ} - E_{int}^{MP2/Tr-AVTZ} \right). \qquad (4.1)$$

In addition for water–benzene and water–anthracene, CCSD and CCSD(T) calculations were carried using the F12 method[169, 170] and the cc-pVTZ-F12 (VTZ-F12) basis set.[174]

Interaction energies were also calculated using the spin-component scaled MP2 (SCS–MP2) of Grimme,[127] in which the antiparallel and parallel spin correlation terms are scaled by a numerical factors of $\frac{6}{5}$ and $\frac{1}{3}$, respectively. The choice of the antiparallel scaling parameter was motivated by the fact that the MP2 methods typically underestimates correlation in two-electron systems by about 20%; the parallel scaling parameter was obtained empirically by fitting to high-level QCISD(T)[175] values of the reaction energies for a set of 51 reactions.[127]

All reported wavefunction-based interaction energies include the Boys–Bernardi counterpoise correction,[63] with the monomer energies being calculated in the full dimer-centered basis set.

4.3.3 DF–DFT–SAPT

The DF–DFT–SAPT method makes use of DFT orbitals in evaluating the electrostatics and first-order exchange-repulsion corrections to the interaction energy,[2] with the induction and dispersion contributions (along with their exchange counterparts) calculated from response functions.[3, 4] In the absence of CCSD(T) results for the larger acenes, the DF–DFT–SAPT[72] results are used as benchmarks for evaluating the performance of other methods. Tekin and Jansen[139] have shown that for systems dominated by CH-π and π-π interactions, the DF–DFT–SAPT/AVTZ method generally reproduces complete basis set limit CCSD(T) interaction energies to within 0.05 kcal mol^{-1}. Similar accuracy is expected in applying this approach to the water–acene systems. Indeed, for water–benzene the interaction energy calculated using the DF–DFT–SAPT/AVTZ method agrees to within 0.03 kcal mol^{-1} of the CCSD(T)-F12/VTZ-F12 result (although, as discussed below, this

---

[‡]Chapter 3

47

excellent agreement is due to a partial cancelation of errors in the DF–DFT–SAPT calculations). The DF–DFT–SAPT, like the DF–MP2C procedure described above, scales as $\mathrm{O}(\mathcal{N}^4)$.[72]

The LPBE0AC functional[72] was used for the DF–DFT–SAPT calculations. For the asymptotic correction inherent in LPBE0AC, the experimental vertical ionization potentials (IP) from the NIST Chemistry Webbook[82] were used when available. As the experimental IPs for heptacene and nonacene were not available, these quantities were estimated using the Hartree–Fock Koopmans' Theorem (KT)[176] modified *via*

$$\mathrm{IP_X} = \mathrm{IP_X^{KT}} + \left(\mathrm{IP_{Pentacene}^{Experimental}} - \mathrm{IP_{Pentacene}^{KT}} \right), \tag{4.2}$$

where X is either heptacene or nonacene. This results in 0.92 eV correction to the KT ionization energies. Although this approach of estimating the IP could lead to errors of a few tenths of an eV, these errors do not significantly impact the resulting water–acene interaction energies. For example, a change of 0.1 eV in the IP of benzene results in a 0.01 kcal mol^{-1} change in the interaction energy of water–benzene. For the density fitting, the cc-pV(x+1)Z JK-fitting set of Weigend[88] was employed for all non-dispersion terms, and the AVxZ MP2-fitting set of Weigend and co-workers[89] was used for the dispersion contributions.

We were unable to successfully complete the calculation of the dispersion energy of water–nonacene using the DF–DFT–SAPT procedure. However the DF–MP2C procedure uses a closely related scheme for evaluating the dispersion energy and gives the same dispersion contributions for water–heptacene and water–nonacene, and moreover gives a dispersion contribution for water–heptacene within 0.1 kcal mol^{-1} of the DF–DFT–SAPT result when used with the LPBE0AC functional.

4.3.4 DFT-based methods

Among the dispersion-corrected DFT methods, the DFT–D2 scheme,[115] which involves the addition of damped atom-atom $\mathrm{C_6^{ij}R_{ij}^{-6}}$ correction terms to the DFT intermolecular energies, is the simplest scheme. A drawback to the DFT–D2 scheme is the lack of sensitivity of the $\mathrm{C_6^{ij}}$ coefficients to the chemical environment. This is partially addressed in the DFT–D3[155] method which

introduces dispersion coefficients that depend on the coordination number of the atoms involved and also includes damped $C_8^{ij}R_{ij}^{-8}$ contributions.[155] In the present study, the DFT–D2 and DFT–D3 schemes are used with the PBE,[142] revPBE,[177] and BLYP[143,144] density functionals together with the AVTZ basis set. The resulting interaction energies are corrected for BSSE using the counterpoise procedure.

The vdW–TS method[116] also applies damped atom-atom $C_6^{ij}R_{ij}^{-6}$ corrections to DFT energies, but it differs from DFT–D2 in that the C_6^{ij} coefficients are adjusted using effective atomic volumes obtained from Hirshfeld partitioning[146] of the charge densities. The vdW–TS calculations were performed with tier 3 and tier 4 numerical atom-centered basis sets[147] for hydrogen and carbon/oxygen, respectively. These basis sets have been designed for use in FHI-AIMS. The tier 3 basis set provides a $5s3p2d1f$ description of the hydrogen atoms, and the tier 4 basis set provides a $6s5p4d3f2g$ description of the carbon/oxygen atoms. The largest vdW–TS calculation, that on water–nonacene, employed 3864 basis functions.

The DFT/CC method of Rubeš and co-workers[112,161] adds to the DFT energy atom-atom correction terms parameterized to differences between CCSD(T)/CBS and PBE interaction energies for water–benzene. The DFT/CC method has been successfully used to categorize both solid[178] and molecule–surface interactions.[112,152,161] The reference energies used for the DFT/CC calculations were taken from References 112 and 178. The base PBE energies for DFT/CC method were calculated with the AVTZ basis set and were corrected for BSSE using the counterpoise procedure.

The dispersion-corrected atom-centered potential (DCACP) method of Roethlisberger and co-workers[118,120] modifies Göedecker–Teter–Hutter (GTH) pseudopotentials[140] by adding an f channel to correct for deficiencies in the density functional employed. The calculations with the DCACPs were carried out with a plane-wave basis set and using periodic boundary conditions. This approach was applied to acenes through heptacene and all calculations employed a planewave cutoff of 3401 eV and a box size of $30 \times 16 \times 16$ Å. The high cut-off energy was necessitated by use of the GTH pseudopotentials.

The vdW–DF1[156] and vdW–DF2[157] GGA functionals of Langreth and co-workers represent

the exchange-correlation energy functional as

$$E_{XC}[\rho] = E_X + E_C^{LDA} + E_C^{non-local}, \tag{4.3}$$

where the non-local correlation functional $\left(E_C^{nonlocal}\right)$ involves integration over the electronic densities (ρ) at two points ($\mathbf{r}$ and $\mathbf{r}'$) with a non-local kernel ($\Phi(\mathbf{r},\mathbf{r}')$),

$$E_C^{non-local} = \frac{1}{2} \int \int \rho(\mathbf{r})\Phi(\mathbf{r},\mathbf{r}')\rho(\mathbf{r}') \, d\mathbf{r} \, d\mathbf{r}'. \tag{4.4}$$

As recommended by the developers, for vdW–DF1 and vdW–DF2, the revPBE and modified PW86[179] (called PW86R[180]) exchange density functionals were used, respectively. The vdW–DF calculations were performed with charge densities from VASP[162–165] calculations obtained using VASP-native pseudopotentials together with a planewave cutoff of 800 eV and a supercell with ~ 10 Å of vacuum in all directions.

4.3.5   RPA-based methods

The random phase approximation (RPA) method is a many-body method which treats a subset of correlation effects (described by ring diagrams) to all orders.[181] There are multiple variants of the RPA method, and in this work three different RPA schemes, denoted RPA, RPA+2OX, and RPA/(HF+PBE), are considered. In each case the energy includes exact exchange contributions computed using the Hartree–Fock expression using either the Hartree–Fock or Kohn–Sham orbitals. The RPA plus second-order exchange (RPA+2OX) approach[5,6] adds a second-order exchange energy correction to the total RPA energy. In the RPA/(HF+PBE) scheme, suggested to us by Ren and Blum,[7] the RPA/PBE correlation correction is added to the Hartree–Fock energy. For the RPA and RPA+2OX schemes the interaction energies obtained using orbitals from HF, PBE, revPBE and BLYP calculations are reported. The RPA calculations were performed with a modified tier 3 numerical atom-centered basis set with the highest angular momentum basis functions from the full tier 3 basis set (*i.e.* the f functions from hydrogen, the g functions from oxygen, and the f and g functions from carbon) being deleted. In addition, the core $1s$ orbitals were frozen.

4.4 RESULTS AND DISCUSSION

Before turning to the discussion on the interaction energies obtained using the various theoretical methods, it is instructional to examine the trends in the energy gaps between the highest occupied molecular orbital (HOMO) and lowest unoccupied molecular orbital (LUMO) as a function of the length of the acene. The orbital energies have been calculated at the Hartree–Fock level using the 6-31G* basis set.[182, 183] This basis was chosen to avoid the low-lying unfilled orbitals corresponding to approximate continuum functions[184] that would be present with a basis set including diffuse functions. The resulting HOMO–LUMO gaps are 12.7, 7.9, 5.8, 4.7, and 4.1 eV along the sequence benzene, anthracene, pentacene, heptacene, and nonacene. This leads one to anticipate growing multiconfigurational character in the wavefunctions with increasing length of the acene. It has even been suggested that the linear acenes larger than pentacene have triplet ground states,[185] although more recent theoretical work indicates that they have singlet ground states[186] as assumed in our study. Reference 186 also demonstrates the expected increase in the multiconfigurational character with increasing length of the acene, raising the possibility that some theoretical methods may not properly describe the water–acene interaction energies for the larger acenes.

4.4.1 DF–DFT–SAPT Results

From Table 4.2, which summarizes the results of the DF–DFT–SAPT calculations, it is seen that the net interaction energy between the water molecule and the acene is nearly independent of the size of the acene. The electrostatic and exchange-repulsion contributions both experience a sizable reduction in magnitude in going from benzene to anthracene, with these changes being of opposite sign and approximately compensating for one another. The exchange-repulsion contribution is essentially constant from anthracene to nonacene, whereas the electrostatic interaction energy continues to decrease in magnitude along the sequence of acenes, with the change in the electrostatic energy in going from water–heptacene to water–nonacene being only 0.03 kcal mol^{-1}. The induction energy, discussed in more detail below, is nearly constant across the series of acenes

Table 4.2: Contributions to the DF–DFT–SAPT interaction energies (kcal mol^{-1}) of the water–acene dimers.

Term	Benzene	Anthracene	Pentacene	Heptacene	Nonacene
$E_{Elst}^{(1)}$	−2.82	−2.29	−2.07	−2.01	−1.98
$E_{Exch}^{(1)}$	3.25	2.85	2.84	2.85	2.85
$E_{Ind}^{(2)}$	−1.28	−1.22	−1.24	−1.26	−1.28
$E_{ExInd}^{(2)}$	0.83	0.76	0.76	0.77	0.77
δ_{HF}	−0.26	−0.21	−0.21	−0.20	−0.21
Net Induction	−0.71	−0.67	−0.69	−0.69	−0.72
$E_{Disp}^{(2)}$	−3.38	−3.66	−3.72	−3.79	(−3.78)[a]
$E_{ExDisp}^{(2)}$	0.46	0.43	0.43	0.43	(0.43)[b]
Net Dispersion	−2.92	−3.23	−3.29	−3.36	(−3.36)
DF–DFT–SAPT	−3.20	−3.34	−3.21	−3.21	−3.21

[a] As discussed in Section 4.3.3, the DF–DFT–SAPT calculation of the dispersion energy of water–nonacene was unsuccessful. The dispersion energy for water–nonacene was taken to be the same as that for water–heptacene as DF–MP2C calculations give the same dispersion energy for these two systems.
[b] The exchange-dispersion energy of water–nonacene has been assumed to be the same as that for water–heptacene.

Table 4.3: Electrostatic interaction energies (kcal mol^{-1}) between DPP2[187] atomic charges on water and the atomic multipoles of the acenes.

Term	Benzene	Anthracene	Pentacene	Heptacene
Charge-Charge	-1.31	-2.36	-2.34	-2.26
Charge-Dipole	1.79	3.33	3.27	3.15
Charge-Quadrupole	-2.27	-2.72	-2.55	-2.44
Charge-Octopole	-0.03	0.17	0.26	0.28
Charge-Hexadecapole	-0.05	-0.09	-0.11	-0.11
Total multipole	-1.87	-1.67	-1.47	-1.39
Charge-penetration	-0.95	-0.62	-0.60	-0.62
DF–DFT–SAPT	-2.82	-2.29	-2.07	-2.01
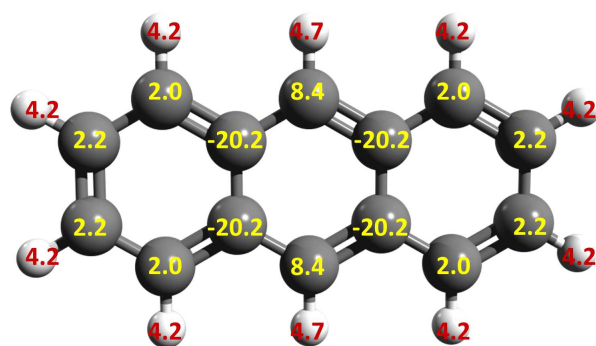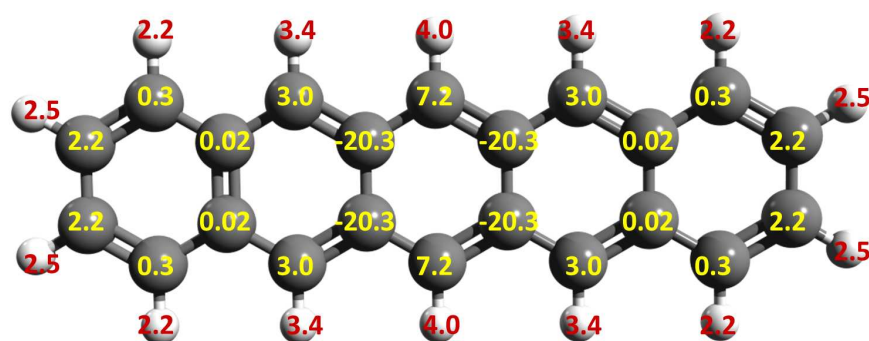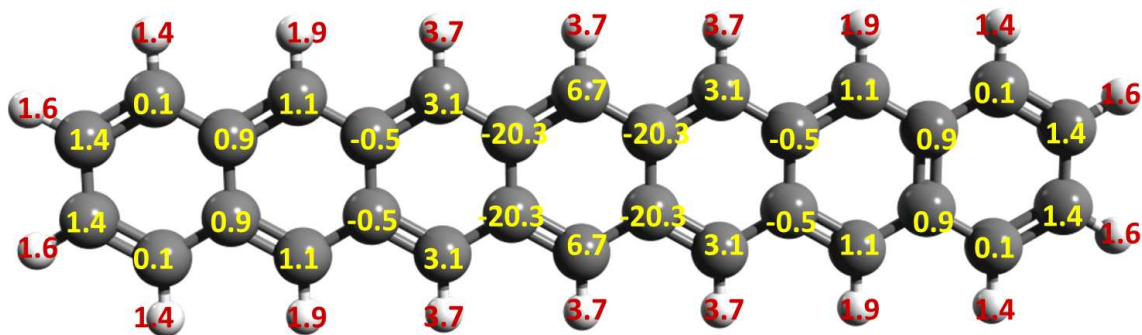
Figure 4.4: Differences between Mulliken atomic charges (in millielectrons) of the acenes in the presence and absence of the water monomer. Results are reported for (a) anthracene, (b) pentacene, and (c) heptacene.

while the dispersion energy grows in magnitude from water–benzene to water–heptacene, and being essentially the same for water–heptacene and water–nonacene. The fall off in the electrostatic contribution is approximately compensated by the growing dispersion contribution with increasing length of the acene.

For benzene, anthracene, pentacene, and heptacene, the atomic multipoles through hexadecapoles were calculated using a distributed multipole analysis (DMA),[100–103] performed with the GDMA[103] program and using MP2/cc-pVDZ charge densities from Gaussian03[104] calculations. The resulting atomic multipoles (through the quadrupoles) are reported in the supporting information (SI)[§]. The analysis was not done for nonacene as the atomic multipole moments for the carbon atoms of the central ring are well converged by heptacene. The charges, dipole moments, and quadrupole moments associated with the carbon atoms of the central ring undergo appreciable changes in going from benzene to anthracene, but they are essentially unchanged along the anthracene–pentacene–heptacene sequence. The electrostatic interaction between water and the acene can be divided into contributions from the permanent atomic moments and charge-penetration which is the result of the charge density of one monomer "penetrating" the charge density of the other monomer.[93] The charge-penetration contributions were estimated by subtracting from the SAPT electrostatic interaction energies the electrostatic interaction energies calculated using the distributed moments through the hexadecapoles of the acenes and the point charges of the DPP2 model[187] for the water monomer. As seen from Table 4.3, this procedure gives a charge-penetration energy of -0.95 kcal mol^{-1} for water–benzene and about -0.6 kcal mol^{-1} for a water monomer interacting with the larger acenes. These results are essentially unchanged upon use of moments for the acenes obtained using the larger cc-pVTZ basis set[167] or when employing higher atomic multipoles on the water monomer.

The net induction energy is defined as $E_{ind}^{(2)} + E_{ex-ind}^{(2)} + \delta(HF)$, where the $\delta(HF)$ accounts in an approximate manner for the higher-order induction and exchange-induction contributions. The net induction energies are about -0.7 kcal mol^{-1} for each of the water–acene systems. At first sight the near constancy of the induction energy is somewhat surprising. The net induction en-

---

[§]In the original publication, the linear acene DMA results were given in the supporting information. This table has been included here as Table 4.8.

ergies can be decomposed into a sum of three contributions, atomic polarization, charge-flow polarization, and intermonomer charge-transfer.[93] The nature of the charge-flow polarization is illustrated in Figure 4.4 where we report the change in the atomic charges of anthracene, pentacene, and heptacene caused by the presence of the water molecule. These results were obtained from Mulliken population analysis[188] of the Hartree–Fock/cc-pVDZ wavefunctions of the water–acene complexes. As expected, the electric field from the water molecule causes flow of electron density from remote carbon atoms to the central ring. Using the atomic charges from the Mulliken analysis, we estimate that charge-flow polarization and intermonomer charge-transfer combined contribute roughly half of the induction energy for the water–acene systems, and that these contributions are relatively independent of the size of the acene. Thus, the insensitivity of the induction energy with the size of the acene can be understood in terms of the relatively small contributions of atomic polarization in these complexes.

The dispersion contribution grows by 0.31 kcal mol^{-1} in magnitude in going from water–benzene to water–anthracene, by 0.06 kcal mol^{-1} in going from water–anthracene to water–pentacene, and by another 0.07 kcal mol^{-1} in going to water–heptacene. For water–anthracene the dispersion contribution to the interaction energy is nearly identical to that for water–heptacene. These changes are small compared to the net dispersion contributions (defined as $E^{(2)}_{\text{disp}} + E^{(2)}_{\text{ex-disp}}$).

4.4.2 Basis set sensitivity of the interaction energies

Before considering in detail the interaction energies obtained with the other methods, it is useful to first consider the sensitivity of the results to the basis sets employed. In Table 4.4, we report for water–benzene and water–anthracene interaction energies obtained using the DF–MP2, DF–MP2C and DF–DFT–SAPT methods, in each case with both the AVTZ and AVQZ basis sets. In addition, for the DF–MP2 and DF–MP2C methods, F12 results are included. The DF–DFT–SAPT interaction energies increase by 0.06–0.10 kcal mol^{-1} in magnitude in going from the AVTZ to the AVQZ basis set, whereas the corresponding increase in the DF–MP2 and DF–MP2C interaction energies is 0.09–0.15 kcal mol^{-1}. Moreover, with the latter two methods, the interaction energy increases by another 0.05–0.08 kcal mol^{-1} in magnitude in going from the AVQZ basis set to the

Table 4.4: Influence of the basis set on the water–benzene and water–anthracene interaction energies (kcal mol^{-1}).

Theoretical Method	AVTZ	AVQZ
Water–benzene		
DF–MP2	-3.28	-3.39
DF–MP2–F12	-3.47	-3.47
DF–MP2C	-3.06	-3.20
DF–MP2C–F12	-3.25	-3.27
DF–DFT–SAPT	-3.20	-3.30
Water–anthracene		
DF–MP2	-3.66	-3.77
DF–MP2–F12	-3.85	-3.84
DF–MP2C	-3.17	-3.29
DF–MP2C–F12	-3.35	-3.37
DF–DFT–SAPT	-3.34	-3.40

F12/AVTZ procedure. The changes in the DF–MP2 and DF–MP2C interaction energies in going from the F12/AVTZ to the F12/AVQZ approaches are 0.02 kcal mol^{-1} or less. These results justify the use of the DF–DFT–SAPT/AVTZ approach to provide the benchmark results for assessing other theoretical methods.

Thus for the MP2 and MP2C methods, the CBS-limit interaction energies are about 0.2 kcal mol^{-1} larger in magnitude than the results obtained using the AVTZ basis set. A similar sensitivity to the basis set is found for the CCSD(T) interaction energy of water–benzene as seen from Table 4.5. Moreover, the DF–MP2C and CCSD(T) procedures give nearly identical interaction energies (we revisit the DF–MP2C interaction energies in the next section). It is also found that the DF–DFT–SAPT calculations with the AVTZ basis set give interaction energies within a few hundredths of a kcal mol^{-1} of the MP2C and CCSD(T) results obtained using the AVQZ/F12 method.

Although the interaction energies calculated with the DF–DFT–SAPT method are less sensitive to the basis set than those calculated with the DF–MP2C or CCSD(T) methods, it is clear that in the CBS-limit the DF–DFT–SAPT interaction energies would be about 0.1 kcal mol^{-1} larger in magnitude than those obtained using the AVTZ basis set, resulting in slight overbinding of the water–acene complexes.

4.4.3 Wavefunction-based results

Although the Hartree–Fock approximation predicts a monotonic fall off in the magnitude of the interaction energy with increasing size of the acene, this is not the case for the DF–DFT–SAPT method, the various DF–MP2 methods, or for the CCSD method. In each of these methods, the interaction energy increases in magnitude in going from water–benzene to water–anthracene and then drops off for the larger acenes. The origin of this behavior is clear from analysis of the results in Table 4.2 and Table S1¶. Namely, the carbon atoms of benzene carry a greater negative charge than do the carbon atoms of the central ring of the large acenes, causing the exchange-repulsion energy to be greater in the case of water–benzene. This is the factor primarily responsible for the smaller in magnitude interaction energy in water–benzene than in water–anthracene.

¶Table 4.8

58

Table 4.5: Net interaction energies (kcal mol^{-1}) for the water–acene systems as described by wave-function based methods.

Method	Benzene	Anthracene	Pentacene	Heptacene	Nonacene
DF–DFT–SAPT	−3.20	−3.34	−3.21	−3.21	−3.21
DF–HF	−0.74	−0.48	−0.29	−0.23	−0.21
DF–MP2	−3.28	−3.66	−3.63	−3.62	−3.61
DF–MP2–F12	−3.47	−3.85	−3.80		
DF–SCS–MP2	−2.61	−2.87	−2.82	−2.80	−2.79
DF–MP2C	−3.06	−3.17	−3.06	−3.02	−3.01
DF–MP2C–F12	−3.25	−3.35	−3.23		
CCSD	−2.63	−2.77	−2.69		
CCSD–F12a	−2.80	−2.89			
CCSD–F12b	−2.76	−2.85			
CCSD(T)	−3.05	−3.26			
CCSD(T)–F12a	−3.21	−3.37			
CCSD(T)–F12b	−3.17	−3.33			

The interaction energies for the wavefunction based methods are presented in Table 4.5. For water–benzene, water–anthracene, and water–pentacene the DF–MP2–F12 calculations overestimate the binding energies by 0.27–0.59 kcal mol^{-1} in magnitude, with the discrepancy growing with increasing size of the acene. On the other hand, the DF–SCS–MP2 method underestimates the magnitude of the total interaction energies by 0.39 to 0.61 kcal mol^{-1}. Comparison of the CCSD and CCSD(T) results for water–benzene and water–anthracene shows that the inclusion of triple excitations increases the interaction energies in magnitude by 0.4–0.5 kcal mol^{-1}. Thus it appears that the underestimation of the magnitude of the interaction energies with the DF–SCS–MP2 method is due to the neglect of triple excitations.

The close agreement of the DF–MP2C, DF–DFT–SAPT and CCSD(T) interaction energies for the water–acene systems warrants further discussion. A detailed analysis of wavefunction-based SAPT [SAPT(HF)][12, 13] calculations on water–benzene reveals that intramonomer correlation a -0.1 kcal mol^{-1} contribution to the dispersion portion of the interaction energy and a positive contribution to both the exchange and electrostatic contributions to the interaction energy, with the net change in the exchange plus electrostatics interaction being 0.65 kcal mol^{-1}. On the other hand, in the DF–MP2C approach there is a change of $+0.2$ kcal mol^{-1} in the dispersion energy upon replacing the uncoupled Hartree–Fock dispersion contribution with the coupled Kohn–Sham value.

Thus the good agreement between interaction energies obtained with the DF–MP2C method and DF–DFT–SAPT approaches appears to be is due in part to a cancelation of errors in the former. A closer examination of the SAPT(HF) results for intramonomer correlation on the dispersion energy reveals that there are both large positive and negative corrections. It appears that although the DF–MP2C method does not recover the 0.65 kcal mol^{-1} contribution of correlation effects to the exchange and electrostatic energies, this is compensated by the failure to recover the -0.68 kcal mol^{-1} change in the dispersion energy due to intramonomer triple excitations.

Table 4.6: Net interaction energies (kcal mol^{-1}) for the water–acene systems as described by DFT-based methods.

Method	Benzene	Anthracene	Pentacene	Heptacene	Nonacene[a]	MAE[b]
DF–DFT–SAPT	−3.20	−3.34	−3.21	−3.21	−3.21	
PBE	−1.87	−1.50	−1.36	−1.32	−1.31	1.76
PBE+D2	−3.66	−3.69	−3.60	−3.57	−3.56	0.38
PBE+D3	−3.60	−3.75	−3.67	−3.65	−3.64	0.43
PBE+D3/TZ[c]	−3.41	−3.54	−3.45	−3.43	−3.42	0.21
revPBE	−0.23	0.14	0.29	0.32	0.33	3.41
revPBE+D2	−3.21	−3.50	−3.44	−3.42	−3.42	0.16
revPBE+D3	−3.50	−3.75	−3.68	−3.66	−3.65	0.41
revPBE+D3/TZ[c]	−3.41	−3.66	−3.58	−3.56	−3.55	0.31
BLYP	−0.27	0.21	0.35	0.37	0.38	3.44
BLYP+D2	−3.13	−3.29	−3.23	−3.22	−3.22	0.03
BLYP+D3	−3.59	−3.83	−3.77	−3.75	−3.75	0.50
BLYP+D3/TZ[c]	−3.23	−3.47	−3.41	−3.39	−3.39	0.14
vdW–TS/PBE	−3.77	−4.01	−3.94	−3.92	−3.89	0.67
vdW–TS/BLYP	−2.50	−2.77	−2.68	−2.65	−2.64	0.59
DFT/CC	−3.23	−3.38	−3.31	−3.29	−3.29	0.06
DCACP/PBE	−2.70	−2.62	−2.48	−2.45		0.68
DCACP/BLYP	−3.08	−3.30	−3.25	−3.23		0.05
vdW–DF1	−2.89	−3.30	−3.38	−3.27		0.14
vdW–DF2	−3.21	−3.38	−3.29	−3.27		0.05

[a] Only a subset of methods were applied to nonacene to check for convergence with respect to system size in the interaction energies.
[b] Mean absolute error (MAE) relative to DF–DFT–SAPT. MAEs were calculated only for benzene through nonacene when water–nonacene interaction energies are available, else they were calculated for benzene through heptacene.
[c] D3/TZ denotes DFT–D3 parameters optimized with Ahlrichs' TZVPP basis set. See Reference 155 for more information.

4.4.4 DFT-based results

Table 4.6 reports interaction energies obtained using the PBE, revPBE, and BLYP density functionals with and without correcting for long-range dispersion. In considering these results, it should be kept in mind that while GGA functionals do not capture long-range dispersion interactions, they can describe short-range dispersion, and also that some dispersion-corrected DFT methods, such as DCACP and DFT–D actually correct for deficiencies in DFT other than the absence of long-range dispersion interactions.[189]

From Table 4.6 it can be seen that while the PBE functional recovers about half of the total interaction energies for the water–acene systems, the revPBE and BLYP functionals predict binding only in the water–benzene case. The failure to obtain bound complexes with the BLYP and revPBE functionals is due to their larger (compared to PBE) exchange-repulsion contributions.[123] Indeed this behavior of the revPBE functional was the motivation for the switch from revPBE in vdW–DF1 to PW86 in vdW–DF2.[157]

The DFT–D2 method does well at reproducing the DF–DFT–SAPT interaction energies with mean absolute errors (MAEs) of 0.39, 0.15 and 0.02 kcal mol^{-1} for PBE, revPBE, and BLYP, respectively. For all of the density functionals considered, the DFT–D3 approach overestimates the magnitude of the interaction energies by about 0.5 kcal mol^{-1}. This overestimation is partially reduced if one uses the DFT–D3 parametrization based on the TZVPP[190] basis set[155] (denoted as DFT–D3/TZ in Table 4.6).

The vdW–TS procedure based on the PBE functional overestimates the magnitude of the total interaction energies, with a MAE of 0.67 kcal mol^{-1}, while the vdW–TS procedure based on the BLYP functional considerably underestimates the magnitude of the interaction energies. Given the fact that the vdW–TS method employs dispersion corrections that depend on the chemical environments, it is surprising that it performs poorer than DFT–D2 for the water–acene systems.

The DFT/CC method gives interaction energies very close to the DF–DFT–SAPT results (MAE of 0.05 kcal mol^{-1}). The DCACP/BLYP approach also gives interaction energies in excellent agreement with the DF–DFT–SAPT results (MAE of 0.06 kcal mol^{-1}) while the DCACP/PBE approach, on the other hand, does not fair as well (MAE of 0.68 kcal mol^{-1}). Both the vdW–DF1

and vdW–DF2 functionals give interaction energies close to the DF–DFT–SAPT values, with the vdW–DF2 proving more successful at reproducing the trend in the interaction energies along the sequence of acenes obtained from the DF–DFT–SAPT calculations.

4.4.5   RPA-based results

As seen from Table 4.7, the RPA calculations using HF orbitals give interaction energies about 0.9 kcal mol^{-1} smaller than the DF–DFT–SAPT results. The errors are reduced to about 0.6 kcal mol^{-1} when using RPA based on DFT orbitals for each of the three functionals considered. The underestimation of the interaction energies is apparently a consequence of the limitations in the RPA method at describing short-range correlation effects (which are not recovered by a sum over ring diagrams only). Interestingly, Scuseria and co-workers have shown that the RPA method based on Hartree–Fock orbitals corresponds to an approximate coupled-cluster doubles approximation.[191] The present PBA/HF calculations on water–benzene, water–anthracene, and water–pentacene gives binding energies 0.25–0.38 kcal mol^{-1} smaller in magnitude than the corresponding CCD results (which, in turn, are nearly identical to the CCSD results in Table 4.5).

The RPA+2OX method does not correctly reproduce the trend in the interaction energies along the sequence of acenes. It appears that the small HOMO/LUMO gaps in the DFT calculations on the larger acenes result in non-physical second-order exchange corrections. There is a significant improvement in the interaction energies as calculated with the RPA/(HF+PBE) method, which gives interaction energies 0.2–0.3 kcal mol^{-1} smaller in magnitude than the DF–DFT–SAPT results, which in turn are expected to be about 0.1 kcal mol^{-1} smaller in magnitude than the exact interaction energies for the geometries employed. However, it is possible that the improved results obtained with this approach are fortuitous as it obviously does not address the problem of RPA not properly describing short-range correlation effects.

63

Table 4.7: Net interaction energies (kcal mol^{-1}) for the water–acene systems as described by RPA methods.

Method	Benzene	Anthracene	Pentacene	Heptacene	Nonacene[a]	MAE[b]
DF–DFT–SAPT	−3.20	−3.34	−3.21	−3.21	−3.21	
RPA/HF	−2.38	−2.42	−2.31	−2.27	−2.25	0.91
RPA/PBE	−2.60	−2.70	−2.62	−2.59		0.61
RPA/revPBE	−2.52	−2.69	−2.61	−2.59		0.64
RPA/BLYP	−2.54	−2.73	−2.66	−2.63		0.60
RPA+2OX/HF	−2.56	−2.53	−2.38	−2.37		0.78
RPA+2OX/PBE	−3.18	−2.91	−2.66	−2.25		0.49
RPA+2OX/revPBE	−3.15	−3.01	−2.76			0.28
RPA+2OX/BLYP	−3.19	−3.03	−2.78			0.25
RPA/HF+PBE	−2.90	−3.11	−3.05	−3.02		0.22

[a] Only a subset of methods were applied to nonacene to check for convergence with respect to system size in the interaction energies.
[b] Mean absolute error (MAE) relative to DF–DFT–SAPT. MAEs were calculated using results for benzene through nonacene when water–nonacene interaction energies are available, else they were calculated for benzene through heptacene.
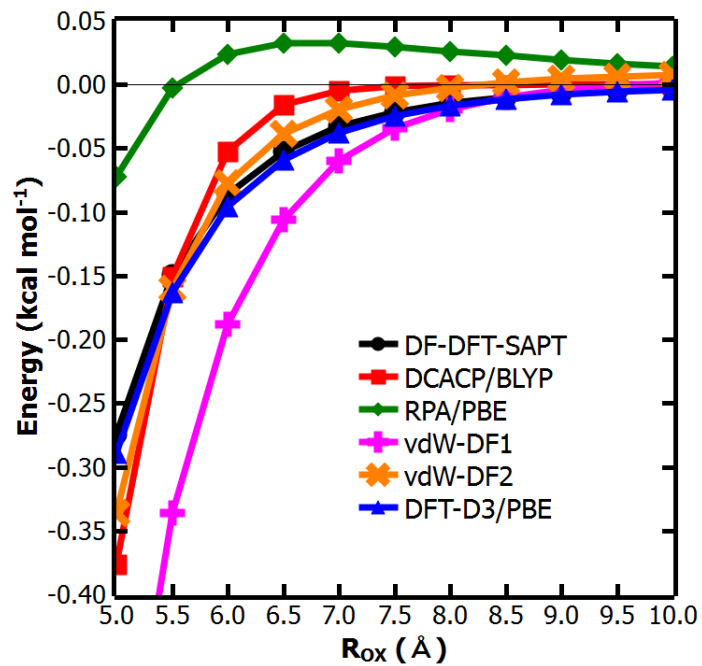
Figure 4.5: Long-range interactions of water–benzene calculated with various methods.

4.4.6 Long-range interactions

All of the results discussed above have been for a water–acene complex with the water–acene separation close to the potential energy minima (for the assumed orientation). Figure 4.5 plots the long-range interaction energies of various theoretical methods. For the DF–DFT–SAPT method the sum of the dispersion and exchange-dispersion contributions is plotted, and for the DCACP/BLYP the difference between the interaction energies with and without the DCACP correction is plotted. For the DFT–D3/PBE method the dispersion contribution is plotted. For the vdW–DF1, vdW–DF2, and RPA approaches, the differences of the correlation energies of the dimers and the correlation energies of the monomers are plotted (using only the non-local correlation terms in the case of the vdW–DF methods).

From Figure 4.5, it is seen that the DFT–D3/PBE curve closely reproduces the DF–DFT–SAPT dispersion curve, indicating that this method is properly describing the dispersion energy in the asymptotic region. Both the vdW–DF2 and DCACP/BLYP methods give dispersion contributions that fall off too rapidly for $R_{OX} \geq 5.5$ Å (as noted in Reference 192, the vdW–DF2 tends to underestimate the C_6 coefficients[192]). The vdW–DF1 curve, while being close to the SAPT curve for $R \gtrsim 8$ Å, is much more attractive than the DF–DFT–SAPT curve for $R_{OX} \leq 7.5$ Å.

The long-range interaction energy from the RPA/PBE calculations is repulsive from $R_{OX} = 5.5$ to 10 Å (the longest distance considered). This is due to the fact that the correlation correction in the RPA method also describes the intramonomer correlation, which alters the electrostatic interaction between the water monomer and the benzene molecule.

4.5   CONCLUSIONS

In the current study we examined the applicability of a large number of theoretical methods for describing a water molecule interacting with a series of linear acenes. The DF–DFT–SAPT calculations, which provide the benchmark results against which the other methods are compared, give interaction energies of water–benzene, water–anthracene, water–pentacene, and water–heptacene,

ranging from -3.20 to -3.24 kcal mol^{-1}. This small spread in interaction energies is largely due to the fact that the decreasing magnitude of the electrostatic interaction energy with increasing size of the acene is partially compensated by the growing (in magnitude) dispersion contribution. The DF–MP2C–F12/AVTZ approach, gives interaction energies in excellent agreement with the DF–DFT–SAPT results, although this good agreement appears to be due, in part, to a cancelation of errors in the DF–MP2C method.

Four of the DFT-corrected methods considered — BLYP–D2, DCACP/BLYP, DFT/CC and vdW–DF2 — are found to give interaction energies for the water–acene systems very close to the DF–DFT–SAPT results. The revPBE–D2, BLYP–D3/TZ, vdW–DF1, and PBE–D3/TZ approaches also are reasonably successful at predicting the interaction energies at our standard geometries. However these successes do not necessarily carry over to other geometries. In particular, as seen in Figure 4.5, both the DCACP and vdW–DF2 methods underestimate long-range dispersion interactions in magnitude.

Even though the HOMO/LUMO gap decreases with increasing size of the acene, there is no indication that any of the methods considered are encountering problems in the calculation of the water–acene interaction energy even for acenes as large as nonacene.

4.6   ACKNOWLEDGEMENTS

4.7   SUPPORTING INFORMATION

Table 4.8: Multipole moments (in atomic units) for the carbon and hydrogen atoms of benzene (C_6H_6), anthracene ($C_{14}H_{10}$), pentacene ($C_{24}H_{12}$), and heptacene ($C_{30}H_{18}$).

Atom Type	q				$|\mu|$				Q_{20}				$|Q_{22c+22s}|$			
	C_6H_6	$C_{14}H_{10}$	$C_{24}H_{12}$	$C_{30}H_{18}$	C_6H_6	$C_{14}H_{10}$	$C_{24}H_{12}$	$C_{30}H_{18}$	C_6H_6	$C_{14}H_{10}$	$C_{24}H_{12}$	$C_{30}H_{18}$	C_6H_6	$C_{14}H_{10}$	$C_{24}H_{12}$	$C_{30}H_{18}$
C1	−0.09	−0.06	−0.06	−0.06	0.11	0.15	0.16	0.16	−1.14	−1.18	−1.18	−1.17	0.09	0.12	0.12	0.12
C2		−0.05	−0.05	−0.05		0.11	0.12	0.12		−1.22	−1.23	−1.23		0.11	0.13	0.13
C3		−0.07	−0.06	−0.06		0.16	0.16	0.16		−1.16	−1.18	−1.17		0.03	0.12	0.12
C4		−0.08	−0.05	−0.05		0.12	0.11	0.12		−1.14	−1.22	−1.22		0.09	0.12	0.13
C5			−0.07	−0.06			0.16	0.16			−1.16	−1.18			0.03	0.12
C6			−0.08	−0.05			0.12	0.11			−1.14	−1.22			0.09	0.12
C7				−0.07				0.16				−1.16				0.03
C8				−0.08				0.12				−1.14				0.09
H1	0.09	0.10	0.10	0.10	0.14	0.15	0.15	0.15	−0.13	−0.13	−0.13	−0.13	0.11	0.06	0.05	0.05
H2		0.10	0.10	0.10		0.14	0.15	0.15		−0.13	−0.13	−0.13		0.08	0.05	0.05
H3		0.09	0.10	0.10		0.14	0.14	0.14		−0.13	−0.13	−0.13		0.11	0.08	0.08
H4			0.09	0.09			0.14	0.14			−0.13	−0.13			0.11	0.11

APPENDIX A

APPENDIX INTRODUCTION

Appendices B and C include two papers to which I have contributed, but was not the first author. For the paper reproduced in Appendix B, I contributed the SAPT and the LMO–EDA interaction energies in addition to the discussion. For the paper reproduced in Appendix C, I contributed the two- and three-body SAPT interaction energies used in the fitting of the DPP2 water model.

<div align="center">**APPENDIX B**</div>

ASSESSMENT OF THE PERFORMANCE OF COMMON DENSITY FUNCTIONAL METHODS FOR DESCRIBING THE INTERACTION ENERGIES OF $(H_2O)_6$ CLUSTERS

B.1 ABSTRACT

Localized molecular orbital energy decomposition analysis (EDA) and symmetry-adapted perturbation theory (SAPT) calculations are used to analyze the 2- and 3-body interaction energies of four low-energy isomers of $(H_2O)_6$ in order to gain insight into the performance of several popular density functionals for describing the electrostatic, exchange-repulsion, induction, and short-range dispersion interactions between water molecules. The energy decomposition analysis indicate that all density functionals considered significantly overestimate the contributions of charge-transfer to the interaction energies. Moreover, in contrast to some studies that state that DFT does not include dispersion interactions, we adopt a broader definition and conclude that for $(H_2O)_6$ the short-range

---

dispersion interactions recovered in the DFT calculations account about 75% or more of the net (short- plus long-range) dispersion energies obtained from the SAPT calculations.

B.2 INTRODUCTION

Density functional theory (DFT)[193–195] has emerged as the method of choice for the calculation of the electronic structure of complex materials. However, there are many important systems for which the commonly used density functional methods are not adequate.[55, 196–198] Key among these are systems in which dispersion interactions are important, and this has generated considerable interest in the development of procedures for correcting DFT for long-range dispersion interactions.[114, 116, 122, 156, 199–205] In recent years, several simulations of liquid water using density functional methods have appeared.[206–210] Not surprisingly, this has generated debate about the role of dispersion interactions for various properties of water.[207, 211, 212]

In order to gain insight into the suitability of various density functional methods for characterizing water, several groups have studied the low-energy ring, cage, prism, and book forms of $(H_2O)_6$,[117, 201, 213–215] for which high-level *ab initio* calculations are feasible.[201, 216, 217] Although calculations with the Hartree–Fock (HF) and with generalized gradient (GGA) or hybrid density functionals predict the ring isomer to be the most stable,[201] MP2[218] and CCSD(T)[95] calculations predict it to be the least stable of these four isomers.[201, 216, 217] This has been attributed to the greater importance of dispersion interactions in the cage and prism isomers than in the more open book and ring isomers.[201, 213] Indeed, significant improvement in the relative energies of the four isomers is achieved upon inclusion of corrections for dispersion, either with damped atom-atom $C_6^{ij}R_{ij}^{-6}$ corrections[201] or by use of the vdW–DF approach of Langreth and co-workers.[122, 215]

In the present work, we use energy decomposition methods to assess the performance of several popular DFT functional methods for characterizing the interaction energies of four low-energy isomers of $(H_2O)_6$. For each cluster, the net interaction energies and their 2-, 3-, and higher-body contributions are calculated using five popular density functional methods as well as using

the Hartree–Fock, MP2, and CCSD(T) methods. In addition, the 2- and 3-body interaction energies are decomposed into electrostatic, exchange-repulsion, polarization, charge-transfer, and short-range dispersion contributions using symmetry-adapted perturbation theory (SAPT)[13] and localized molecular orbital energy decomposition analysis (LMO–EDA). Two different EDA procedures — the localized molecular orbital (LMO–EDA) method of Su and Li,[8] and the absolutely localized molecular orbital (ALMO–EDA) method of Head–Gordon and co-workers[9] — are used. The former provides estimates of the electrostatic, exchange-repulsion, induction, and short-range dispersion contributions recovered in the various DFT methods, and the latter allows for the separation of the induction contributions into polarization and charge-transfer components.

B.3 METHODOLOGY

The low-energy ring, cage, prism, and book isomers of $(H_2O)_6$ considered in this work are depicted in Figure B1. All results are reported for structures optimized at the MP2/aug-cc-pVDZ[10] level, under the constraint of rigid monomers. The exchange-correlation functionals examined, include the BLYP,[143, 144] PW91,[219] and PBE[142] generalized-gradient (GGA)-type functionals, as well as the B3LYP[144, 220–222] and PBE0[76] hybrid functionals, which contain a component of the exact exchange. The BLYP, PW91, and PBE functionals have all been employed in simulations of liquid water.[206–209]

The net interaction energy of a cluster with n monomers can be decomposed into one- through n-body interactions, where the one-body term is due to the geometrical distortion of the monomers upon incorporation into the cluster, and the 2- and 3-body interactions are defined by

$$\Delta E_2 = \sum_{i=1}^{N-1} \sum_{j=i+1}^{N} \left[E(i,j) - E(i) - E(j) \right] \qquad (B.1)$$

and

$$\Delta E_3 = \sum_{i=1}^{N-2} \sum_{j=i+1}^{N-1} \sum_{k=j+1}^{N} \left[E(i,j,k) - E(i,j) - E(i,k) - E(j,k) + E(i) + E(j) + E(k) \right] \qquad (B.2)$$
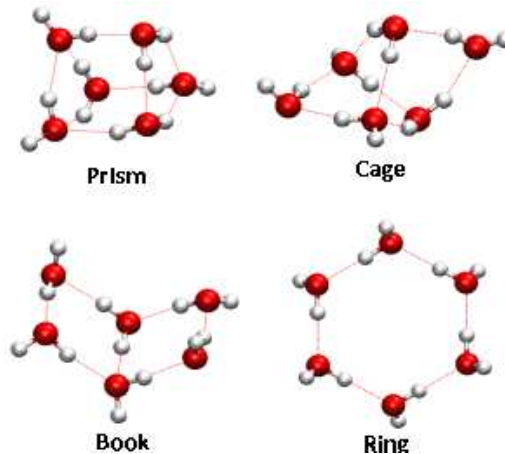
Figure B1: Structures of the four low-energy isomers of $(H_2O)_6$ studied in this paper.

where E(i), E(i,j), and E(i,j,k) are, respectively, the energies of the monomer i, dimer (i,j), and trimer (i,j,k) cut out of the full cluster.[223–226] Analogous expressions exist for the 4- and higher-body interaction energies. The n-body expansion is expected to converge rapidly for water clusters,[226–228] and as a result, we report 4+5+6-body interaction energies, obtained by subtracting the 2- and 3-body interaction energies from the net interaction energies, rather than individual 4-, 5-, and 6-body interaction energies.

The net interaction energies and the 2-, 3-, and 4+5+6-body contributions to the interaction energies of the four $(H_2O)_6$ isomers were calculated using each of the above density functional methods as well as using the HF, MP2, and CCSD(T) methods. (Due to the use of rigid monomers, the one-body terms are zero.) The DFT calculations were performed using the aug-cc-pVTZ (AVTZ)[74, 167] basis set, and the HF and MP2 calculations were performed using the aug-cc-pV5Z (AV5Z)[229] basis set. The CCSD(T)/AV5Z energies were estimated by combining CCSD(T) energies calculated with the aug-cc-pVDZ (AVDZ)[74, 167] basis set and MP2 energies calculated with the AVDZ[74, 167] and AV5Z[229] basis sets as described by Equation B.3:

$$E\,[CCSD(T)/AV5Z] \approx E\,[CCSD(T)/AVDZ] + E\,[MP2/AV5Z] - E\,[MP2/AVDZ] \qquad (B.3)$$

The SAPT procedure adopts as its initial wave function the product of the Hartree–Fock wave functions of the non-interacting monomers, and uses perturbation theory to separate the various terms comprising the interactions between monomers. Exchange effects are accounted for by exchange of electrons between orbitals localized on different monomers. This gives a decomposition of the net interaction energy into electrostatic, exchange-repulsion, induction, dispersion, exchange-induction and exchange-dispersion contributions. Charge-transfer contributions are incorporated in the induction terms. For the various 2-body contributions, corrections due to intramonomer correlation were also calculated.[13] The SAPT calculations were carried out using the AVTZ (2-body) and AVDZ (3-body) basis sets, and are free of basis set superposition errors (BSSE).[63]

The LMO–EDA method is used to decompose the interaction energies into electrostatic, exchange-repulsion, intermonomer correlation, and induction contributions.[8] In the LMO–EDA method, as applied to DFT, intermonomer correlation $\left(E_c^{AB}\right)$ is calculated using

$$E_c^{AB} = E_c\left[\rho_{AB}\right] - \left(E_c\left[\rho_A\right] + E_c\left[\rho_B\right]\right) \tag{B.4}$$

where ρ_{AB} and $\rho_{A/B}$ denote the total Kohn–Sham charge densities of the dimer and the two non-interacting monomers, respectively. The intermonomer correlation can also be interpreted as the short-range contribution to the dispersion energy. The ALMO–EDA method is used to dissect the induction interactions into polarization and charger-transfer contributions, where polarization refers to the distortion of the charge density of a monomer due to the electric fields from the other monomers. Both the LMO–EDA and ALMO–EDA calculations were carried out using the AVTZ basis set and included counterpoise corrections for BSSE. Although one can question whether these decomposition procedures are fully consistent with the philosophy of density functional theory, we believe that they can serve as valuable tools in assessing the performance of various DFT functionals.

It should be noted that the exchange-repulsion energies consist of both exchange and repulsion contributions. (In the DFT literature, it is common to report the exchange only portions of the

exchange-repulsion energies.) At the Hartree–Fock level of theory, the 2-body exchange contribution is given in terms of the exchange integrals involving r_{ij}^{-1}, where i and j are identified with two different monomers, whereas the repulsion contribution involves integrals over the kinetic energy and electron-nuclear Coulombic operators, with the former dominating.[230]

The MP2 geometry optimizations and single-point calculations of the n-body energies were performed using Gaussian03[104] and MOLPRO,[73] respectively. The ALMO–EDA calculations were performed with Q-CHEM3.2,[111] the LMO–EDA calculations were performed with GAMESS,[132] and the SAPT calculations were carried out with the SAPT2008[231] and SAPT3b[232] programs interfaced with the ATMOL1024[233] integral and SCF routines.

B.4   RESULTS AND DISCUSSION

B.4.1   Net Interaction Energies

Figure B2 reports the net interaction energies of the four $(H_2O)_6$ isomers obtained at the various levels of theory. As noted in previous studies, the MP2 and CCSD(T) interaction energies are very similar.[213,234,235] However, higher-order correlation effects do play a minor role, with the prism, cage, and book isomers calculated to be, respectively, 0.4, 0.3, and 0.1 kcal mol^{-1} more stable at the CCSD(T)/AV5Z than at the MP2/AV5Z level, while the stability of the ring isomer is essentially unaffected by inclusion of higher-order correlation effects. At the CCSD(T) level of theory the prism isomer is predicted to be the most stable and the ring isomer the least stable, lying 1.6 kcal mol^{-1} higher in energy. All density functional methods considered predict the book and ring isomers to be more stable than the prism and cage isomers, in agreement with the Hartree–Fock calculations but in contrast to the MP2 and CCSD(T) calculations.

While the HF and BLYP calculations both predict the ring isomer to be about 2.2 kcal mol^{-1} more stable than the prism isomer, this energy difference drops to 1.7 kcal mol^{-1} with the B3LYP functional and to only 0.8 kcal mol^{-1} with the PBE, PBE0, and PW91 functionals. Hence, it is clear that there are factors other than the neglect of long-range dispersion interactions in the DFT

76
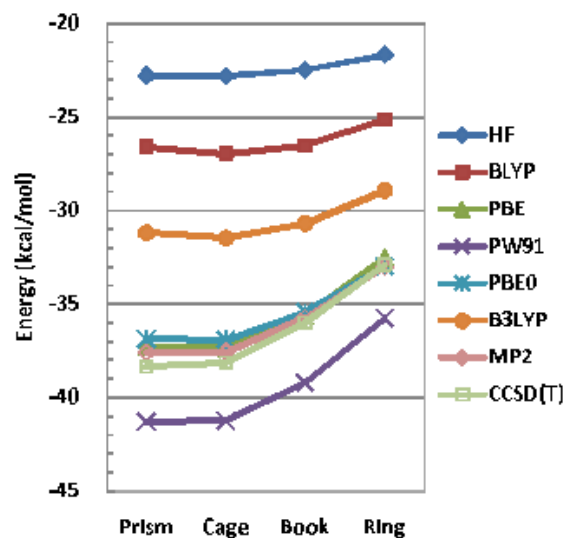
Figure B2: Net interaction energies of the $(H_2O)_6$ isomers from different theoretical methods.

calculations contributing to the discrepancies between the net interaction energies calculated using the CCSD(T) and DFT methods.

B.4.2 Two-body Energies

The 2-body energies for the four $(H_2O)_6$ isomers are reported in Figure B3. The PBE and PBE0 functionals give 2-body energies fairly close to the CCSD(T) values, while the BLYP and B3LYP functionals considerably underestimate and the PW91 functional overestimates the 2-body energies in magnitude. All methods considered — HF, MP2, CCSD(T), and DFT — predict the relative stabilities to be ring < book < cage ∼ prism when only 2-body energies are considered, with the prism-ring energy difference being 1.1 kcal mol^{-1} for the HF method and 5.4 kcal mol^{-1} for the CCSD(T) method. The PW91, PBE, and PBE0 functionals give prism–ring 2-body energy differences of 3.8–5.5 kcal mol^{-1}, while the BLYP and B3LYP functionals give prism–ring 2-body energy differences about three times smaller than the CCSD(T) result. The ensuing analysis of the
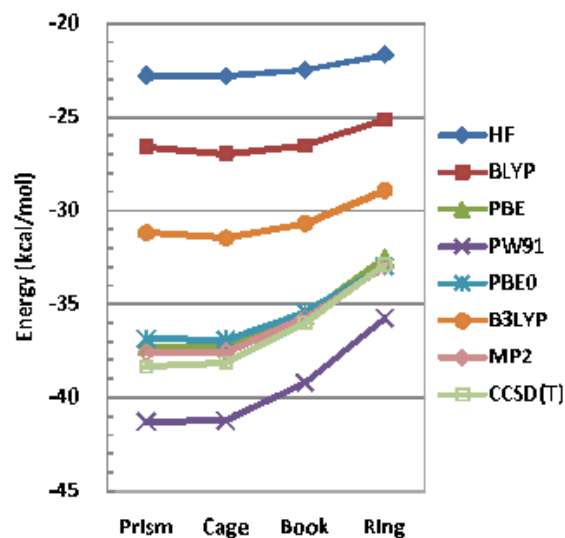
Figure B3: 2-body interaction energies of the $(H_2O)_6$ isomers from different theoretical methods.

individual contributions to the 2-body energies provides insight into the origins of this behavior.

Figure B4 reports the electrostatic, exchange-repulsion, induction, and dispersion contributions to the 2-body interaction energies of the $(H_2O)_6$. The electrostatic energies from the HF and SAPT calculations vary only slightly across the series of four hexamers. The inclusion of intramonomer correlation corrections in the SAPT procedure weakens the electrostatic interaction energies relative to their Hartree-Fock values by 1.0–1.5 kcal mol^{-1}. With the SAPT method the electrostatic energy for the prism isomer is about 1 kcal mol^{-1} more attractive than for the ring isomer. The electrostatic interaction energies associated with the various density functional methods and determined using the LMO–EDA analysis fall within 2.5 kcal mol^{-1} of the SAPT results, with the PBE0 functional giving electrostatic energies closest to the SAPT results. However, the DFT methods give larger electrostatic energy differences (2.0–2.9 kcal mol^{-1}) between the ring and prism isomers than found in the SAPT calculations.

In the SAPT procedure inclusion of intramonomer correlation increases the exchange-repulsion energies of each of the four $(H_2O)_6$ isomers by about 9 kcal mol^{-1} compared to their
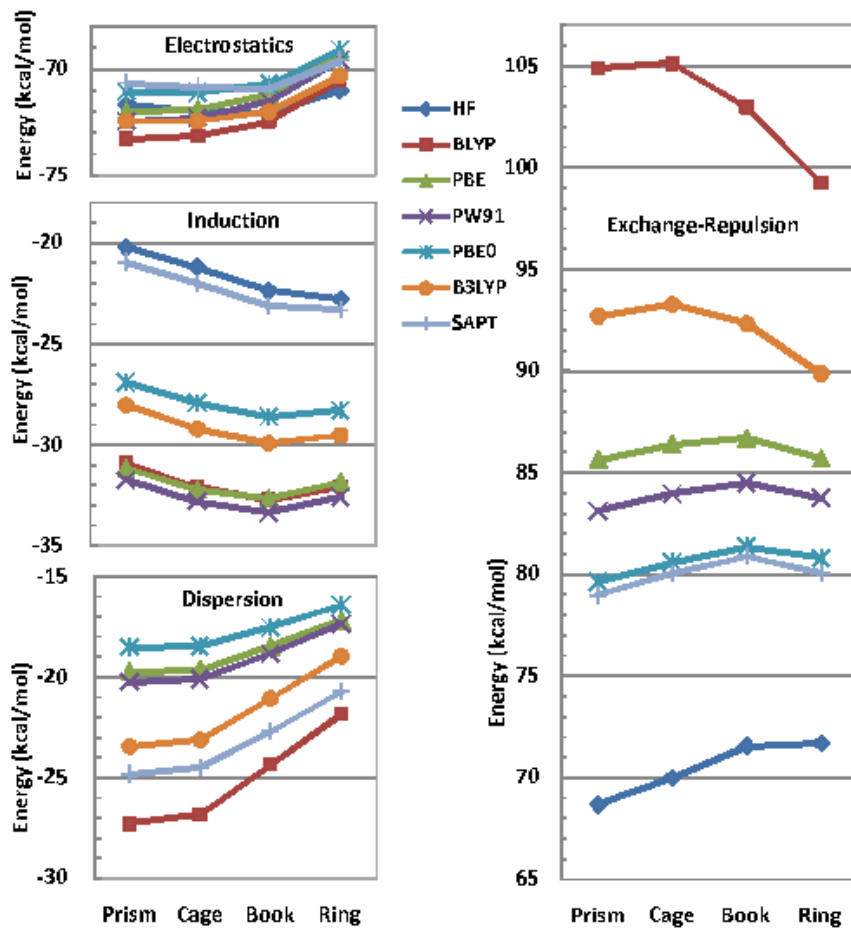
Figure B4: Electrostatics, exchange-repulsion, induction, and dispersion contributions to the 2-body interaction energies of the $(H_2O)_6$ isomers calculated using different theoretical methods. For the DFT methods the energy decomposition was accomplished using the LMO–EDA procedure.
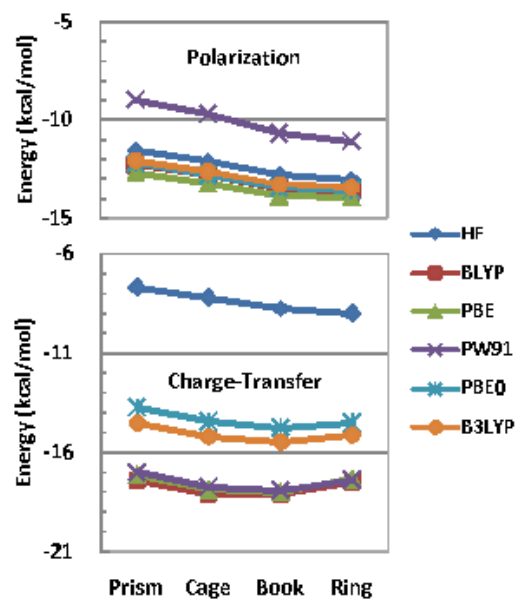
Figure B5: Polarization and charge-transfer contributions to the 2-body induction energies of the $(H_2O)_6$ isomers. For the DFT methods the decomposition of the induction energies was accomplished using the ALMO–EDA procedure.

Hartree–Fock values. The density functional methods all give larger exchange-repulsion energies (as deduced using the LMO–EDA analysis) than obtained from the SAPT calculations, with the differences from the SAPT values being 0.5–0.8, 3.6–4.1, 5.7–6.7, 9.9–13.7, and 19.2–25.9 kcal mol^{-1} with the PBE0, PW91, PBE, B3LYP, and BLYP functionals, respectively. While the trends in the exchange-repulsion energies for the PBE, PBE0, and PW91 functionals closely reproduce that from the SAPT calculations, this is not the case for the BLYP and B3LYP functionals. Specifically, while the exchange-repulsion energy from the SAPT calculations is about a 1 kcal mol^{-1} larger for the ring than for the prism, the exchange-repulsion energies associated with the BLYP and B3LYP functionals are significantly larger for the prism than for the ring isomer.

The SAPT calculations give 2-body induction energies about 1 kcal mol^{-1} more negative than the corresponding Hartree–Fock values, whereas LMO–EDA analysis with the hybrid and non-hybrid functionals give, respectively, induction energies as much as 5–7 and 10–11 kcal mol^{-1} larger in magnitude than the SAPT values. The large discrepancy between the DFT and SAPT values of the induction energies is a result of overestimation of charge-transfer contributions in the DFT calculations. This is confirmed by using the ALMO–EDA procedure to dissect the induction contributions into polarization and charge-transfer contributions. (In analyzing these results it should be kept in mind that induction energies obtained from the LMO–EDA and ALMO–EDA transfer procedures differ slightly due to differences in the localization procedures used in the two approaches.) The resulting 2-body polarization and charge-transfer contributions for the four $(H_2O)_6$ isomers are reported in Figure B5, from which it is seen that the differences between the DFT and SAPT values of the induction energies are indeed due to the overestimation of the charge-transfer contributions in the former. As expected, this problem is somewhat less severe with the hybrid functionals. The tendency of DFT calculations to overestimate charge-transfer contributions has been noted previously.[236]

Figure B4 also reports the 2-body dispersion contributions to the interaction energies calculated using the SAPT procedure and extracted from the DFT energies using the LMO–EDA procedure. The SAPT calculations give 2–body dispersion contributions to the interaction energies that range from -20.7 kcal mol^{-1} for the ring isomer to -24.8 kcal mol^{-1} for the prism isomer. These results

include contributions from exchange-dispersion as well as of changes in the dispersion energies resulting from correlation of the isolated monomers. Interestingly, for the four isomers of $(H_2O)_6$ these two corrections to the dispersion energies approximately cancel. The LMO–EDA analysis gives dispersion contributions to the interaction energies of -16.4 to -20.3 kcal mol^{-1} for the PBE, PBE0, and PW91 functionals, -19.0 to -23.5 kcal mol^{-1} for the B3LYP functional, and -21.8 to -27.3 kcal mol^{-1} with the BLYP functional, where the ranges indicate the spread as one progresses from the ring to the prism isomers. Hence the LMO–EDA analysis demonstrates that all functionals considered recover a significant fraction of the dispersion interactions between the monomers of the $(H_2O)_6$ clusters, with the BLYP functional actually overestimating the dispersion contributions. We have also carried out the LMO–EDA analysis using the local density approximation (LDA).[237] With LDA, the calculated inter-monomer correlation energies are about two to three times smaller than obtained with the GGAs and hybrid functional. This is a consequence of the LDA functional capturing only local intermonomer correlation resulting from overlap of the monomer charge distributions.

It is also of interest to examine how well the different functionals do at reproducing the SAPT value of the difference between the 2-body dispersion energies of the ring and prism isomers. In this context, we note that the PBE, PBE0, and PW91 functionals recover about two-thirds of the 4.1 kcal mol^{-1} dispersion energy difference between the ring and prism isomers calculated by the SAPT procedure. The BLYP and B3LYP functionals, on the other hand, overestimate the difference between the dispersion energies of the prism and ring isomers, giving values of 5.5 and 4.5 kcal mol^{-1}, respectively. These results indicate that the incorrect ordering of the $(H_2O)_6$ isomers obtained from calculations with the BLYP and B3LYP functionals is actually not due to their inadequate treatment of dispersion, but rather, is due to other deficiencies (in particular, in the exchange-repulsion energies) in these functionals.

B.4.3 Three-body Energies

It has been noted in several earlier studies that electron correlation effects are relatively unimportant for the 3- and higher-body interactions in water clusters.[238–240] This is confirmed in Figure
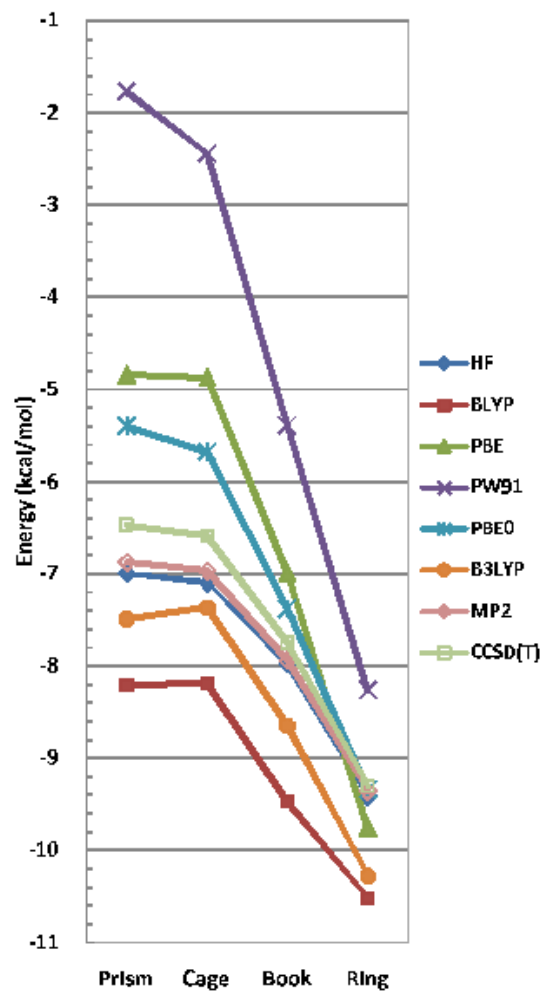
Figure B6: 3-body interaction energies of the $(H_2O)_6$ isomers from different theoretical methods.
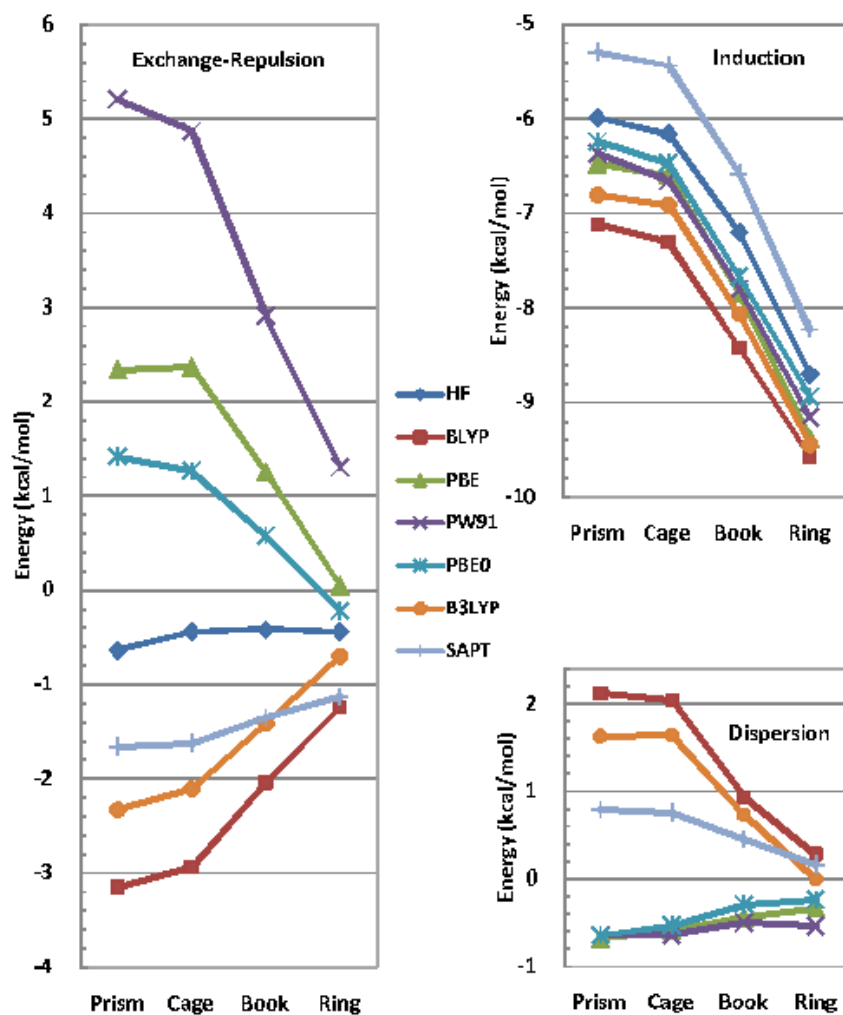
Figure B7: Exchange-repulsion, induction, and dispersion contributions to the 3-body interaction energies of the $(H_2O)_6$ isomers calculated using different theoretical methods. For the DFT methods the energy decomposition was accomplished using the LMO–EDA procedure.
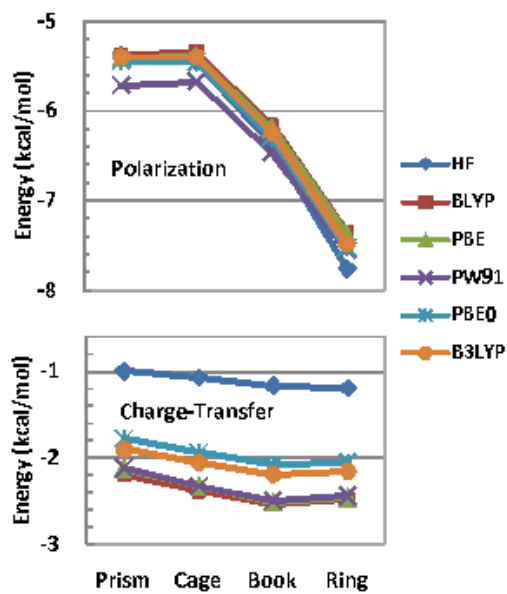
Figure B8: Polarization and charge-transfer contributions to the 3-body induction energies of the $(H_2O)_6$ isomers. For the DFT methods the decomposition of the induction energies was accomplished using the ALMO–EDA procedure.

B6 from which it is seen that the 3-body contributions calculated at the HF, MP2, and CCSD(T) levels of theory are very close to one another. Of the density functionals considered, only the B3LYP and PBE0 functionals give 3-body interaction energies within 1 kcal mol^{-1} of the CCSD(T) results. Most strikingly, the PBE and PW91 functionals give much larger differences between the 3-body interaction energies of the ring and prism isomers than obtained from the CCSD(T) calculations.

The 3-body interaction energies can be divided into exchange-repulsion, induction, and dispersion contributions. In the SAPT procedure, exchange-induction and exchange-dispersion are incorporated in the induction and dispersion contributions, respectively. The 3-body exchange-repulsion, induction, and dispersion contributions to the interaction energies are reported in Figure B7. The EDA/HF values of the 3-body exchange-repulsion energies are quite small for all four isomers, being close to -0.5 kcal mol^{-1}. The SAPT values for the 3-body exchange-repulsion energies are 0.7–1.2 kcal mol^{-1} more negative than the corresponding EDA/HF results. Since the 3-body contributions calculated using the SAPT procedure do not include correlation corrections, the small differences between the SAPT and EDA/HF values of the 3-body exchange-repulsion energies are primarily consequences of our associating the entire 3-body δ(HF) corrections to the SAPT 3-body induction and to differences in the localization procedures used in the two approaches. Thus the HF results should be the more appropriate reference in this case. The LMO–EDA analysis indicates that the 3-body exchange-repulsion energies from the DFT calculations vary much more strongly along the ring–book–cage–prism sequence than do the corresponding results from the Hartree–Fock calculations, with the trends found for the PW91, PBE, and PBE0 functionals and for the BLYP and B3LYP functionals being in opposite directions. The differences between the HF and DFT values of the 3-body exchange-repulsion interaction energies grow along the ring–book–cage–prism sequence, being as large as 5.8 kcal mol^{-1} for the prism isomer in the case of the PW91 functional.

The SAPT calculations give 3-body induction energies 0.5–0.7 kcal mol^{-1} smaller in magnitude than the Hartree–Fock calculations. As for the 3-body exchange contributions, the EDA/HF results are expected to be the more appropriate reference. All five density functional methods give

3-body induction energies that are larger in magnitude than the HF values, with the deviation from the HF results being on the order of 0.7 to 1.2 kcal mol^{-1} with the B3LYP and BLYP functionals, but only about 0.3 to 0.7 kcal mol^{-1} with the PW91, PBE, and PBE0 functionals.

The polarization and charge-transfer contributions to the 3-body induction energies were calculated using the ALMO–EDA procedure and are reported in Figure B8. All functionals are found to give values of the 3-body polarization energies close to the HF values, while the density functional methods give 3-body charge-transfer energies 0.8–1.4 kcal mol^{-1} larger in magnitude than the HF values, with the discrepancies from the HF values being less with the hybrid functionals.

The 3-body dispersion energies obtained with the various theoretical methods are reported in Figure B7. The SAPT calculations give 3-body dispersion energies that are positive, ranging from 0.16 kcal mol^{-1} for the ring to 0.79 kcal mol^{-1} for the prism isomer. The corresponding results from the LMO-EDA analysis with the BLYP and B3LYP functionals are also positive but much larger in magnitude, e.g., for the prism isomer being as large as 2.12 and 1.63 kcal mol^{-1}, respectively. In contrast, for the PBE, PBE0, and PW91 functionals the LMO-EDA analysis gives 3-body dispersion energies ranging from -0.24 to -0.68 kcal mol^{-1} for the water hexamers. Thus, none of the functionals considered give 3-body dispersion energies in good agreement with the SAPT results.

Figure B9 reports the net 4+5+6-body interaction energies from the various theoretical methods. With the CCSD(T) calculations these higher-body interaction energies range from -0.4 kcal mol^{-1} for the prism to -1.4 kcal mol^{-1} for the ring isomer. The BLYP and B3LYP functionals give 4+5+6-body interaction energies close to the CCSD(T) results, while the PW91, PBE, and PBE0 functionals give 4+5+6-body interaction energies that are too large in magnitude, especially for the cage and prism isomers. The LMO-EDA analysis reveal that the errors in the PW91, PBE, and PBE0 values of the 4+5+6-body interaction energies are largely due to the exchange-repulsion contributions. Interestingly, for these three functionals the errors in the 4+5+6- and 3-body energies approximately cancel.
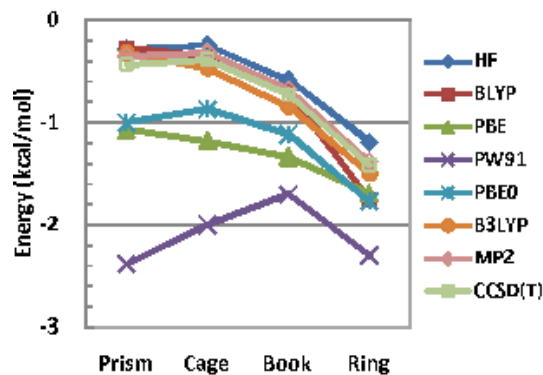
Figure B9: 4+5+6-body interaction energies of the $(H_2O)_6$ isomers from different theoretical methods.

B.5   CONCLUSION

Two types of energy decomposition have been employed in analyzing the interaction energies of selected low-energy isomers of $(H_2O)_6$ as described by several DFT and wavefunction-based methods. Specifically, the net interaction energies were decomposed into their 2-, 3-, and 4+5+6-body contributions, and each of these was further dissected into electrostatics, exchange-repulsion, induction, and dispersion contributions. The latter decomposition was accomplished by means of symmetry-adapted perturbation theory and localized molecular orbital EDA methods.

Of the functionals considered, the PBE0 functional gives net and 2-body interaction energies closest to the CCSD(T) results. However, none of the density functional methods, including PBE0, do a good job at reproducing the CCSD(T) values of the 3-body interaction energies, although the largest errors in the 3-body energies calculated with the PBE0 functional are only about 1 kcal mol^{-1} (for the cage and prism isomers), and these errors are largely canceled by errors in the opposite direction in the 4+5+6-body interaction energies. It is relevant to note that Tkatchenko and von Lilienfeld in a recent study of argon clusters and solid argon, have concluded that for these systems the success of dispersion-corrected DFT methods is, in part, due to a partial cancelation

between the errors in the 2- and 3-body contributions.[241]

The energy decomposition analysis reveal that, with the exception of the PBE0 functional, all functionals considered have sizable errors in each of the individual contributions to the 2-body interaction energies. Although the PBE0 functional gives electrostatic and 2-body exchange-repulsion energies in close agreement with the SAPT values, it does have large errors in the 2-body induction and dispersion energies, overestimating the former by 5.5–6.7 kcal mol^{-1} in magnitude and underestimating the latter by about 4.3–6.3 kcal mol^{-1} in magnitude. These two errors approximately cancel, with the result that the PBE0 functional gives 2-body interaction energies close to the CCSD(T) results (although failing to give the correct energy ordering of the isomers). The decomposition analysis also allows us to establish that the major source of the error in the 3-body energies from the density functional calculations derives from the exchange-repulsion interactions. The LMO–EDA procedure also indicates that none of the functionals properly describe the 3-body dispersion interactions in the water clusters.

As noted in Section B.2, several strategies have been devised to account for long-range dispersion contributions in DFT calculations. One of the challenges in correcting DFT methods for dispersion is to avoid overbinding due to the deficiencies in the exchange-correlation functional.[180,242–244] Energy decomposition analysis, such as those used in the present study, provide additional insight into the factors at play in the application of DFT methods to weakly interacting systems. Specifically, the LMO–EDA calculations reveal that the choice of exchange functional is important for establishing the magnitudes of the exchange-repulsion energies as well as for the magnitude of the charge-transfer contributions to the interaction energy. All functionals examined overestimate the magnitude of the charge-transfer contributions to the interaction energies of the water hexamers. This tendency has been observed previously for a variety hydrogen-bonded complexes by Piquemal et al.[236] who attributed it to the presence of self-interaction errors. Since both exchange-repulsion and charge-transfer depend exponentially on intermolecular separation, this problem can be partially remedied by adoption of an exchange functional which results in overly repulsive exchange-repulsion contributions. For example, partial cancelation between these two sources of error occurs with the PBE functional where the errors in the 2+3-

body exchange-repulsion and 2+3-body charge-transfer contributions to the hexamer interaction energies (as judged by comparison with the SAPT results) are 6.8 to 10.7 and -9.6 to -10.9 kcal mol^{-1}, respectively. The PBE0 functional, on the other hand, gives exchange-repulsion energies close to the SAPT values, and thus will not benefit between cancelation of errors in the exchange-repulsion and charge-transfer contributions. Obviously, the adoption of functionals employing exact exchange eliminates the problems caused by overestimation of charge-transfer from the exchange term, but then results in exchange-repulsion energies close to the HF values, which, in turn, are appreciably smaller than the SAPT values which are destabilized by correlation of the monomers.

The second major "insight" gained from the comparison of the SAPT and LMO–EDA analysis of the interaction energies of the $(H_2O)_6$ isomers is that GGA and hybrid functionals actually recover a significant fraction (over 75%) of the intermonomer correlation energies in these systems. In this work we have equated the intermonomer correlation energies recovered in the DFT calculations with short-range contributions to the dispersion energies. However, it is important to note that what is meant by dispersion energy is interpreted differently by different researchers. For example, in a recent paper it is stated that most popular density functionals completely neglect dispersion.[245] Such a statement seems to be based on a definition in which only the long-range intermonomer correlation contributions are regarded as dispersion. We have adopted a broader definition, consistent with that used in the SAPT procedure, in which dispersion consists of all contributions to the interaction energy involving simultaneous dipole-allowed electronic excitations from two (or more) monomers (or atoms). With this more encompassing definition dispersion includes both short-range and long-range contributions, and it is appropriate to refer to the correlation contributions deduced from LMO–EDA analysis as short-range dispersion contributions. The fact that the LMO–EDA analysis with the BLYP functional gives dispersion energies greater in magnitude than those obtained from the SAPT calculations does not imply that the BLYP functional recovers long-range dispersion contributions. Rather, it means that this functional overestimates the short-range intermonomer correlation effects.

We have also applied the LMO–EDA decomposition to PBE calculations on the argon dimer

at its equilibrium geometry. In this case it is found that the density functional calculations recover only about 30% of the dispersion energy obtained from SAPT calculations.[246] This indicates that the potential energy minima found for inert gas dimers with some GGA density functional methods actually has two origins: (1) a non-physical contribution due to the exchange functional (which we associate primarily with overestimation of charge-transfer) and (2) a physical contribution due to recovery of short-range dispersion effects. We believe that this is an important observation since it is generally assumed that such binding derives solely from deficiencies in the functional. We note also that the overestimation of charge transfer partially compensating for underestimation of true dispersion effects has been noted previously in the literature.[236]

In concluding, it is important to recall that it is not possible to precisely map correlation effects in a wavefunction treatments onto correlation as described by DFT calculations.[247] In particular, we note that it has been established that LDA and GGA functionals recover some long-range left-right correlation through their exchange functionals and that this is related to self-interaction errors.[247–249] Presumably, this recovery of left-right correlation is partially responsible for the exchange-repulsion energies from DFT being closer to the SAPT than to the Hartree-Fock values. On the other hand, the self-interaction error is accompanied by overestimation of charge transfer in the DFT calculations which leads to an artificial attraction. This underscores the difficulty in designing DFT methods for describing weakly bonded systems.

B.6   ACKNOWLEDGEMENTS

APPENDIX C

A SECOND GENERATION DISTRIBUTED POINT POLARIZABLE WATER MODEL

This work was published as[*]: Revati Kumar, Fangfang Wang, Glen R. Jenness, and Kenneth D. Jordan *The Journal of Chemical Physics*, 132, (2010), 014309-1–014309-12

C.1   ABSTRACT

A distributed point polarizable model (DPP2) for water, with explicit terms for charge-penetration, induction, and charge-transfer, is introduced. The DPP2 model accurately describes the interaction energies in small and large water clusters and also gives an average internal energy per molecule and radial distribution functions of liquid water in good agreement with experiment. A key to the success of the model is its accurate description of the individual terms in the n-body expansion of the interaction energies.

C.2 INTRODUCTION

Most Monte Carlo and molecular dynamics simulations are carried out using model potentials (force fields)[10,94,107,212,250–265] and, as a result, there is a continued interest in the development of improved model potentials. The "holy grail" of research in this area is the development of model potentials that are applicable over a wide range of conditions and for a wide range of properties. There is a growing consensus that this requires explicit inclusion of many-body effects.[93,94,107,258,264,266–270] Water, in particular, has been a hotbed of activity of model potential development, with a large number of many-body polarizable potentials having been introduced over the past few years.[10,94,107,212,259–267,269,271–274] This is a consequence of the fundamental importance of water in chemistry and biology as well as of the expectation that approaches that prove successful for describing the interactions in water can be carried over to other systems.

In recent years, several polarizable models of water parameterized to high-level electronic structure calculations on small water clusters have appeared.[10,107,212,254,260,273,275,276] These have proven highly successful at describing a range of properties of water clusters as well as of bulk water. However, studies from our group have revealed that even some of the most successful of these models do not perform well for water clusters with geometrical arrangements highly distorted from those of the minimum energy structures of low-energy isomers of the neutral clusters. Such distorted structures are encountered, for example, in $(H_2O)_n^-$ clusters and in complexes of water clusters with anions.[277,278]

These considerations led our group to introduce a distributed point polarizable (DPP) model designed to describe water clusters at both "normal" geometries as well as those encountered in the charged clusters.[10] This model is now an integral part of the excess electron-water cluster code developed in our group.[277,278] In the present study we introduce several improvements to the DPP water model, with the new model being designated DPP2. In the following sections we describe the design of the new model and apply it to water clusters as large as $(H_2O)_{21}$ as well as to bulk water.

93

C.3   THEORETICAL METHODOLOGY

Before describing the DPP2 model, it is useful to summarize first the major features of the earlier DPP model. The DPP model shares several features with the TTM2 models from the Xantheas group.[260, 279, 280] Specifically, both the DPP and TTM2 models (as well as the new DPP2 model) employ the experimental geometry of the gas phase monomer (*i.e.*, OH distances of 0.957 Å and an HOH angle of $104.52°$, point charges of $0.5742e$ on the H atoms and $-1.1484e$ on an *M*-site, located on the rotational axis, displaced 0.25 Å from the O atoms towards the H atoms, and three mutually interacting, atom-centered point polarizable sites, with Thole-type[281] damping between the charges and induced dipoles and between the induced dipoles. The major differences between the DPP and TTM2 models are:

1. Charge-charge interactions are damped in the latter but not in the former,

2. A slightly larger damping factor for the charge-induced dipole interactions is employed in the DPP model, and

3. Repulsive (exponential) interactions are included between all atoms of different monomers in the DPP model, whereas repulsive (inverse power law) interactions are employed between O atoms only in the TTM2 model.

Both models also include dispersion interactions between the O atoms of different monomers, but with these interactions being damped in the DPP model, but not in the TTM2 models.

By comparing with the results of large basis set MP2 calculations it has been found that overall the DPP model performs better than the polarizable TTM and AMOEBA[107] water models, especially for geometries encountered in the $(H_2O)_n^-$ clusters.[10] (The AMOEBA model also employs three mutually interacting atom-centered polarizable sites with Thole damping.) However, even for a cluster as small as $(H_2O)_6$ the relative energies from the DPP model differ by as much as 0.8 kcal mol^{-1} from the *ab initio* results. The primary motivation for the development of the DPP2 model is to achieve more accurate energies for water clusters, both at their local minima as well as in distorted structures.

In designing the DPP2 model, use has been made of the results of symmetry-adapted pertur-
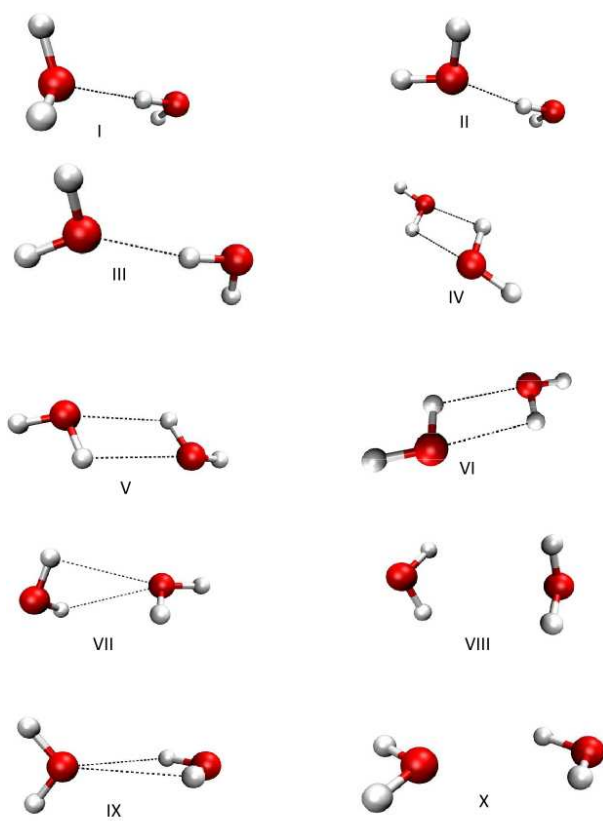
Figure C1: The Smith dimer set.
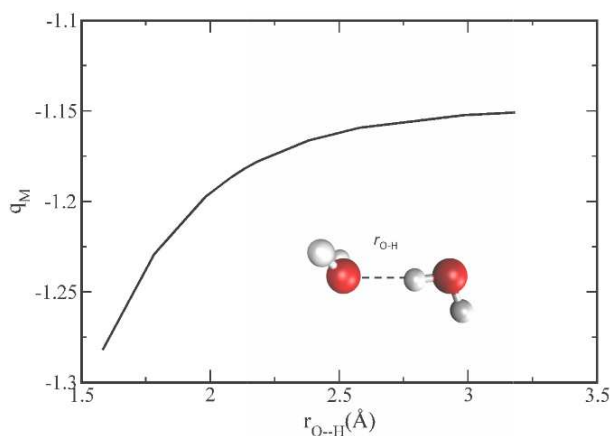
Figure C2: The variation of the charge on the *M*-site with the OH distance in the dimer.

bation theory (SAPT),[11, 12] absolutely localized molecular orbitals energy decomposition analysis (ALMO–EDA),[9] and CCSD(T)[95] calculations on the water dimer as well as of CCSD(T) calculations of the three-body energies of four isomers of $(H_2O)_6$. The SAPT procedure is used to dissect dimer interaction energies into electrostatic, exchange-repulsion, induction, and dispersion contributions. Because the SAPT procedure does not separate the induction into separate polarization and charge-transfer (CT) contributions, use has been made of the EDA procedure in QChem[111] to calculate the charge-transfer contributions. Although the separation of induction into charge-transfer and polarization contributions is not unique, the EDA procedure has been found to give physically reasonable values for the charge-transfer contributions and to give results that are not strongly basis set dependant.[9]

The individual contributions to the interaction energies were used, as described below, in parameterizing the DPP2 model which, by design, is a rigid monomer model. In future work we plan to extend the DPP2 model to allow for monomer relaxation.

96

Table C1: Parameters in the DPP2 model.

Interaction	Parameter	Value	Units
Dispersion	C_{OO}	-277.21	kcal mol^{-1}Å^6
	δ_{OO}	31.92	Å^{-1}
	C_{OH}	-131.49	kcal mol^{-1}Å^6
	δ_{OH}	3.7738	Å^{-1}
	C_{HH}	-25.96	kcal mol^{-1}Å^6
	δ_{HH}	10.98	Å^{-1}
Charge-transfer	A_{CT}	-1107.7	kcal mol^{-1}
	B_{CT}	3.70976	Å^{-1}
Charge-penetration	λ	-2.9957	Å^{-1}
Induction	α_O	1.22	Å^3
	α_H	0.28	Å^3
	a_{DD} (Dipole-Dipole damping)	0.30	
	a_{CD} (Charge-Dipole damping)	0.21	
Repulsion	A_{OO}	369.0	kcal mol^{-1}
	B_{OO}	4.99867	Å^{-1}
	A_{OH}	5373.9	kcal mol^{-1}
	B_{OH}	3.52188	Å^{-1}
	A_{HH}	2101.05	kcal mol^{-1}
	B_{HH}	3.20194	Å^{-1}
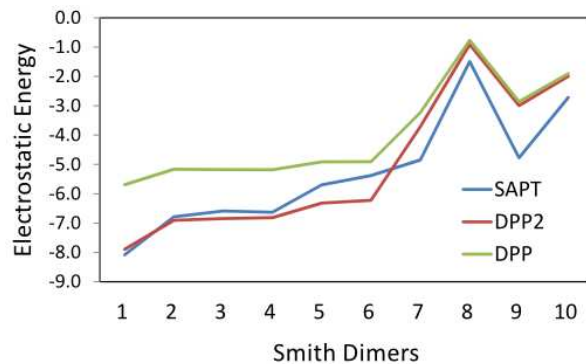
Figure C3: Electrostatic energies (kcal mol^{-1}) from the SAPT procedure and the DPP and the DPP2 models for the ten Smith dimers.
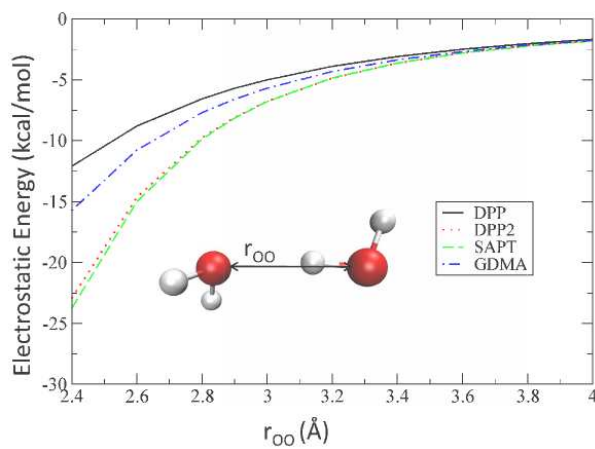
Figure C4: Electrostatic energy (kcal mol^{-1}) as a function of the OO distance for the water dimer. Results are reported for the SAPT procedure and for the DPP, DPP2, and GDMA models. The differences between the GDMA and SAPT results provides estimates of the charge-penetration contributions.
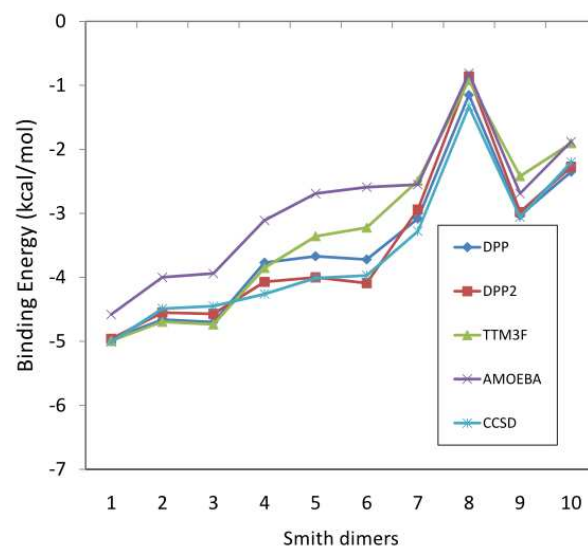
Figure C5: Binding energies (kcal mol^{-1}) of the ten Smith dimers. Results are reported for the DPP model and DPP2 models as well as from CSSD(T)/AV5Z calculations.

C.3.1 Electrostatics

Most force fields for water use three point charges to model the charge distribution of the monomer. The limitations of such simple models for describing the electrostatic interactions between water molecules at distances typically encountered in clusters and the bulk are well appreciated, and, not surprisingly, several recent water models (*e.g.*, AMOEBA[107] and ASPW4[282]) use atom-centered distributed multipole expansions, or additional off-atom charge sites (*e.g.*, SAPT5s[283] and CC-pol[212]). However, even these improved representations of the electrostatics do not account for charge-penetration,[93] which can, in fact, be more important for the energetics than expanding the number of point charges or adopting higher atom-centered multipoles.[284] Piquemal and co-workers have developed a Gaussian electrostatic model (GEM)[285] which includes explicit terms for the effects of charge-penetration and have incorporated it in their SIBFA force field.[267,269] Charge-penetration has also been included in the effective fragment model of Freitag and co-workers.[286]

In the DPP2 model we retain the use of three charge sites, but introduce charge-penetration using a procedure of Piquemal *et al.*[284] In this approach the electrostatic interaction between the point charges, q_i and q_j associated with two water monomers is given by

$$E_{es} = \frac{q_i^*(r_{ij})q_j^*(r_{ij})}{r_{ij}} \qquad (C.1)$$

where $q_i^*(r_{ij})$ is related to q_i as follows:

$$q_i^*(r_{ij}) = 2q_i - \left\{ Z_i - [Z_i - q_i]\left[1 - \exp\left(\frac{\lambda r_{ij} Z_i}{Z_i - q_i} \right) \right] \right\} \qquad (C.2)$$

In Equation C.2, Z_i is the number of valence electrons associated with atom *i*, i.e, 1 for H and 6 for O and can be viewed as the effective nuclear charge. As in the TTM2-R and DPP models, q_H is taken to be $0.5742e$, and the countering negative charge of $-1.1484e$ is located on the *M*-site. The +6 charge associated with the O nucleus, is also displaced to the *M*-site. The value of the λ parameter was obtained by least-squares fitting the electrostatic energies from SAPT calculations on the ten stationary points on the water dimer potential energy surface (the so-called Smith dimer set)[287] depicted in Figure C1. The value of λ and of the other parameters in the DPP2 model are

summarized in Table C1.

The charge-penetration, or de-shielding effect, is greater for the O atoms (*M*-sites in our model) than for the H atoms. In Figure C2 we plot the charge at the *M*-site of the acceptor monomer as a function of the distance between the associated O atom and the donor H atom of the other monomer (the dihedral angles defining the relative orientation of the two monomers are fixed at their equilibrium values). Although the changes of the effective charges are quite small at the equilibrium geometry of the dimer, they do lead to a 2.4 kcal mol^{-1} enhancement of the electrostatic interaction energy.

Figure C3 compares, for the Smith set, the electrostatic energies from the DPP and DPP2 models with those from the SAPT calculations, and Figure C4 shows the corresponding results for the water dimer as a function of the OO distance, keeping the dihedral angles fixed at the optimized values for the equilibrium geometry. As expected, and in agreement with Piquemal *et al.*, the electrostatic energies are much better represented by the DPP2 model which includes charge-penetration than by the DPP model which does not. Still, the DPP2 value of the electrostatic interaction for the structure IX of the Smith set is about 1.7 kcal mol^{-1} less attractive than that obtained from the SAPT calculations. However, the errors in the DPP2 values of the electrostatic energies are largely compensated for by the exchange-repulsion term, described below, and the total interaction energies calculated with the DPP2 model are, in fact, very close to the CCSD(T) results, with the largest discrepancy for the Smith dimers being only 0.3 kcal mol^{-1} (see Figure C5).

Figure C4 also includes the electrostatic energies for the dimer obtained from a distributed multipole expansion employing on all atoms multipoles through the quadrupole and determined from a GDMA analysis[103, 288] of the MP2/AVTZ[74, 167] charge density. From this figure it is seen that the DDP2 model is more successful than the GDMA model, which neglects charge-penetration, at reproducing the electrostatic energies from the SAPT calculations. At the limit of r_{ij} tending to zero, Equation C.2 is no longer physical. However as can be seen from Figure C4, the DPP2 model does extremely well at reproducing the SAPT electrostatic interaction energy in the water dimer at OO distances as short as 2.4 Å.

Table C2: Components of the molecular polarizability (Å^3) of the water monomer[a] .

Component	DPP	DPP2	Experiment[289]
α_{xx}	1.62	1.57	1.53
α_{yy}	1.29	1.36	1.42
α_{zz}	1.37	1.44	1.47
$\alpha_{average}$	1.43	1.46	1.47

[a] The monomer is oriented in the *xz* plane, with the principal axis along the z-axis

C.3.2 Polarization

The DPP2 model, like the DPP, TTM2, and AMOEBA models, uses mutually interacting atom-centered point polarizable sites, with Thole-type damping between the charges and induced dipoles and between the induced dipoles, to describe the polarization interactions. In the DPP, TTM2, and AMOEBA models the values of the atomic polarizabilities were taken from the work of Thole,[281] while the damping coefficients were modified from Thole's values to give a better fit to the *ab initio* values of the cluster energies. In the DPP model, the coefficient damping the interactions between the induced dipoles was adjusted so that the model gives three-body energies for the book, prism, cage, and ring isomers of $(H_2O)_6$ close to those from MP2/AVTZ calculations.

In the DPP2 model we have re-adjusted the atomic polarizabilities (keeping the same damping constants as the DPP model) to give, simultaneously, the best fit to the atomic polarizability components of the water molecule and the three-body energies (evaluated at the CCSD(T)/AV5Z[74, 167] level) of the four low-lying isomers of the hexamer. The three-body energy of each hexamer was obtained by considering each trimer contained in the hexamer and evaluating its three-body interaction energy from

$$E_{ABC}^{3Body} = E_{ABC} - (E_{AB} + E_{AC} + E_{BC}) + (E_A + E_B + E_C) \qquad (\text{C.3})$$

where the energies of the trimer, dimers, and monomers are given by E_{ijk}, E_{ij}, and E_i, respectively. The net three-body energy of the hexamer is then calculated by adding the three-body energies of all constituent trimers. The molecular polarizabilities of the water monomer as described by the DPP and DPP2 models and from experiment are summarized in Table C2, and the atomic polarizabilities and damping constants are summarized in Table C1. Interestingly, the values of the atomic polarizabilities employed in the DPP2 model and optimized as described above are close to those used in the recently introduced TTM4-F water model of Burnham *et al.*[276]

In the remainder of this subsection the procedure used to calculate the polarization energy is described. The induced dipole μ_i on atom i with polarizability α_i is given by:

$$\mu_i = \alpha_i \left[\mathbf{E}_i + \sum_{j \neq i} \mathbf{T}_{ij} \cdot \mu_j \right] \tag{C.4}$$

where $\mathbf{E}_i$ is the electric field defined as

$$\mathbf{E}_i = \sum_{j \neq i} f_3(r_{ij}) \frac{q_j^*(r_{ij}) \vec{r}_{ij}}{r_{ij}^3} \tag{C.5}$$

The summation in Equation C.5 involves all partial charges, $q_j^*(r_{ij})$ (as defined by Equation C.1) on molecules other than the one containing site i. The dipole tensor $\mathbf{T}_{ij}$ is a 3×3 matrix whose elements are:

$$T_{ij}^{\beta \gamma} = f_5(r_{ij}) \frac{3 r_{ij}^{\beta} r_{ij}^{\gamma}}{r_{ij}^5} - f_3(r_{ij}) \frac{\delta_{\beta \gamma}}{r_{ij}^3} \tag{C.6}$$

where β and γ denote the Cartesian components x,y, or z, $\delta_{\beta \gamma}$ corresponds to the Kronecker δ function, and the Thole-type damping functions $f_3(r_{ij})$ and $f_5(r_{ij})$ are given by

$$f_3(r_{ij}) = 1 - \exp\left(-a \frac{r_{ij}^3}{(\alpha_i \alpha_j)^{\frac{1}{2}}} \right) \tag{C.7}$$

and

$$f_5(r_{ij}) = 1 - \left(1 + a \frac{r_{ij}^3}{(\alpha_i \alpha_j)^{\frac{1}{2}}} \right) \exp\left(-a \frac{r_{ij}^3}{(\alpha_i \alpha_j)^{\frac{1}{2}}} \right) \tag{C.8}$$

103
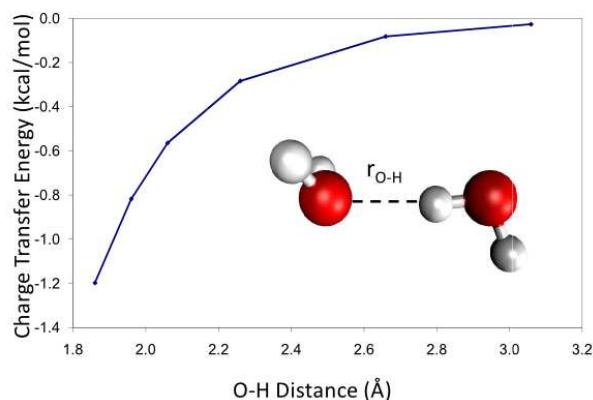
Figure C6: Charge-transfer energy (kcal mol^{-1}) of the water dimer as a function of the distance between the monomera with fixed flap angles. The results were obtained from an EDA analysis.

Separate values of the damping constant a are employed for the charge-dipole and dipole-dipole interactions. The induced dipoles are solved iteratively, and the induction energy is given by

$$E_{pol} = -0.5 \sum_i \mathbf{E}_i \cdot \mu_i \qquad (\text{C.9})$$

As mentioned earlier, the charges employed in the electric field evaluation are given by Equation C.2 and thus take into account the effect of charge-penetration. However, the inclusion of charge-penetration causes only small changes (≤ 0.1 kcal mol^{-1}) in the polarization energies of the hexamer.

C.3.3 Charge-Transfer

Figure C6 reports the charge-transfer contribution to the interaction energy of the water dimer as a function of the OO distance. These results were obtained from an ALMO–EDA analysis of the

Hartree–Fock/AVTZ wavefunctions. At the equilibrium geometry of the water dimer, the charge-transfer contribution to the interaction energy estimated from the ALMO–EDA analysis is -0.9 kcal mol^{-1}, which is nearly 20% of the net interaction energy. For this reason it was decided to include a term to account explicitly for two-body charge-transfer contributions in the DPP2 model. This was accomplished by fitting the EDA values of the charge-transfer energies of the dimer at several values of the OO separation to exponentials in the intermolecular distances between H and O atoms of the different monomers, *i.e.*,

$$E_{CT} = -A_{ct} \sum_{i,j} \exp\left(-B_{ct} r_{O_i H_j}\right) \qquad (C.10)$$

In the DPP2 model the net induction energies are given by the sum of the charge-transfer energies estimated by Equation C.10 and the polarization energies calculated using the point-inducible dipoles as described in Section C.3.2. Figure C8 compares for the Smith dimer set the induction energies from the SAPT calculations and from the DPP and DPP2 models. Two sets of SAPT results are included, SAPT(a) which includes only the induction terms explicitly calculated by the SAPT procedure, and SAPT(b) which includes also the δ(HF) corrections[231] which recover the higher-order induction and exchange-induction interactions not recovered in the perturbative SAPT analysis.

Overall, for the Smith dimer set the DPP2 model more closely reproduces the SAPT(a) results for the induction energies than does the DPP model. The largest discrepancies between the DPP2 and SAPT(a) results are for the symmetrical bridging structures V and VI, for which the DPP2 contributions are about 0.3 kcal mol^{-1} more negative, primarily due to an overestimation of the magnitude of the charge-transfer contributions for these structures. On the other hand, the largest discrepancy between DPP2 and SAPT(b) induction contributions for the Smith dimer set is for the global minimum where the discrepancy is 0.5 kcal mol^{-1} (with the DPP2 value being smaller in magnitude).

Much of the discrepancy between the DPP2 and SAPT two-body induction energies derives from limitations of a model potential employing only three point charges to describe the charge

distribution of the monomer and only point inducible dipoles to describe the polarization. In any case, the fact that the DPP2 model slightly underestimates the induction energies from SAPT calculations is, to a large extent, compensated by the approach used to determine the exchange-repulsion terms in the DPP2 model (discussed in Section C.3.5).

C.3.4 Dispersion interaction

In the DPP2 model the dispersion interaction between two monomers is represented as

$$E_d = \frac{C_{OO}f(r_{OO}, \delta_{OO})}{r_{OO}^6} + \sum_{i,j} \frac{C_{OH}f\left(r_{O_iH_j}, \delta_{OH}\right)}{r_{O_iH_j}^6} + \sum_{i,j} \frac{C_{HH}f\left(r_{H_iH_j}, \delta_{HH}\right)}{r_{H_iH_j}^6} \qquad (C.11)$$

where the $f(r, \delta)$ factors are the Tang–Toennies damping functions,[290] and the C and δ parameters were obtained by fitting to dispersion energies (dispersion + exchange-dispersion) from SAPT calculations for a set of dimer structures generated starting with the equilibrium structure of the dimer, and scanning along the OO distance, optimizing the flap angles (see Figure C9) for each OO distance. The SAPT dispersion contributions were evaluated at second-order perturbation theory and the induction-dispersion and the exchange-induction-dispersion contributions which appear at third order, essentially cancel.[291]

Figure C10 compares the SAPT, DPP, and DPP2 values of the dispersion energies for the Smith dimer set. Overall, the dispersion energies, calculated using the DPP2 model closely reproduce those from the SAPT calculations, with the largest discrepancies being for structures IV, V, and VI, for which the DPP2 model gives the dispersion contributions 0.2–0.3 kcal mol^{-1} too small in magnitude. This is a significant improvement over the earlier DPP model. We also considered models with only OO dispersion or only OH dispersion, but that these proved to be inferior to the DPP2 model which allows for dispersion interactions between all atoms of different monomers.
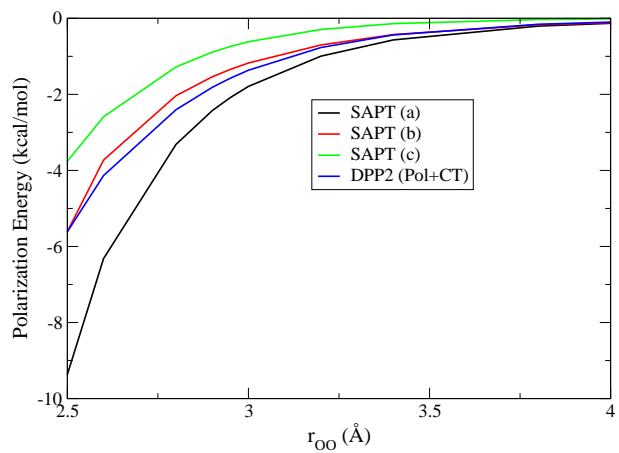
Figure C7: Induction energies (kcal mol^{-1}) of the water dimer as the OO distance is scanned keeping the flap angles fixed at the values for the equilibrium structure of the water dimer. Results are reported for the third-order SAPT procedure and for the DPP and DPP2 models. The SAPT results are reported without (a) and with (b) the δ(HF) corrections.
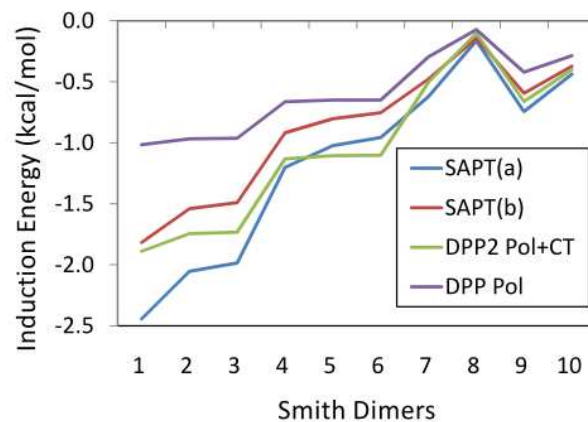
Figure C8: Induction energies (kcal mol^{-1}) for the ten Smith dimers. Results are reported for the SAPT procedure and for the DPP and DPP2 models. The SAPT results are reported with (a) and without (b) the $\delta(\text{HF})$ corrections.
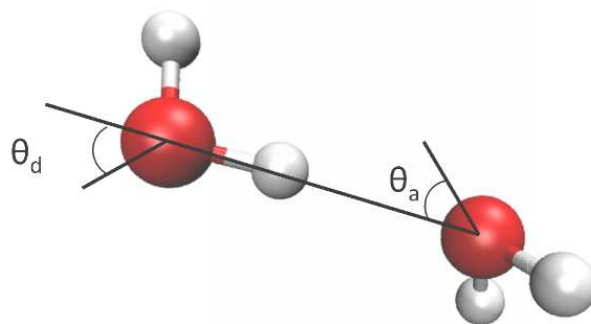
Figure C9: Definition of the the flap angles θ_a and θ_b for the water dimer.
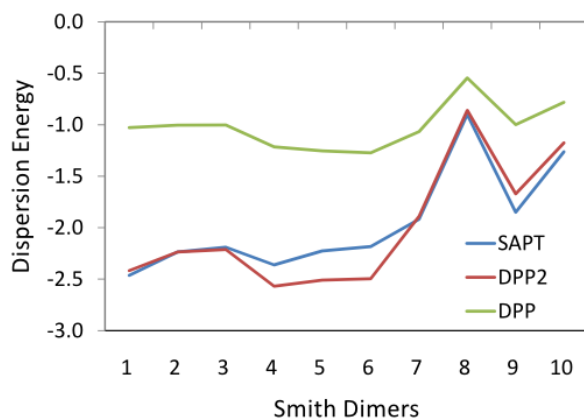
Figure C10: Dispersion energies (kcal mol^{-1}) for the ten Smith dimers. Results are reported for the SAPT procedure and for the DPP and DPP2 models.
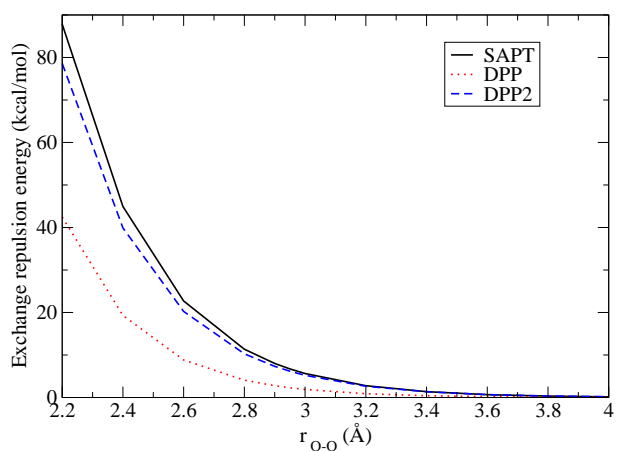
Figure C11: Exchange-repulsion energy (kcal mol^{-1}) of the water dimer as a function of the OO distance, keeping the angles fixed at their values for the equilibrium structure of the dimer. Results are reported for the SAPT procedure and for the DPP and DPP2 models.
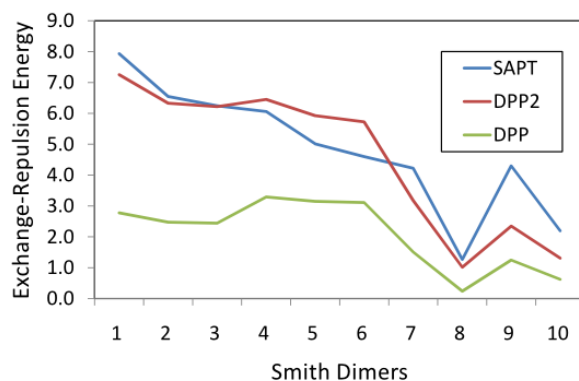
Figure C12: Exchange-repulsion energies (kcal mol^{-1}) for the ten Smith dimers from SAPT calculation and from the DPP and DPP2 models.

C.3.5   Exchange-Repulsion

The exchange-repulsion between two water monomers in the DPP2 model is represented as

$$E_{ex-rep} = A_{OO}exp\left(-B_{OO}r_{OO}\right) + A_{OH}\sum_{i,j}exp\left(-B_{OH}r_{O_iH_j}\right) + A_{HH}\sum_{i,j}exp\left(-B_{HH}r_{H_iH_j}\right) \quad (\text{C.12})$$

Although the parameters in this expression could be determined by fitting to the SAPT exchange-repulsion contributions, the success of the model at predicting net interaction energies is enhanced by adopting instead the following procedure. Approximate CCSD(T)/AV5Z calculations were carried out for a set of 15 dimer structures generated by performing a scan in the OO distance (from 2.4 to 4.0 Å), keeping the flap angles (Figure C9) fixed at their equilibrium geometry values, as well as for 15 dimer structures with OO distances of 2.8, 2.9, and 3.0 Å with the angle θ_a scanned from 10° to 50°, keeping θ_b (see Figure C9) fixed at the value optimized for the potential energy minimum. At each of these geometries, the electrostatic, induction, and dispersion contributions from the DPP2 model were subtracted from the CCSD(T) interaction energies, and the resulting energy differences were then used to fit the parameters in the repulsive potential.

110

The approximate CCSD(T)/AV5Z energies used in this procedure were obtained by combining the MP2 energies calculated with the AVTZ and AV5Z basis sets, with the CCSD(T)/AVTZ energies using

$$E(CCSD(T)/AV5Z) \approx E(CCSD(T)/AVTZ) + E(MP2/AV5Z) - E(MP2/AVTZ) \qquad (C.13)$$

Explicit corrections for basis set superposition error (BSSE)[63] were not applied as BBSE is negligible with the AV5Z basis set.

Figure C11 compares the exchange-repulsion energies for the water dimer obtained from the DPP and DPP2 models as well as from the SAPT calculations. The DPP2 model is seen to closely reproduce the SAPT results even though the DPP2 exchange-repulsion energies were not fit to the SAPT exchange-repulsion energies. For small OO distances the DPP2 repulsion energies are slightly smaller than the SAPT exchange-repulsion energies. This is a consequence of the fact that the repulsive term in the DPP2 model is also compensating for the small errors in the electrostatics and induction energies (including the $\delta(HF)$ terms) as represented in the DPP2 model. Figure C12 reports the DPP and DPP2 exchange-repulsion energies as well as the SAPT values for the ten Smith dimers. The DPP2 model again performs significantly better than the DPP model in representing the exchange-repulsion energies.

The potential energy curves for the water dimer, calculated using the CCSD(T) procedure and from the DPP2 model, are shown in Figure C13. Overall, the agreement between the DPP2 and CCSD(T) potential energy curves is excellent, although compared to the CCSD(T) potential, the DPP2 potential is slightly more attractive for R $\leq$ 2.85 Å and slightly less attractive for R $\geq$ 2.9 Å.

Compared to some recent parameterizations of water force fields, we have used a relatively small set of dimer structures. Specifically, the Smith dimer set was used to determine the λ parameter in the charge-penetration term, and the parameters in the exchange-repulsion, dispersion, and charge-transfer terms in the model were all determined from electronic structure calculations on structures generated from scans about the dimer equilibrium structure. As will be seen below the DPP2 model is successful at describing water clusters in a wide range of structures. Thus, it appears that the strategy of parameterizing separately the electrostatic, induction, charge-transfer

111

and exchange-repulsion terms to energies from *ab initio* energy decomposition analysis requires fewer geometrical structures than global fits of potentials.

C.4   TESTING THE DPP2 MODEL

To test the performance of the DPP2 model, the interaction energies of the ten Smith dimers (Figure C5), four low-energy isomers of $(H_2O)_6$, and two low-energy isomers of $(H_2O)_{21}$ were calculated. In addition, calculations were also carried out for five neutral $(H_2O)_6$ clusters at geometries of $(H_2O)_6^-$ isomers. For the Smith dimer set and for the $(H_2O)_6$ isomers, geometries optimized at the MP2/AVTZ level with rigid monomer constraints were employed. For the $(H_2O)_6^-$ species the geometries were taken from Reference 278, where they were optimized using the AVDZ[74, 167] basis set augmented with diffuse *s* and *p* functions to describe the weakly bound excess electron. For the $(H_2O)_{21}$ isomers we started with the fully optimized RI–MP2[292]/AVDZ structures of Cui *et al.*[293] and adjusted the internal angles and bond lengths of the monomers to the monomer gas-phase values. For each of the hexamer structures, the two- and three-body contributions and the net interaction energies were calculated using the approximate CCSD(T)/AV5Z method described above (except that the CCSD(T)/AVDZ and MP2/AVDZ energies were used in place of the CCSD(T)/AVTZ and MP2/AVTZ energies, respectively). The interaction energies of the two isomers of $(H_2O)_{21}$ were calculated at the RI–MP2/AVQZ level.

The geometry optimizations were carried out using Gaussian03,[104] and the single-point RI–MP2 and CCSD(T) calculations were done with MOLPRO[73] and ACES,[294] respectively. The SAPT calculations were carried out with the SAPT2008 program,[231, 295] and the ALMO–EDA analyses were performed using QChem.[111]

Finally, the DPP2 model potential was used to perform NVT Monte Carlo simulations on liquid water at T = 298 K. The simulations used a cubic box, of length 19.728 Å, containing 256 molecules (which corresponds to a density of 0.996 g cc^{-1}),[256] replicated by means of periodic boundary conditions. Long-range interactions were treated with a spherical cutoff of 9.5 Å. The
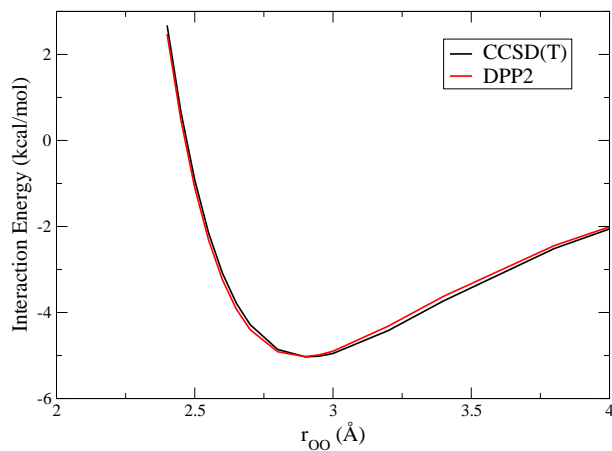
Figure C13: Comparison of the potential energy curve of the water dimer, with flap angles fixed to their equilibrium values, from CCSD(T)/AV5Z calculations and the DPP2 model.

Table C3: Interaction energies (kcal mol^{-1}) of four low-energy isomers of $(H_2O)_6$.

Method	Ring	Book	Cage	Prism	RMSD[a]
Dang–Chang	−39.04	−39.15	−39.06	−39.38	5.50
AMOEBA	−44.03	−44.62	−44.58	−44.62	0.47
TTM3-F	−40.56	−41.23	−42.03	−42.21	3.12
DPP	−44.03	−44.65	−45.34	−45.30	0.24
DPP2	−43.47	−44.47	−45.25	−45.22	0.11
MP2	−43.75	−44.38	−44.86	−44.84	0.26
CCSD(T)	−43.64	−44.49	−45.12	−45.26	0.00

[a] RMSD values are reported relative to the CCSD(T)/AV5Z results

Table C4: Two-body energies (kcal mol^{-1}) of four low-energy isomers of the water hexamer.

Method	Ring	Book	Cage	Prism	RMSD[a]
Dang–Chang	−30.40	−32.70	−34.00	−33.74	5.22
AMOEBA	−32.48	−35.46	−37.26	−37.70	0.63
TTM3-F	−33.85	−36.08	−37.83	−37.66	0.57
DPP	−33.66	−35.90	−37.91	−38.20	0.39
DPP2	−32.34	−35.65	−37.98	−37.98	0.38
CCSD(T)	−32.93	−36.01	−38.15	−38.26	0.00

[a] RMSD values are reported relative to the CCSD(T)/AV5Z results

Table C5: Three-body energies (kcal mol^{-1}) of four low-energy isomers of the water hexamer.

Method	Ring	Book	Cage	Prism	RMSD[a]
Dang–Chang	−7.30	−5.80	−4.76	−5.17	1.79
AMOEBA	−10.76	−9.30	−8.09	−7.65	1.43
TTM3-F	−5.79	−4.73	−4.03	−4.24	2.87
DPP	−8.80	−7.73	−6.90	−6.59	0.30
DPP2	−9.25	−7.83	−6.81	−6.66	0.15
CCSD(T)	−9.30	−7.75	−6.59	−6.47	0.00

[a] RMSD values are reported relative to the CCSD(T)/AV5Z results
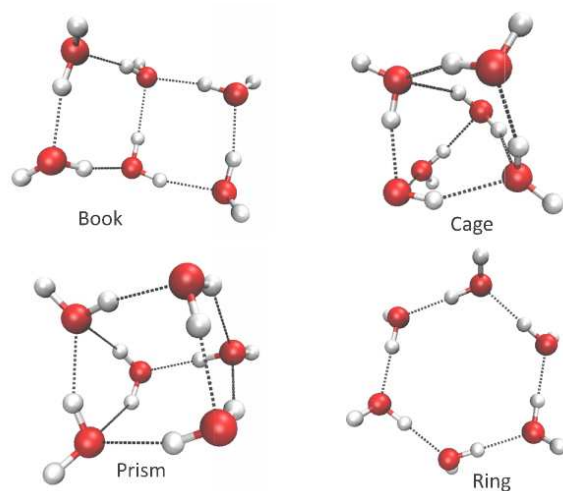
Figure C14: Structures of four low energy minima of the water hexamer.

simulations were carried out for 0.5×10^6 Monte Carlo moves. Test calculations with the TIP4P,[256] SPCE,[255] and TIP3P[256] models showed that for the properties calculated in this study, the use of a cutoff introduced negligible errors compared with simulations with an Ewald[296] treatment of the long-range electrostatics.[297]

C.4.1 Hexamers

The two-body, three-body, and net interaction energies calculated using the DPP, DPP2, TTM3-F,[298] AMOEBA, and Dang–Chang models for the four low-lying local minima of the neutral $(H_2O)_6$ cluster (Figure C14) are compared with the corresponding CCSD(T) results in Tables C3, C4, and C5, respectively. TTM3-F is the latest in the TTM series of models developed by Xantheas and co-workers. The TTM3-F model, unlike the earlier TTM2 models, but in common with the Dang–Chang model, employs only a single polarizable site. The results in these tables were obtained using the MP2 optimized geometries (with frozen monomers) to eliminate differ-
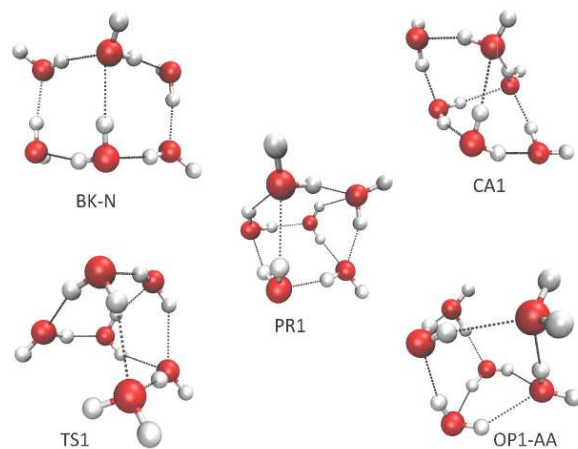
Figure C15: Five low-energy stationary points of $(H_2O)_6^-$.

Table C6: Total interaction energies (kcal mol^{-1}) of four low-energy isomers of the water hexamer at the optimized geometries for each method.

Method	Ring	Book	Cage	Prism	RMSD[a]
Dang–Chang	−39.39	−40.43	−40.85	−41.00	4.21
AMOEBA[b]	−43.52	−44.58	−44.90	−44.54	0.38
TTM3-F[b]	−41.13	−41.94	−42.80	−43.22	2.36
CC-pol[c]	−42.91	−43.90	−44.75	−45.41	0.51
DPP	−44.43	−45.12	−45.95	−46.02	0.76
DPP2	−43.58	−44.89	−45.90	−45.75	0.50
CCSD(T)	−43.64	−44.49	−45.12	−45.26	0.00

[a] RMSD values are reported relative to the CCSD(T)/AV5Z results
[b] Using rigid monomer optimization

[c] Vibrationally averaged monomer geometries are employed[212]

Table C7: Relative energies (kcal mol^{-1}) of the neutral water hexamer at geometries of the $(H_2O)_6^-$ isomers. Calculations carried out using geometries from Reference 278, with the exception of CC-pol for which vibrationally averaged monomer geometries are employed (Reference 212).

Method	BK-N	CA1	PR1	TS1	OP1-AA	RMSD[a]
Dang–Chang	0.00	2.07	1.09	5.29	6.08	1.53
AMOEBA	0.00	2.45	1.51	8.18	9.37	0.56
TTM3-F	0.00	1.26	0.21	4.60	5.99	1.82
CC-pol	0.00	1.76	0.11	6.2	7.83	0.80
DPP	0.00	1.88	0.62	6.26	8.15	0.59
DPP2	0.00	1.98	0.84	6.88	8.72	0.20
CCSD(T)	0.00	1.98	1.12	7.18	8.93	0.00

[a] The RMSD values are reported relative to the CCSD(T)/AV5Z results

ences that would result using different geometries for the different approaches.

For both the net interaction energies and for the two- and three-body contributions, the best agreement with the CCSD(T) results is obtained with the DPP2 model. In particular, for the total energies, the RMSD values (using the CCSD(T) results as the reference) are 5.50, 3.12, 0.47, 0.24, and 0.11 kcal mol^{-1} with the DC,[94] TTM3-F,[298] AMOEBA, DPP, and DPP2 models, respectively.

Equally important as a model's ability to predict absolute energies is its ability to predict properly the relative energies. Thus it is noteworthy that the TTM3-F model, even though it considerably underestimates the magnitudes of the net interaction energies, does an excellent job at predicting the relative energies of the local minima of the $(H_2O)_6$ isomer test set. In particular, the RMSD error for the relative energies predicted by the TTM3-F model is only 0.16 kcal mol^{-1}, while that for the DPP2 model is 0.11 kcal mol^{-1}.

Table C3 also reports the interaction energies calculated at the MP2/AV5Z level of theory. Interestingly, while high-order correlation effects beyond those recovered at the MP2 level stabilize

117

the cage, prism, and book isomer by 0.1–0.4 kcal mol^{-1}, they destabilize the ring isomer by 0.1 kcal mol^{-1}. From Table C4 it is seen that the AMOEBA, TTM3-F, DPP, and DPP2 models are all quite successful at predicting the CCSD(T) two-body energies, with the RMSD errors being 0.63, 0.57, 0.39, and 0.38 kcal mol^{-1}, respectively. The situation is quite different for the three-body energies (Table C5), for which the DPP and DPP2 models give results much closer to the CCSD(T) calculations than do the AMOEBA, Dang–Chang, and TTM3-F models, with the AMOEBA model considerably overestimating and the Dang–Chang and TTM3-F model considerably underestimating the three-body energies in magnitude.

The geometries of the four $(H_2O)_6$ isomers were also optimized, under the constraint of rigid monomers, using each of the model potentials considered above as well as using the CC-pol model,[212] which employs monomer bond lengths and angles that correspond to the vibrationally-averaged gas-phase monomer. The resulting interaction energies are tabulated in Table C6. When geometries optimized with each method are employed the RMSD errors in the net interaction energies are 4.21, 0.38, 2.36, 0.51, 0.75, and 0.50 kcal mol^{-1} for the Dang–Chang, AMOEBA, TTM3-F, CC-pol, DPP, and DPP2 models, respectively. While these results suggest that the AMOEBA, CC-pol, and DPP2 models all perform quite well at describing the net interaction energies when geometries optimized with each model are employed, the DPP2 model is the most successful of these at reproducing the CCSD(T) values of the relative energies.

A key motivation for the development of the DPP and DPP2 water models is to describe accurately water clusters in the highly distorted structures encountered in the presence of excess electrons or anions. To this end, we have also examined five $(H_2O)_6$ clusters with geometries corresponding to those for selected low-energy isomers of $(H_2O)_6^-$ (Figure C15).[278] For these geometries, the interaction energies have been calculated using the CCSD(T)/AV5Z approach described above as well as using the DC, TTM3-F, AMOEBA, DPP, and DPP2 models. We also calculated the interaction energies using the CC-pol model with the monomer bond-lengths and bond angles adjusted to the CC-pol values.

The relative energies of this group of $(H_2O)_6$ structures are reported in Table C7, from which it is seen that the DPP2 model most closely reproduces the CCSD(T) results, with a RMSD error
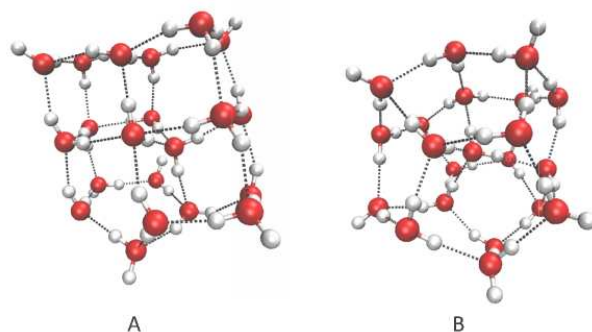
Figure C16: Structures of two isomers of the $(H_2O)_{21}$ cluster.

in the relative energies of only 0.20 kcal mol^{-1}. For the AMOEBA and CC-pol models the RMSD errors are 0.59 kcal mol^{-1} and 0.80 kcal mol^{-1}, respectively, whereas the TTM3-F model, which performed quite well for the relative energies of the local minima of neutral $(H_2O)_6$, fares much poorer, with a RMSD error of 1.8 kcal mol^{-1}. In order to check that the geometry differences are not the major factor responsible for the differences between between the CC-pol and CCSD(T) results, we also calculated CCSD(T)/AV5Z interaction energies for the BK-N and PR1 isomers using the CC-pol geometries, generated as described above. For these geometries, the CCSD(T) calculations give an energy difference of 1.39 kcal mol^{-1} between the two isomers, whereas the CC-pol model predicts that the two isomers are separated by only 0.11 kcal mol^{-1}. Hence, even as sophisticated a model as CC-pol does not fare well in describing water clusters at the geometries into which they are distorted by an excess electron.

C.4.2 $(H_2O)_{21}$

In this section, two low-energy isomers of $(H_2O)_{21}$ are examined to determine whether the good performance of the DDP2 model found for $(H_2O)_2$ and $(H_2O)_6$ persists for appreciably larger clusters. The two isomers considered have very different structures (see Figure C16). The

Table C8: Interaction energies (kcal mol^{-1}) of isomers **A** and **B** of the $(H_2O)_{21}$ cluster calculated using different model potentials. All results for MP2/AVDZ optimized structures, modified as described in the text.

Method	Isomer	
	A	B
Dang–Chang	-191.75	-192.61
AMOEBA	-209.22	-214.27
TTM3-F	-202.53	-202.26
CC-pol	-216.64	-219.09
DPP	-217.60	-220.90
DPP2	-214.85	-217.41
RI–MP2[a]	-213.00	-215.80

[a] Obtained using the AVQZ basis set

Table C9: Three-body energies (kcal mol^{-1}) of isomers **A** and **B** of $(H_2O)_{21}$. All results for MP2/AVDZ optimized structures, modified as described in the text.

Method	Isomer	
	A	B
Dang–Chang	−31.16	−33.37
AMOEBA	−41.70	−45.44
TTM3-F	−27.24	−28.56
CC-pol	−35.52	−38.83
DPP	−36.24	−38.49
DPP2	−38.27	−40.61
RI–MP2[a]	−39.31	−41.47

[a] RI–MP2 results from Reference 226

geometries used are taken from Reference 226, but with the OH bond lengths and HOH angles of the monomers "restored" to their gas-phase values. The energies of the two isomers were calculated at the RI–MP2/AVQZ level and with the DPP, AMOEBA, DC, TTM3-F, CC-pol, and DPP2 model potentials. For calculation with the CC-pol model the OH bond lengths and HOH angles of the monomers were adjusted to the values employed in that model. From Table C8 it is seen that for these two $(H_2O)_{21}$ isomers the DPP2 model gives net interaction energies within 2 kcal mol^{-1} of the RI–MP2/AVQZ values, whereas the AMOEBA and CC-pol results differ by as much as 3.8 kcal mol^{-1} from the RI–MP2 results. (The TTM3-F interaction energies differ by up to 13.5 kcal mol^{-1} from the RI–MP2 results). For both isomers the DPP2 model predicts stronger cluster binding than do the RI–MP2/AVQZ calculations.

The DPP2 model predicts isomer **B** to be 2.6 kcal mol^{-1} more stable than isomer **A**, in excellent agreement with the MP2 energy difference of 2.8 kcal mol^{-1} while the Dang–Chang, AMOEBA, and TTM3-F models give relative stabilities of the two isomers very different from
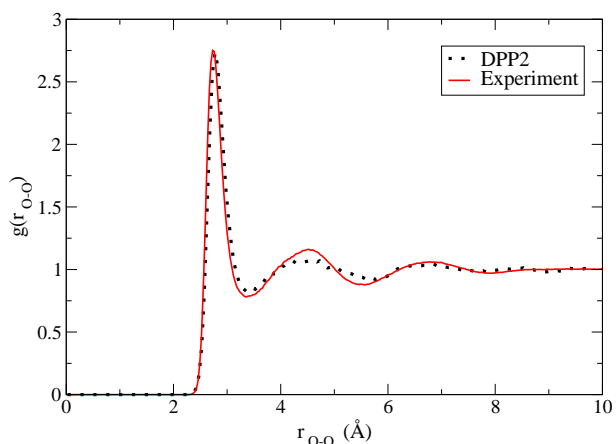
Figure C17: OO radial distribution function of water at T = 298 K from Monte Carlo simulations with the DPP2 model and from experiment (Reference 299).

the RI–MP2 results (with the TTM3-F model, in fact, predicting isomer **B** to be more stable). The CC-pol model predicts a relative stability of 2.5 kcal mol^{-1} which is also in good agreement with the MP2 results. As seen from Table C9, the DPP2 model more closely reproduces the *ab initio* (RI–MP2/AVTZ) three-body energies of the two isomers than do the other model potentials considered.

C.4.3   Liquid Water

As mentioned in the introduction, a major challenge in force field development is to accurately describe systems ranging from small clusters to the condensed phase. For this reason it is valuable to test how well the DPP2 model performs for liquid water. To accomplish this we have carried out Monte Carlo simulations of liquid water at T = 298 K. The resulting OO, OH, and HH radial distribution functions, shown in Figures C17–C19, are all in close agreement with experiment.[299]

The average internal energy per molecule for each of the Dang–Chang, AMOEBA, TTM3-F, DPP, and DPP2 models and from experiment is tabulated in Table C10. The internal energies for

122
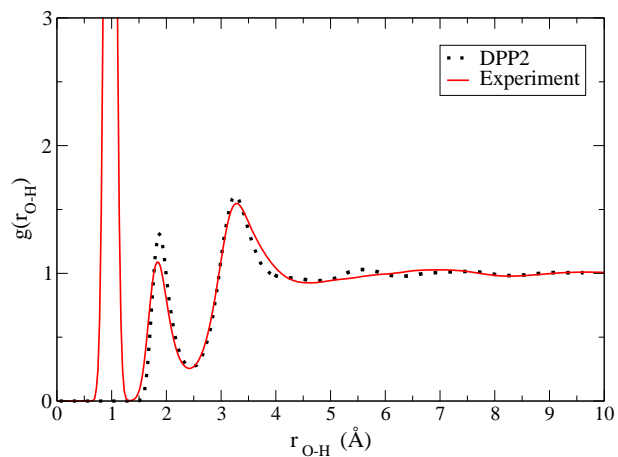
Figure C18: OH radial distribution function of water at T = 298 K from Monte Carlo simulations with the DPP2 model and from experiment (Reference 299).
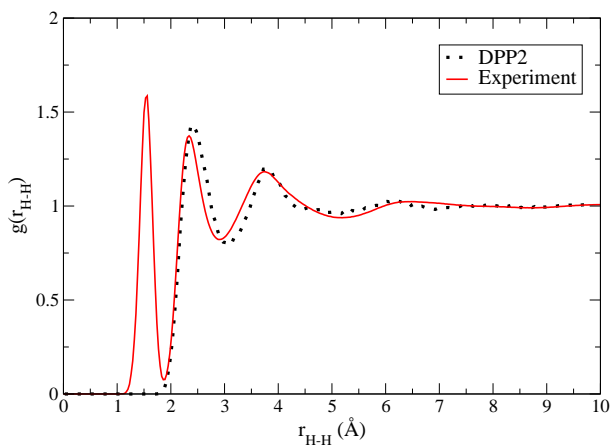
Figure C19: HH radial distribution function of water at T = 298 K from Monte Carlo simulations with the DPP2 model and from experiment (Reference 299).

Table C10: The internal energy (kcal mol^{-1}) per molecule of liquid water at T = 298 K.

Method	Internal energy
Dang–Chang[94]	−9.8
AMOEBA[107]	−9.0
TTM3-F[298]	−10.7
CC-pol[212]	−10.9
DPP	−10.7
DPP2[a]	−10.1
Expt.[256]	−9.9

[a] This work

the Dang–Chang, AMOEBA, TTM3-F, and DPP models are taken from the literature. The average internal energy per molecule calculated for the DPP2 model is −10.1 kcal mol^{-1}, which is close to the experimental value of −9.91 kcal mol^{-1}.[256] This excellent agreement between theory and experiment, at first sight, is surprising since the DPP2 model, by design, does not include monomer flexibility, and the simulations neglected nuclear quantum corrections. However, Manolopoulos *et al.* have shown that for many properties monomer flexibility and nuclear quantum effects have opposing tendencies, with the result that properties calculated from classical simulations with rigid monomers can be close to those from quantum simulations using flexible monomers.[300]

As a further test of how well various model potentials are doing at describing the interactions between water molecules in arrangements important in the liquid, we took twenty dimers and twenty trimers, selected at random from structures sampled in the DPP2 Monte Carlo simulations of liquid water, and for each of these clusters calculated the interaction energies using the TTM3-F, AMOEBA, and DPP2 force-fields and the CCSD(T)/AV5Z method. The RMSD errors for the interaction energies with respect to the CCSD(T) results of this set of dimers are 0.40, 0.60, 0.11, and 0.15 kcal mol^{-1} for the TTM3-F, AMOEBA, CC-pol and DPP2 force-fields, respectively. In the

case of the trimers the corresponding RMSD errors are 0.53, 0.68, 0.34, and 0.42 kcal mol^{-1}. (The CC-pol interaction energies are compared to those from CCSD(T) calculations with the monomers constrained to the CC-pol monomer geometry.) Thus it is seen that the CC-pol and DPP2 force fields are more successful than the TTM3-F or AMOEBA models at describing the energetics of the dimers and the trimers sampled in the Monte Carlo simulations of the liquid, with the CC-pol model performing slightly better than the DPP2 model.

C.5   CONCLUSION

In this study, we have presented a new force field for water, designated DPP2, which includes explicit terms for charge-penetration and charge-transfer. The model was parameterized so that its individual contributions — electrostatics (including charge-penetration), induction (including charge-transfer), dispersion, and exchange-repulsion — closely reproduce, for selected structures on the water dimer, corresponding results obtained from SAPT and ALMO–EDA calculations. The model accurately describes the two- and three-body interaction energies as well as the net interaction energies of both small and large water clusters, both at their equilibrium structures and at the highly distorted geometries encountered in $(H_2O)_n^-$ clusters.

Comparison is made with the predictions of other recently introduced polarizable force fields including TTM3-F, CC-pol, and AMOEBA. The DPP2 and CC-pol models are found to be more successful than the TTM3-F and AMOEBA models at reproducing the *ab initio* interaction energies of the various clusters examined. The DPP2 model, by far, is the most successful at describing the energetics of the water clusters in geometries encountered in $(H_2O)_6^-$.

The DPP2 model gives for bulk water radial distribution functions and an internal energy in excellent agreement with experiment. Examination of dimers and trimers sampled in the finite temperature Monte Carlo simulations shows that the DPP2 model accurately represents the energies of these species, as does the CC-pol model.

In future work, we plan to extend the DPP2 model to allow for flexible monomers (*i.e.*, for OH

stretching and HOH bending), which will permit it to be used to calculate vibrational spectra and to address the role of monomer flexibility on cluster and condensed phase systems. The strategy used to develop the DPP2 force field water should be applicable to other small molecules.

C.6   ACKNOWLEDGMENTS

APPENDIX D

SUPPORTING NUMERICAL DATA

D.1   INTRODUCTION

This appendix is dedicated to providing additional numerical data for the previous chapters. Included are experimental binding energies for the water–benzene and water–anthracene systems, timing and computer resources required for the water–acene systems, and the numerical data used in Appendix B.

D.2   SUPPORTING INFORMATION FOR THE WATER–ACENE INTERACTIONS

D.2.1   Experimental data on the water–acene interactions

Table D1 gives a comparison of experimental interaction energies with the calculated interaction energies using the DF–DFT–SAPT, MP2C, and MP2C–F12 methods for water–benzene. As discussed in Chapter 4, all three methods are capable of producing CCSD(T) quality results. However, since the water–benzene geometry used in Chapters 3 and 4 is a model geometry designed to mimic the interaction between a water molecule and an infinite graphene sheet, a direct comparison between the experimental interaction energy and those presented in Chapters 3 and 4 cannot

Table D1: Interaction energies (D_e, in kcal mol^{-1}) for water–benzene and water–anthracene.

Method	Water–benzene
DF–DFT–SAPT	−3.29
MP2C	−3.10
MP2C–F12	−3.34
Experiment[a]	−3.45±0.09[b]
	−3.26±0.25[c]
	−3.21±0.58[d]

[a] Includes a ZPE correction of −1.01 kcal mol^{-1}.
[b] Reference 99
[c] Reference 301
[d] Reference 302

be made.

In order to ensure a direct comparison between theory and experiment, the geometry of the water–benzene complex was optimized at the MP2/aug-cc-pVDZ level. The vibrational frequencies and the zero-point energy (ZPE) for water–benzene were then calculated for the optimized geometry using the harmonic approximation at the MP2/aug-cc-pVDZ level. The theoretically calculated ZPE was combined with the experimental D_0 to give the "experimental" D_e of water–benzene. The experimental interaction energies are compared to the DF–DFT–SAPT, MP2C, and MP2C–F12 interaction energies calculated using the optimized geometries. This set of methods were shown in Chapter 4 to produce near CCSD(T) quality results with the computational expense greatly reduced, which makes them ideal for comparison with the experimental interaction energies. From Table D1, all three methods give interaction energies within the experimental error bars for water–benzene.

D.2.2 Timings and computer resources

Table D2 gives the computer resources used in calculating the DF–DFT–SAPT, DF–MP2, DF–MP2–F12, CCSD(T), and CCSD(T)–F12 interaction energies for the water–acene systems. Computer resources were provided through the Center for Molecular and Material Simulations (CMMS) at the University of Pittsburgh. All calculations were run with the MOLPRO2009.1 program package, with the exception of the water–nonacene DF–DFT–SAPT energies, which were run with the MOLPRO2010.1 program package.

Table D2: Computational resources used (in hours and GB) in the water–acene studies

System	Processor	Total CPU time	Hard disk
DF–DFT–SAPT			
Water–benzene[a]	Intel Nehalem 2.66 GHz	8.24	1.84
Water–anthracene[a]	Intel Nehalem 2.66 GHz	21.28	13.44
Water–coronene[b]	Intel Nehalem 2.66 GHz	36.64	24.48
Water–pentacene[a]	Intel Nehalem 2.66 GHz	231.12	44.55
Water–heptacene[a,c]	Intel Nehalem 2.66 GHz	545.40	104.65
Water–DBC[b,c]	Intel Nehalem 2.66 GHz	403.38	212.09
Water–nonacene[a,c]	Intel X5650 2.67 GHz	452.70	97.06
DF–MP2[a]			
Water–benzene	Intel Nehalem 2.66 GHz	0.24	0.37
Water–anthracene	Intel Nehalem 2.66 GHz	2.72	1.73
Water–pentacene	Intel Nehalem 2.66 GHz	12.12	4.81
Water–heptacene	Intel Nehalem 2.66 GHz	37.52	10.08
Water–nonacene	Intel Nehalem 2.66 GHz	167.24	16.88
DF–MP2–F12[a]			
Water–benzene	Intel Nehalem 2.66 GHz	1.16	14.21
Water–anthracene	Intel Nehalem 2.66 GHz	27.60	179.22
Water–pentacene	Intel Nehalem 2.66 GHz	115.93	907.88
CCSD(T)[a]			
Water–benzene	Intel Nehalem 2.66 GHz	28.80	130.95
Water–anthracene	Intel Nehalem 2.66 GHz	766.50	375.15
CCSD(T)–F12[d]			
Water–benzene	Intel Nehalem 2.66 GHz	30.56	37.14
Water–anthracene	Intel Nehalem 2.66 GHz	836.62	376.89

[a] aug-cc-pVTZ basis set
[b] A(2.0)VTZ basis set
[c] Not including the $\delta(\text{HF})$ correction
[d] cc-pVTZ-F12 basis set

D.3 NUMERICAL DATA FOR THE WATER HEXAMERS

The Tables D3–D16 tabulates the exact numerical data graphed in Figures B2–B9 from Appendix B.

Table D3: Net 2-body interaction energies for the water hexamers (in kcal mol^{-1}).

Method	Prism	Cage	Book	Ring
HF	−22.78	−22.80	−22.49	−21.68
BLYP	−26.61	−26.96	−26.56	−25.14
PBE	−37.27	−37.36	−35.65	−32.52
PW91	−41.32	−41.25	−39.21	−35.76
PBE0	−36.88	−36.91	−35.47	−33.00
B3LYP	−31.22	−31.47	−30.68	−28.92
MP2	−37.60	−37.57	−35.76	−33.01
CCSD(T)	−38.36	−38.15	−36.01	−32.93

Table D4: 2-body electrostatic interaction energies for the water hexamers (in kcal mol^{-1}).

Method	Prism	Cage	Book	Ring
HF	-22.78	-22.80	-22.49	-21.68
BLYP	-26.61	-26.96	-26.56	-25.14
PBE	-37.27	-37.36	-35.65	-32.52
PW91	-41.32	-41.25	-39.21	-35.76
PBE0	-36.88	-36.91	-35.47	-33.00
B3LYP	-31.22	-31.47	-30.68	-28.92
MP2	-37.60	-37.57	-35.76	-33.01
CCSD(T)	-38.36	-38.15	-36.01	-32.93

Table D5: 2-body exchange-repulsion interaction energies for the water hexamers (in kcal mol^{-1}).

Method	Prism	Cage	Book	Ring
HF	68.69	69.99	71.54	71.70
BLYP	104.86	105.12	102.97	99.27
PBE	85.64	86.39	86.69	85.68
PW91	83.12	83.95	84.49	83.76
PBE0	79.62	80.60	81.36	80.79
B3LYP	92.70	93.28	92.33	89.88
SAPT	78.98	80.05	80.88	80.03

Table D6: 2-body induction interaction energies for the water hexamers (in kcal mol^{-1}).

Method	Prism	Cage	Book	Ring
HF	−20.20	−21.22	−22.36	−22.77
BLYP	−30.91	−32.09	−32.71	−32.04
PBE	−31.15	−32.21	−32.66	−31.83
PW91	−31.74	−32.80	−33.33	−32.58
PBE0	−26.91	−27.92	−28.61	−28.29
B3LYP	−28.02	−29.18	−29.93	−29.52
SAPT	−20.96	−21.99	−23.11	−23.32

Table D7: 2-body polarization interaction energies for the water hexamers (in kcal mol^{-1}).

Method	Prism	Cage	Book	Ring
HF	−11.58	−12.11	−12.79	−13.09
BLYP	−12.25	−12.83	−13.49	−13.63
PBE	−12.65	−13.23	−13.86	−13.94
PW91	−8.96	−9.70	−10.69	−11.07
PBE0	−12.22	−12.79	−13.44	−13.57
B3LYP	−12.03	−12.60	−13.26	−13.43

Table D8: 2-body charge-transfer interaction energies for the water hexamers (in kcal mol^{-1}).

Method	Prism	Cage	Book	Ring
HF	−7.66	−8.19	−8.75	−9.00
BLYP	−17.37	−18.07	−18.15	−17.50
PBE	−17.14	−17.86	−17.98	−17.36
PW91	−17.00	−17.74	−17.91	−17.37
PBE0	−13.74	−14.43	−14.76	−14.51
B3LYP	−14.50	−15.18	−15.45	−15.11

Table D9: 2-body dispersion interaction energies for the water hexamers (in kcal mol^{-1}).

Method	Prism	Cage	Book	Ring
BLYP	−27.29	−26.84	−24.35	−21.84
PBE	−19.74	−19.65	−18.47	−17.16
PW91	−20.25	−20.10	−18.83	−17.37
PBE0	−18.52	−18.47	−17.52	−16.41
B3LYP	−23.45	−23.11	−21.06	−18.96
SAPT	−24.83	−24.50	−22.71	−20.72

Table D10: Net 3-body interaction energies for the water hexamers (in kcal mol^{-1}).

Method	Prism	Cage	Book	Ring
HF	−6.99	−7.10	−7.98	−9.41
BLYP	−8.21	−8.19	−9.47	−10.52
PBE	−4.84	−4.87	−6.99	−9.75
PW91	−1.77	−2.44	−5.39	−8.26
PBE0	−5.40	−5.68	−7.38	−9.34
B3LYP	−7.49	−7.37	−8.65	−10.28
MP2	−6.88	−6.96	−7.94	−9.36
CCSD(T)	−6.47	−6.59	−7.75	−9.30

Table D11: 3-body exchange-repulsion interaction energies for the water hexamers (in kcal mol^{-1}).

Method	Prism	Cage	Book	Ring
HF	−0.64	−0.44	−0.42	−0.44
BLYP	−3.15	−2.94	−2.04	−1.24
PBE	2.34	2.37	1.26	0.05
PW91	5.21	4.87	2.91	1.30
PBE0	1.42	1.27	0.58	−0.22
B3LYP	−2.33	−2.11	−1.41	−0.70
SAPT	−1.66	−1.62	−1.35	−1.13

Table D12: 3-body induction interaction energies for the water hexamers (in kcal mol^{-1}).

Method	Prism	Cage	Book	Ring
HF	−5.99	−6.16	−7.20	−8.70
BLYP	−7.12	−7.31	−8.42	−9.58
PBE	−6.48	−6.60	−7.84	−9.38
PW91	−6.37	−6.66	−7.80	−9.16
PBE0	−6.24	−6.47	−7.67	−8.94
B3LYP	−6.81	−6.91	−8.06	−9.44
SAPT	−5.29	−5.44	−6.58	−8.23

Table D13: 3-body polarization interaction energies for the water hexamers (in kcal mol^{-1}).

Method	Prism	Cage	Book	Ring
HF	−5.37	−5.45	−6.37	−7.76
BLYP	−5.37	−5.34	−6.16	−7.35
PBE	−5.40	−5.38	−6.20	−7.38
PW91	−5.71	−5.67	−6.46	−7.55
PBE0	−5.44	−5.45	−6.29	−7.53
B3LYP	−5.40	−5.40	−6.24	−7.49

Table D14: 3-body charge-transfer interaction energies for the water hexamers (in kcal mol^{-1}).

Method	Prism	Cage	Book	Ring
HF	−0.99	−1.07	−1.17	−1.19
BLYP	−2.20	−2.38	−2.54	−2.48
PBE	−2.14	−2.33	−2.52	−2.46
PW91	−2.12	−2.33	−2.50	−2.44
PBE0	−1.78	−1.94	−2.09	−2.06
B3LYP	−1.90	−2.05	−2.19	−2.15

Table D15: 3-body dispersion interaction energies for the water hexamers (in kcal mol^{-1}).

Method	Prism	Cage	Book	Ring
BLYP	2.12	2.04	0.93	0.28
PBE	−0.68	−0.59	−0.44	−0.34
PW91	−0.64	−0.64	−0.50	−0.54
PBE0	−0.65	−0.53	−0.30	−0.24
B3LYP	1.63	1.64	0.73	0.00
SAPT	0.79	0.76	0.45	0.16

Table D16: 4+5+6-body interaction energies for the water hexamers (in kcal mol^{-1}).

Method	Prism	Cage	Book	Ring
HF	-0.29	-0.25	-0.59	-1.19
BLYP	-0.27	-0.36	-0.70	-1.75
PBE	-1.07	-1.18	-1.34	-1.69
PW91	-2.38	-2.00	-1.70	-2.30
PBE0	-1.00	-0.87	-1.12	-1.77
B3LYP	-0.32	-0.47	-0.85	-1.50
MP2	-0.35	-0.32	-0.68	-1.38
CCSD(T)	-0.43	-0.38	-0.73	-1.41

APPENDIX E

SYMMETRY-ADAPTED PERTURBATION THEORY (SAPT)

E.1   INTRODUCTION

In the current document, extensive use of the symmetry-adapted perturbation theory (SAPT) method has been made. Our group has found SAPT to be a valuable tool for giving insight into the various physical components that make up the total interaction energy. In this Appendix, both the Hartree–Fock based SAPT [SAPT(HF)] and DFT based SAPT (DFT–SAPT) methods will be briefly outlined. For a more in-depth exposure to SAPT, I refer the reader to References 11–13 for SAPT(HF) and to References 2–4 for DFT–SAPT.

E.2   HF BASED SAPT [SAPT(HF)]

The interaction energy between two monomers (A and B) is typically calculated using the supermolecular method,

$$E_{int}^{AB} = E_{AB} - E_A - E_B, \qquad (E.1)$$

where E_{AB} is the total energy of the dimer and $E_{A/B}$ is the energy of monomer A/B. While Equation E.1 is applicable to any electronic structure method, it gives no physical insight into the nature of the interaction energy. However, since the interaction between two monomers is small, it can be

treated using perturbation theory. The Hamiltonian of the dimer system will be defined as

$$H_{AB} = F_A + W_A + F_B + W_B + V_{AB},$$ (E.2)

where $F_{A/B}$ is the Fock operator for monomer A/B, $W_{A/B}$ is the correlation operator for monomer A/B, and V_{AB} is the operator describing the interaction between the two monomers. Since W also tends to be small, an additional perturbation expansion can be done for monomers A and B. Thus, the perturbation expansion in SAPT involves three terms — V_{AB}, W_A, and W_B — which leads to an interaction energy that can be expressed as a triple sum,

$$E_{int} = \sum_n^\infty \sum_i^\infty \sum_j^\infty E_{pol}^{(nij)},$$ (E.3)

where the n, i, and j indices denotes the order in V_{AB}, W_A, and W_B, respectively. Here, the zeroth-order wavefunction of the dimer is taken as a product of the unperturbed wavefunctions of the individual monomers $\Phi_{AB} = \Phi_A \Phi_B$.[11,13] The expansion in Equation E.3 is commonly referred to as the polarization expansion, and hence the subscript *pol* in Equation E.3.[13,93]

The effects of electronic exchange between the two monomer charge densities has been neglected in Equation E.3. In the region of the potential energy minima the two monomer charge densities overlap, and thus exchange effects become important. Therefore the perturbation expansion in Equation E.3 needs to be modified to allow for electronic exchange between the two charge densities. Such a perturbation expansion is said to be *symmetry-adapted*, and is achieved by modifying the zeroth-order wavefunction by the application of an antisymmetrizer operator, $\mathscr{A}$, which exchanges electrons between the two monomers.[11] The zeroth-order wavefunction is now written as $\Phi_{AB} = \mathscr{A}\Phi_A\Phi_B$, and Equation E.3 becomes

$$E_{int}^{SAPT} = \sum_n^\infty \sum_i^\infty \sum_j^\infty \left(E_{pol}^{(nij)} + E_{exch}^{(nij)} \right),$$ (E.4)

where $E_{pol}^{(nij)}$ represents the terms arising from the polarization expansion and $E_{exch}^{(nij)}$ represents the terms arising from the application of the antisymmetrizer $\mathscr{A}$. In practice Equation E.4 is truncated at $n=2$ and $i+j=4$, which results in a perturbation expansion that is equivalent to fourth-order many-body perturbation theory (MBPT4).[11,13]

In the subsequent sections, the terms that arise from the expansion in the intermolecular potential, V_{AB}, will be briefly explained. As the terms arising from the correlation terms are rather complex, they will not be discussed here, and instead I will refer the reader to References [11]–[13] for further details on the intramonomer correlation terms.

E.2.1 Electrostatics

The first order polarization energy is[2,72]

$$E_{pol}^{(10)} = \langle \Phi_A^0 \Phi_B^0 | V_{AB} | \Phi_A^0 \Phi_B^0 \rangle, \tag{E.5}$$

where $\Phi_{A/B}$ is the unperturbed wavefunction of monomer A/B. A more physical representation of $E_{pol}^{(10)}$ can be obtained by expressing Equation E.5 in terms of the charge densities of monomer A/B,[13]

$$E_{pol}^{(10)} = \int \int \rho_A(\mathbf{r}_1) \frac{1}{\mathbf{r}_{12}} \rho_B(\mathbf{r}_2) \, d\mathbf{r}_1 d\mathbf{r}_2, \tag{E.6}$$

where the charge density $\rho_{A/B}$ is obtained by integrating over the coordinates of the all electrons in monomer A/B minus one. From Equation E.6 it is easily seen that $E_{pol}^{(10)}$ represents the interaction between two charge distributions; thus it is referred to as the electrostatic energy and is written as $E_{elst}^{(10)}$. In the limit of the asymptotic separation, $E_{elst}^{(10)}$ can be represented as a sum of the interacting permanent multipole moments.[11,13] However in the non-asymptotic region, $E_{elst}^{(10)}$ also contains charge-penetration effects,[93] which is discussed in Chapters 2–4 in connection with the water–acene interaction energies.

E.2.2 Exchange

The antisymmetrizer operator can be written as

$$\mathscr{A} = \frac{N_A! N_B!}{(N_A + N_B)!} \mathscr{A}_A \mathscr{A}_B (1 + \mathscr{P}), \tag{E.7}$$

where $N_{A/B}$ is the number of electrons in monomer A/B, $\mathscr{A}_{A/B}$ is the antisymmetrizer operator of monomer A/B, and $\mathscr{P}$ is the operator that exchanges electrons between the two monomers. The exchange operator, $\mathscr{P}$, can be expressed as a series expansion,

$$\mathscr{P} = \sum_{i=1}^{\infty} \mathscr{P}_i \qquad (E.8)$$

where $\mathscr{P}_i$ interchanges $i + 1$ electrons between the two monomers (*i.e.* $\mathscr{P}_1$ interchanges two electrons, $\mathscr{P}_2$ interchanges three electrons *etc.*)[13] Truncation of the series in Equation E.8 to $\mathscr{P}_i$ leads to Equation E.9 including overlap (S) terms up to S^{i+1}. The first-order exchange energy, $E_{exch}^{(10)}$, is written as[2,13]

$$E_{exch}^{(10)} = \frac{\langle \Phi_A^0 \Phi_B^0 | V - E_{elst}^{(10)} | \mathscr{P} \Phi_A^0 \Phi_B^0 \rangle}{1 + \langle \Phi_A^0 \Phi_B^0 | \mathscr{P} \Phi_A^0 \Phi_B^0 \rangle} \qquad (E.9)$$

where $\mathscr{P}$ is given in Equation E.8.

E.2.3 Induction and Exchange-Induction

The second-order terms in the SAPT expansion contains two contributions: one arising from single excitations and one arising from double excitations. These contributions are referred to as the induction and dispersion energy, respectively. The induction energy will be examined first.

Since single excitations can occur on either monomer A or monomer B, the induction energy can be written as[11,13,72]

$$E_{ind}^{(2)} = E_{ind}^{(2)}(A \rightarrow B) + E_{ind}^{(2)}(B \rightarrow A), \qquad (E.10)$$

where $E_{ind}^{(2)}(A \rightarrow B)$ denotes single excitations on B while A is in the ground state (a similar interpretation can also be made for $E_{ind}^{(2)}(B \rightarrow A)$). $E_{ind}^{(2)}(A \rightarrow B)$ is proportional to $\langle \Phi_A | \Omega_B^2 | \Phi_A \rangle$,[13] where Ω_B is the electrostatic potential arising from the permanent multipole moments on monomer B (*i.e.* monomer B is unperturbed). Thus, the induction energy represents the effect of polarization on one monomer *via* the static electric field from the permanent multipole moments of the other monomer.[13]

The exchange-induction term, $E_{exch-ind}^{(20)}$, represents the interchange of electrons between the two monomers while one monomer is perturbed by the static electric field of the other monomer.

Similar to $E_{exch}^{(10)}$, it involves the exchange operator given in Equation E.8, however the series expansion is truncated to $i = 1$.

E.2.4 Dispersion and Exchange-Dispersion

The dispersion energy is the remaining part of the second-order polarization energy, encompassing the terms arising from double excitations. Analogous to the MP2 energy,[158] the dispersion energy, $E_{disp}^{(20)}$, can be written as[4]

$$E_{disp}^{(20)} = -\sum_{a\neq 0}\sum_{b\neq 0} \frac{|\langle \Phi_A^a \Phi_B^b | V_{AB} | \Phi_A^a \Phi_B^b \rangle|^2}{E_A^a - E_A^0 + E_B^b - E_B^0}. \tag{E.11}$$

The dispersion energy represents instantaneous fluctuations in the charge distribution on both monomers[13,93] and from Equation E.11, it is seen that the dispersion energy is a pure correlation effect that would not be present in a Hartree–Fock treatment.[13,93] The second-order exchange-dispersion energy, $E_{exch-disp}^{(20)}$, represents the effect of electronic exchange during the mutual polarization of both monomers. Similar to $E_{exch-ind}^{(20)}$, the exchange operator in Equation E.8 is truncated to $i = 1$.

E.2.5 $\delta(\mathrm{HF})$

As mentioned in Section E.2, the series expansion in Equation E.4 is typically truncated at second-order in V_{AB}, which results in a complete neglect of third- and higher-order terms. Since the Hartree–Fock interaction energy can interpreted as being in infinite order in the intermolecular potential V_{AB},[303] a correction term can be introduced that represents the missing higher-order terms. The correction term is defined as

$$\delta(\mathrm{HF}) = E_{int}^{HF} - E_{elst}^{(10)} - E_{exch}^{(10)} - E_{ind}^{(20)} - E_{exch-ind}^{(20)}, \tag{E.12}$$

where E_{int}^{HF} is the Hartree–Fock interaction energy calculated using the supermolecular method presented in Equation E.1. As dispersion and exchange-dispersion does not appear in the Hartree–Fock interaction energy, the $\delta(\mathrm{HF})$ correction term is interpreted as the effect of third- and higher-order induction and exchange-induction effects.

E.3 DFT BASED SAPT (DFT–SAPT)

Despite the successes of SAPT(HF), the calculation of the correlation terms makes it computationally prohibitive for larger molecular systems. Williams and Chabalowski[75] suggested if a correlated description of the monomers was used, the costly correlation terms can be avoided. Due to computational considerations, Williams and Chabalowski suggested a DFT description of the monomers would be best suited. While their initial results were rather poor, refinements made by Heßelmann and Jansen[2–4] and Misquitta *et al.*[79] greatly improved on the accuracy of this method, allowing SAPT to be performed on much larger systems than previously allowed by SAPT(HF).

E.3.1 Electrostatics and Exchange

From Equation E.6, it is seen that $E_{elst}^{(10)}$ depends only on the electronic densities of the monomers. Since the electronic density is potentially exact within the framework of density functional theory (DFT) provided that the exact exchange-correlation functional is known, $E_{elst}^{(10)}$ can be calculated exactly. As the exact exchange-correlation functional is not currently known, an approximate exchange-correlation functional needs to be chosen. Heßelmann and Jansen,[2] and Misquitta and Szalewicz[78] found the PBE0[76] hybrid exchange-correlation functional best reproduces the first-order SAPT(HF) electrostatic energy when compared to other density functionals.

The addition of exact exchange in PBE0 is found to be necessary as a pure generalized gradient approximated (GGA) functional does not accurately reproduce the correct $\frac{1}{r}$ asymptotic behavior of the exact exchange-correlation functional. Despite the 25% Hartree–Fock exchange found in PBE0, the asymptotic behavior of the PBE0 exchange-correlation functional behaves as $\frac{1}{4r}$.[2] In order to ensure the correct $\frac{1}{r}$ asymptotic behavior, a fraction of the asymptotically correct LB94[80] density functional is added to the PBE0 density functional using the gradient-regulated connection scheme of Grüning *et al.*[81] The asymptotically corrected PBE0 functional is referred to as PBE0AC.[3]

Since Equation E.9 depends on the non-local operator product $V_{AB}\mathscr{P}$, $E_{exch}^{(10)}$ requires one- and two-electron density matrices[304] (as opposed to the one-electron density terms in $E_{elst}^{(10)}$). However,

144

as DFT is only able to provide one-electron density matrices,[305] the terms involving the two-electron matrix terms are neglected. Fortunately, the use of a one-electron density matrix is found to be a good approximation, and $E_{exch}^{(10)}$ can be calculated with minimal error.[2]

E.3.2 Induction and Exchange-Induction

Unfortunately, the SAPT(HF) expressions for $E_{ind}^{(20)}$ and $E_{exch-ind}^{(20)}$ do not allow for changes to occur in either the Coulomb or exchange-correlation potential due to induced changes in the electronic density. By using a coupled-perturbed Kohn–Sham (CPKS) approach, the perturbations in the electronic density caused by changes to the Coulomb and exchange-correlation potential can be accounted for through the use of density-density response functions,[306] which can then be used in the calculation of the $E_{ind}^{(20)}$ and $E_{exch-ind}^{(20)}$ terms.[3] As $E_{ind}^{(20)}$ depends on density-density response functions (which in turns depends on the density of the system in the presence of an external electric field), $E_{ind}^{(20)}$ can be calculated exactly, provided the exact exchange-correlation potential is known.[307] Analogous to the first-order exchange energy, $E_{exch-ind}^{(20)}$ depends on the operator product $V_{AB}\mathscr{P}$, which due to it's non-locality requires density-density response matrices, which are only a first-order approximation to the exact one- and two-electron density matrices caused by an external electric field. Therefore, while $E_{ind}^{(20)}$ is exact within the CPKS framework, $E_{exch-ind}^{(20)}$ is only an approximation within CPKS.[3]

E.3.3 Dispersion and Exchange-Dispersion

Similar to the second-order induction terms, a CPKS approach using density-density response functions is required for the calculation of the second-order dispersion terms.[4,306] Employing the integral transform of Casimir and Polder,[308] Equation E.11 can be written as a function of density-density response functions,

$$E_{disp}^{(2)} \propto \sum_{p \geq q} \sum_{r \geq s} \sum_{t \geq u} \sum_{v \geq w} \int_0^\infty \alpha_{pq,rs}^A(i\omega) \alpha_{tu,vw}^B(i\omega) d\omega, \qquad (\text{E.13})$$

145

where the $\alpha(\mathrm{i}\omega)$ terms are the frequency dependent linear response functions,[4]

$$\alpha(\mathrm{i}\omega) \propto \sum_{\mathrm{p}} \frac{2\omega_{\mathrm{p}}}{\omega^2 + \omega_{\mathrm{p}}^2}. \qquad (\text{E.14})$$

In Equation E.14, the ω_p are the eigenvalues of the product of two Hessian matrices from time-dependent DFT (TDDFT), which are calculated using the adiabatic local density approximation (ALDA)[307] for the exchange-correlation kernel. While ALDA is only an approximation to the exact exchange-correlation kernel, has been shown to give dispersion energies in excellent agreement with SAPT(HF).[4,72]

E.4 CONCLUSION

SAPT based on a density functional description of the monomers represents a huge savings in computational effort over conventional SAPT(HF). Further computational savings can be made by employing the density fitting (DF) approximation (also referred to as the resolution of the identity, or RI).[72,86] The use of density fitting within the DFT–SAPT framework has allowed the exploration of intermolecular systems whose size would have been prohibitive under the SAPT(HF) framework due it's $\mathrm{O}(\mathcal{N}^7)$ scaling. Recent work on adapting the density fitting approximation to both the zeroth-order and correlation corrections in SAPT(HF) has also recently emerged,[309,310] in addition to an efficient algorithm for evaluating the triple excitation terms found in the correlated SAPT(HF) treatment.[311] Early results suggest that this is a very promising extension of the SAPT(HF) framework, with systems as large as the pentacene dimer being studied with these approximations.

APPENDIX F

COMMONLY USED ABBREVIATIONS

Table F1: List of commonly used abbreviations

Abbreviation	Meaning
ALMO–EDA	Absolutely localized molecular orbital energy decomposition analysis
AVDZ	Dunning's aug-cc-pVDZ basis set
AVTZ	Dunning's aug-cc-pVTZ basis set
AVTZ(-f)	AVTZ basis set with f functions removed from heavy atoms and d functions from light atoms
AVQZ	Dunning's aug-cc-pVQZ basis set
AV5Z	Dunning's aug-cc-pV5Z basis set
CCSD	Coupled cluster using iterative singles and doubles
CCSD(T)	Coupled cluster using iterative singles and doubles with perturbative triples
δ(HF)	Hartree–Fock correction term for SAPT
DF	Density fitting. Identical to resolution of the identity (RI)
DF–DFT–SAPT	DFT based SAPT of Heßelmann $et\ al.$[2–4] with density fitting[72]
DFT	Density functional theory
DFT+D2	Grimme's second-generation dispersion correction for DFT[115]
DFT+D3	Grimme and co-worker's third-generation dispersion correction for DFT[155]
DFT/CC	Rubeš $et\ al.$[112, 161] coupled cluster correction method for DFT
DFT–SAPT	DFT based SAPT of Heßelmann $et\ al.$[2–4]
Disp	2nd–order dispersion interaction
DMA	Distributed multipole analysis
DPP	Distributed point polarizable model of DeFusco $et\ al.$[10]
DPP2	second-generation DPP model covered in Appendix C
EDA	Energy decomposition analysis
Elst	1st-order electrostatics interaction
Exch	1st-order exchange interaction
Exch-Disp	2nd-order exchange–dispersion interaction
Exch-Ind	2nd-order exchange–induction interaction
FDDS	frequency-dependent density susceptibilities
GDMA	Gaussian distributed multipole analysis
HF	Hartree–Fock

Ind	2nd-order induction interactions
LMO–EDA	Localized molecular orbital energy decomposition analysis
MP2	Möller–Plesset 2nd–order perturbation theory
MBPTn	Many-body perturbation theory through order n
RI	Resolution of the identity. Identical to density fitting (DF).
SAPT	Symmetry-adapted perturbation theory
SAPT(DFT)	DFT based SAPT of Misquitta *et al.*[77–79]
Tr-AVTZ	Truncated AVTZ basis set as described in Section 3.3

BIBLIOGRAPHY

[1] Feller, D. and and Jordan, K. D. *J. Phys. Chem. A*, **2000**, *104*, 9971–9975.

[2] Heßelmann, A. and Jansen, G. *Chem. Phys. Lett.*, **2002**, *357*, 464–470.

[3] Heßelmann, A. and Jansen, G. *Chem. Phys. Lett.*, **2002**, *362*, 319–325.

[4] Heßelmann, A. and Jansen, G. *Chem. Phys. Lett.*, **2003**, *367*, 778–784.

[5] Kurth, S. and Perdew, J. P. *Phys. Rev. B*, **1999**, *59*, 10461–10468.

[6] Yan, Z.; Perdew, J. P.; Kurth, S. *Phys. Rev. B*, **2000**, *61*, 16430–16439.

[7] Ren, X. and Blum, V. Private Communication, **2010**.

[8] Su, P. and Li, H. *J. Chem. Phys.*, **2009**, *131*, 014102.

[9] Khaliullin, R. Z.; Bell, A. T.; Head-Gordon, M. *J. Chem. Phys.*, **2008**, *128*, 184112.

[10] Defusco, A.; Schofield, D.; Jordan, K. D. *Mol. Phys.*, **2007**, *105*, 2681.

[11] Rybak, S.; Jeziorski, B.; Szalewicz, K. *J. Chem. Phys.*, **1991**, *95*, 6576–6601.

[12] Jeziorski, B.; Moszynski, R.; Ratkiewicz, A.; Rybak, S.; Szalewicz, K.; and Williams, H. L. In Clementi, E. , editor, *Method and Techniques in Computational and Chemistry: METECC94*, Volume B, pages 79–129. STEF: Cagliari, Italy, 1993.

[13] Jeziorski, B.; Moszynski, R.; Szalewicz, K. *Chem. Rev.*, **1994**, *94*, 1887–1930.

[14] Kolesnikov, A. I.; Zanotti, J.-M.; Loong, C.-K.; Thiyagarajan, P.; and Moravsky, A. P.; Loutfy, R. O.; Burnham, C. J. *Phys. Rev. Lett.*, **2004**, *93*, 035503.

[15] Koga, K.; Gao, G. T.; Tanaka, H.; Zeng, X. C. *Nature*, **2001**, *412*, 802.

[16] Werder, T.; Walther, J. H.; Jaffe, R. L.; Halicioglu, T.; Noca, F.; and Koumoutsakos, P. *Nano Lett.*, **2001**, *1*, 697–702.

[17] Hummer, G.; Rasaiah, J. C.; Noworyta, J. P. *Nature*, **2001**, *414*, 188.

[18] Noon, W. H.; Ausman, K. D.; Smalley, R. E.; Ma, J. *Chem. Phys. Lett.*, **2002**, *355*, 445–448.

[19] Mamontov, E.; Burnham, C. J.; Chen, S.-H.; Moravsky, A. P.; Loong, C.-K.; and de Souza, N. R.; Kolesnikov, A. I. *J. Chem. Phys.*, **2006**, *124*, 194703.

[20] Holt, J. K.; Park, H. G.; Wang, Y.; Stadermann, M.; Artyukhin, A. B.; and Grigoropoulos, C. P.; Noy, A.; Bakajin, O. *Science*, **2006**, *312*, 1034–1037.

[21] Kolesnikov, A.; Loong, C.-K.; de Souza, N.; Burnham, C.; Moravsky, A. *Physica B: Condensed Matter*, **2006**, *385-386*, 272 – and 274. Proceedings of the Eighth International Conference on Neutron and Scattering.

[22] Sinha, S.; Rossi, M. P.; Mattia, D.; Gogotsi, Y.; Bau, H. H. *Physics of Fluids*, **2007**, *19*, 013603.

[23] Whitby, M.; Cagnon, L.; Thanou, M.; Quirke, N. *Nano Lett.*, **2008**, *8*, 2632–2637.

[24] Köfinger, J.; Hummer, G.; Dellago, C. *Proc. Natl. Acad. Sci.*, **2008**, *105*, 132–18–13222.

[25] Barber, A. H.; Cohen, S. R.; Wagner, H. D. *Phys. Rev. B*, **2005**, *71*, 115443.

[26] Avgul, N. N. and Kiselev, A. V. In Jr., P. L. W. , editor, *Chemistry and Physics of Carbon*, and volume 6, pages 1–124. Dekker: New York, 1970.

[27] Markovic, N.; Andersson, P. U.; Någård, M. B.; Pettersson, J. B. C. and . *Chem. Phys.*, **1999**, *247*, 413–430.

[28] Chakarov, D. V.; Oesterlund, L.; Kasemo, B. *Langmuir*, **1995**, *11*, 1201–1214.

[29] Vernov, A. and Steele, W. A. *Langmuir*, **1992**, *8*, 155–159.

[30] Karapetian, K. and Jordan, K. D. *Water in Confining Geometries*, pages 139–150. Springer-Verlag, 2003.

[31] Pertsin, A. and Grunze, M. *J. Phys. Chem. B*, **2004**, *108*, 1357–1364.

[32] Pertsin, A. and Grunze, M. *J. Chem. Phys.*, **2006**, *125*, 114707.

[33] Zhao, X. and Johnson, J. K. *Mol. Sim.*, **2005**, *31*, 1–10.

[34] Thomas, J. A. and McGaughey, A. J. H. *J. Chem. Phys.*, **2007**, *126*, 034707.

[35] Birkett, G. R. and Do, D. D. *J. Phys. Chem. C*, **2007**, *111*, 5735–5742.

[36] González, B. S.; Hernández-Rojas, J.; Bretó, J.; Gomez Llorente, J. M. and . *J. Phys. Chem. C*, **2007**, *111*, 14862–14869.

[37] Gordillo, M. C. and Martí, J. *Chem. Phys. Lett.*, **2000**, *329*, 341–345.

[38] Walther, J. H.; Jaffe, R.; Halicioglu, T.; Koumoutsakos, P. *J. Phys. Chem. B*, **2001**, *105*, 9980–9987.

[39] Koga, K.; Gao, G. T.; Tanaka, H.; Zeng, X. C. *Physica A: Statistical Mechanics and its Applications*, **and 2002**, *314*, 462–469.

[40] Werder, T.; Walther, J. H.; Jaffe, R. L.; Halicioglu, T.; Koumoutsakos, P. and . *J. Phys. Chem. B*, **2003**, *107*, 1345–1352.

[41] Bushuev, Y.; Davletbaeva, S.; Muguet, F. F. *Sensors*, **2005**, *5*, 139–147.

[42] Thomas, J. A. and McGaughey, A. J. H. *J. Chem. Phys.*, **2008**, *128*, 084715.

[43] Arai, N.; Yasuoka, K.; Zeng, X. C. *J. Am. Chem. Soc.*, **2008**, *130*, 7916–7920.

[44] Rasaiah, J. C.; Garde, S.; Hummer, G. *Annu. Rev. Chem. Phys.*, **2008**, *59*, 713.

[45] Alexiadis, A. and Kassinos, S. *Chem. Rev.*, **2008**, *108*, 5014–5034.

[46] Nanok, T.; Artrith, N.; Pantu, P.; Bopp, P. A.; Limtrakul, J. *J. Phys. Chem. A*, **2009**, *113*, 2103–2108.

[47] Wehling, T. O.; Lichtenstein, A. I.; Katsnelson, M. I. *App. Phys. Lett.*, **2008**, *93*, 202110.

[48] Leenaerts, O.; Partoens, B.; Peeters, F. M. *Phys. Rev. B*, **2008**, *77*, 125416.

[49] Benedict, L. X.; Louie, S. G.; Cohen, M. L. *Phys. Rev. B*, **1995**, *52*, 8541–8549.

[50] Andersson, Y.; Langreth, D. C.; Lundqvist, B. I. *Phys. Rev. Lett.*, **1996**, *76*, 102–105.

[51] Hult, E.; Andersson, Y.; Lundqvist, B. I.; Langreth, D. C. *Phys. Rev. Lett.*, **1996**, *77*, 2029–2032.

[52] Kohn, W.; Meir, Y.; Makarov, D. E. *Phys. Rev. Lett.*, **1998**, *80*, 4153–4156.

[53] van Mourik, T. and Gdanitz, R. J. *J. Chem. Phys.*, **2002**, *116*, 9620–9623.

[54] Cybulski, S. M. and Seversen, C. E. *J. Chem. Phys.*, **2003**, *119*, 12704–12707.

[55] Zhao, Y. and Truhlar, D. G. *J. Chem. Theory Comput.*, **2005**, *1*, 415–432.

[56] Johnson, E. R. and Becke, A. D. *J. Chem. Phys.*, **2006**, *124*, 174104.

[57] Alonso, J. and Mañanes, A. *Theo. Chem. Acc.*, **2007**, *117*, 467–472.

[58] Silvestrelli, P. L. *Phys. Rev. Lett.*, **2008**, *100*, 053002.

[59] Grimme, S. *J. Chem. Phys.*, **2006**, *124*, 034108.

[60] Grimme, S.; Máck-Lichtenfeld, C.; Antony, J. *J. Phys. Chem. C*, **2007**, *111*, 11199–11207.

[61] Lin, I.-C. and Rothlisberger, U. *Phys. Chem. Chem. Phys.*, **2008**, *10*, 2730–2734.

[62] Rubes, M. and Bludsky, O. *Phys. Chem. Chem. Phys.*, **2008**, *10*, 2611–2615.

[63] Boys, S. F. and Bernardi, F. *Mol. Phys.*, **1970**, *19*, 553–566.

[64] Hobza, P.; Selzle, H. L.; Schlag, E. W. *J. Phys. Chem.*, **1996**, *100*, 18790–18794.

[65] Tsuzuki, S.; Uchimaru, T.; Matsumura, K.; Mikami, M.; Tanabe, K. *Chem. Phys. Lett.*, **2000**, *319*, 547–554.

[66] Tsuzuki, S.; Honda, K.; Uchimaru, T.; Mikami, M.; Tanabe, K. *J. Am. Chem. Soc.*, **2002**, *124*, 104–112.

[67] Sinnokrot, M. O.; Valeev, E. F.; Sherrill, C. D. *J. Am. Chem. Soc.*, **2002**, *124*, 10887–10893.

[68] Sinnokrot, M. O. and Sherrill, C. D. *J. Phys. Chem. A*, **2004**, *108*, 10200–10207.

[69] Podeszwa, R.; Bukowski, R.; Szalewicz, K. *J. Phys. Chem. A*, **2006**, *110*, 10345–10354.

[70] Sudiarta, I. W. and Geldart, D. J. W. *J. Phys. Chem. A*, **2006**, *110*, 10501–10506.

[71] Tsuzuki, S.; Uchimaru, T.; Mikami, M.; Tanabe, K. *Chem. Phys. Lett.*, **1996**, *252*, 206–210.

[72] Heßelmann, A.; Jansen, G.; Schütz, M. *J. Chem. Phys.*, **2005**, *122*, 014103.

[73] Werner, H.-J.; Knowles, P. J.; Lindh, R.; Manby, F. R.; Schütz, M.; and Celani, P.; Korona, T.; Mitrushenkov, A.; Rauhut, G.; Adler, T. B.; and Amos, R. D.; Bernhardsson, A.; Berning, A.; Cooper, D. L.; Deegan, M. and J. O.; Dobbyn, A. J.; Eckert, F.; Goll, E.; Hampel, C.; Hetzer, G.; and Hrenar, T.; Knizia, G.; Köppl, C.; Liu, Y.; Lloyd, A. W.; Mata, R. A. ; May, A. J.; McNicholas, S. J.; Meyer, W.; Mura, M. E.; Nicklass, A.; and Palmieri, P.; Pflüger, K.; Pitzer, R.; Reiher, M.; Schumann, U.; and Stoll, H.; Stone, A. J.; Tarroni, R.; Thorsteinsson, T.; Wang, M.; Wolf, and A. Molpro, Version 2009.1, A Package of Ab Initio Programs, 2009. see www.molpro.net.

[74] Kendall, R. A.; Thom H. Dunning, J.; Harrison, R. J. *J. Chem. Phys.*, **1992**, *96*, 6796–6806.

[75] Williams, H. L. and Chabalowski, C. F. *J. Phys. Chem. A*, **2001**, *105*, 646–659.

[76] Adamo, C. and Barone, V. *J. Chem. Phys.*, **1999**, *110*, 6158–6170.

[77] Misquitta, A. J.; Jeziorski, B.; Szalewicz, K. *Phys. Rev. Lett.*, **2003**, *91*, 033201.

[78] Misquitta, A. J. and Szalewicz, K. *J. Chem. Phys.*, **2005**, *122*, 214109.

[79] Misquitta, A. J.; Podeszwa, R.; Jeziorski, B.; Szalewicz, K. *J. Chem. Phys.*, **2005**, *123*, 214103.

[80] van Leeuwen, R. and Baerends, E. J. *Phys. Rev. A*, **1994**, *49*, 2421–2431.

[81] Grüning, M.; Gritsenko, O. V.; van Gisbergen, S. J. A.; Baerends, E. J. and . *J. Chem. Phys.*, **2001**, *114*, 652–660.

[82] Lias, S. G. Ionization energy evaluation. NIST Chemistry Webbook, NIST Standard and Reference Database No. 69. http://webbook.nist.gov.

[83] http://astrochemistry.ca.astro.it/database/circumcoronene/circumcoronene.html.

[84] Podeszwa, R. and Szalewicz, K. *Chem. Phys. Lett.*, **2005**, *412*, 488–493.

[85] Bukowski, R.; Podeszwa, R.; Szalewicz, K. *Chem. Phys. Lett.*, **2005**, *414*, 111–116.

[86] Podeszwa, R.; Bukowski, R.; Szalewicz, K. *J. Chem. Theory Comput.*, **2006**, *2*, 400–412.

[87] Vahtras, O.; Almlf, J.; Feyereisen, M. *Chem. Phys. Lett.*, **1993**, *213*, 514–518.

[88] Weigend, F. *Phys. Chem. Chem. Phys.*, **2002**, *4*, 4285.

[89] Weigend, F.; Köhn, A.; Hättig, C. *J. Chem. Phys.*, **2002**, *116*, 3175–3183.

[90] Sala, F. D. and Görling, A. *J. Chem. Phys.*, **2001**, *115*, 5718–5732.

[91] King, H. W. *CRC Handbook of Chemistry and Physics*, pages 12.15–12.18. CRC Press, 88th edition, 2007.

[92] Benedict, W. S.; Gailar, N.; Plyler, E. K. *J. Chem. Phys.*, **1956**, *24*, 1139–1165.

[93] Stone, A. J. *The Theory of Intermolecular Forces*. Oxford University Press, Oxford, U. K., 2002 edition, 1996.

[94] Dang, L. X. and Chang, T.-M. *J. Chem. Phys.*, **1997**, *106*, 8149–8159.

[95] Raghavachari, K.; Trucks, G. W.; Pople, J. A.; Head-Gordon, M. *Chem. Phys. Lett.*, **1989**, *157*, 479–483.

[96] Zhao, Y.; Tishchenko, O.; Truhlar, D. G. *J. Phys. Chem. B*, **2005**, *109*, 19046–19051.

[97] Xu, X. and Jordan, K. D. *Unpublished*, **2009**.

[98] Feller, D. *J. Phys. Chem. A*, **1999**, *103*, 7558–7561.

[99] Courty, A.; Mons, M.; Dimicoli, I.; Piuzzi, F.; Gaigeot, M.-P.; Brenner, and V.; de Pujo, P.; Millie, P. *J. Phys. Chem. A*, **1998**, *102*, 6590–6600.

[100] Stone, A. *Chem. Phys. Lett.*, **1981**, *83*, 233–239.

[101] Price, S. L. and Stone, A. J. *Chem. Phys. Lett.*, **1983**, *98*, 419–423.

[102] Price, S. L.; Stone, A. J.; Alderton, M. *Mol. Phys.*, **1984**, *52*, 987.

[103] Stone, A. J. *J. Chem. Theory Comp.*, **2005**, *1*, 1128.

[104] Frisch, M. J.; Trucks, G. W.; Schlegel, H. B.; Scuseria, G. E.; Robb, M. A. ; Cheeseman, J. R.; Montgomery, J. A.; Vreven, T.; Kudin, K. N.; Burant, and J. C.; Millam, J. M.; Iyengar, S. S.; Tomasi, J.; Barone, V.; Mennucci, and B.; Cossi, M.; Scalmani, G.; Rega, N.; Petersson, G. A.; Nakatsuji, H.; and Hada, M.; Ehara, M.; Toyota, K.; Fukuda, R.; Hasegawa, J.; Ishida, M.; and Nakajima, T.; Honda, Y.; Kitao, O.; Nakai, H.; Klene, M.; Li, X.; Knox, and J. E.; Hratchian, H. P.; Cross, J. B.; Bakken, V.; Adamo, C.; Jaramillo, and J.; Gomperts, R.; Stratmann, R. E.; Yazyev, O.; Austin, A. J.; Cammi, R. ; Pomelli, C.; Ochterski, J. W.; Ayala, P. Y.; Morokuma, K.; Voth, G. A. ; Salvador, P.; Dannenberg, J. J.; Zakrzewski, V. G.; Dapprich, S.; and Daniels, A. D.; Strain, M. C.; Farkas, O.; Malick, D. K.; Rabuck, A. D.; and Raghavachari, K.; Foresman, J. B.; Ortiz, J. V.; Cui, Q.; Baboul, A. G.; and Clifford, S.; Cioslowski, J.; Stefanov, B. B.; Liu, G.; Liashenko, A.; and Piskorz, P.; Komaromi, I.; Martin, R. L.; Fox, D. J.; Keith, T.; and Al-Laham, M. A.; Peng, C. Y.; Nanayakkara, A.; Challacombe, M.; Gill, P. and M. W.; Johnson, B.; Chen, W.; Wong, M. W.; Gonzalez, C.; Pople, J. A. Gaussian 03, Revision C.02. Gaussian, Inc., Wallingford, CT, 2004.

[105] Kairys, V. and Jensen, J. H. *Chem. Phys. Lett.*, **1999**, *315*, 140–144.

[106] Dang, L. X. and Feller, D. *J. Phys. Chem. B*, **2000**, *104*, 4403–4407.

[107] Ren, P. and Ponder, J. W. *J. Phys. Chem. B*, **2003**, *107*, 5933–5947.

[108] Jorgensen, W. L. and Madura, J. D. *Mol. Phys.*, **1985**, *56*, 1381.

[109] Whitehouse, D. B. and Buckingham, A. D. *J. Chem. Soc. Faraday Trans.*, **1993**, *89*, 1909–1913.

[110] Ponder, J. W. Tinker. Software Tools for Molecular Design, Version 4.2, 2004. see http://dasher.wast.edu/tinker1.

[111] Shao, Y.; Fusti-Molnar, L.; Jung, Y.; Kussmann, J.; Ochsenfeld, C.; Brown, and S. T.; Gilbert, A. T. B.; Slipchenko, L. V.; Levchenko, S. V.; O'Neill, and D. P.; Jr., R. A. D.; Lochan, R. C.; Wangand, T.; Beran, G. J. O.; and Besley, N. A.; Herbert, J. M.; Lin, C. Y.; Voorhis, T. V.; Chien, S. H.; and Sodt, A.; Steele, R. P.; Rassolov, V. A.; Maslen, P. E.; Korambath, P. P. ; amd B. Austin, R. D. A.; Baker, J.; Byrd, E. F. C.; Dachsel, H.; and Doerksen, R. J.; Dreuw, A.; Dunietz, B. D.; Dutoi, A. D.; Furlani, T. R. ; Gwaltney, S. R.; Heyden, A.; Hirata, S.; Hsu, C.-P.; Kedziora, G.; and Khalliulin, R. Z.; Klunzinger, P.; Lee, A. M.; Lee, M. S.; Liang, W.; and Lotan, I.; Nair, N.; Peters, B.; Proynov, E. I.; Pieniazek, P. A.; Rhee, and Y. M.; Ritchie, J.; Rosta, E.; Sherrill, C. D.; Simmonett, A. C.; and Subotnik, J. E.; III, H. L. W.; Zhang, W.; Bell, A. T.; Chakraborty, and A. K.; Chipman, D. M.; Keil, F. J.; Warshel, A.; Hehre, W. J.; III, H. and F. S.; Kong, J.; Krylov, A. I.; Gill, P. M. W.; Head-Gordon, M. *Phys. Chem. Chem. Phys.*, **2006**, *8*, 3172–3191.

[112] Rubeš, M.; Nachtigall, P.; Vondrášek, J.; Bludský, O. *J. Phys. Chem. C*, **2009**, *113*, 8412–8419.

[113] Jenness, G. R. and Jordan, K. D. *J. Phys. Chem. C*, **2009**, *113*, 10242–10248.

[114] Grimme, S. *J. Comp. Chem.*, **2004**, *25*, 1463–1473.

[115] Grimme, S. *J. Comp. Chem.*, **2006**, *27*, 1787–1799.

[116] Tkatchenko, A. and Scheffler, M. *Phys. Rev. Lett.*, **2009**, *102*, 073005.

[117] Silvestrelli, P. L.; Benyahia, K.; Grubisiê, S.; Ancilotto, F.; Toigo, and F. *J. Chem. Phys.*, **2009**, *130*, 074702.

[118] von Lilienfeld, O. A.; Tavernelli, I.; Rothlisberger, U.; Sebastiani, D. *Phys. Rev. Lett.*, **2004**, *93*, 153004.

[119] Lin, I.-C.; Coutinho-Neto, M. D.; Felsenheimer, C.; von Lilienfeld, O. A.; and Tavernelli, I.; Rothlisberger, U. *Phys. Rev. B*, **2007**, *75*, 205131.

[120] Tavernelli, I.; Lin, I.-C.; Rothlisberger, U. *Phys. Rev. B*, **2009**, *79*, 045106.

[121] Zhao, Y. and Truhlar, D. G. *Theo. Chim. Acta*, **2008**, *120*, 215–241.

[122] Dion, M.; Rydberg, H.; Schröder, E.; Langreth, D. C.; Lundqvist, B. I. *Phys. Rev. Lett.*, **2004**, *92*, 246401.

[123] Wang, F.; Jenness, G.; Al-Saidi, W. A.; Jordan, K. D. *J. Chem. Phys.*, **2010**, *132*, 134303.

[124] van Gisbergen, S. J. A.; Schipper, P. R. T.; Gritsenko, O. V.; Baerends, and E. J.; Snijders, J. G.; Champagne, B.; Kirtman, B. *Phys. Rev. Lett.*, **1999**, *83*, 694–697.

[125] Cybulski, S. M. and Lytle, M. L. *J. Chem. Phys.*, **2007**, *127*, 141102.

[126] Jurecka, P.; Šponer, J.; Černý, J.; Hobza, P. *Phys. Chem. Chem. Phys.*, **2006**, *8*, 1985–1993.

[127] Grimme, S. *J. Chem. Phys.*, **2003**, *118*, 9095–9102.

[128] Antony, J. and Grimme, S. *J. Phys. Chem. A*, **2007**, *111*, 4862–4868.

[129] Tkatchenko, A.; Robert A. DiStasio, J.; Head-Gordon, M.; Scheffler, M. *J. Chem. Phys.*, **2009**, *131*, 094106.

[130] Pitoňák, M. and Hesselmann, A. *J. Chem. Theory Comput.*, **2010**, *6*, 168–178.

[131] Hermann, A. and Schwerdtfeger, P. *J. Chem. Phys.*, **2009**, *131*, 244508.

[132] Schmidt, M. W.; Baldridge, K. K.; Boatz, J. A.; Elbert, S. T.; Gordon, and M. S.; Jensen, J. H.; Koseki, S.; Matsunaga, N.; Nguyen, K. A.; Su, S.; and Windus, T. L.; Dupuis, M.; Jr, J. A. M. *J. Comp. Chem.*, **1993**, *14*, 1347–1363.

[133] CPMD v3.13 Copyright IBM Corp 1990-2008, Copyright MPI Fuer and Festkoerper-forschung Stuttgart 1997-2001.

[134] Blum, V.; Gehrke, R.; Hanke, F.; Havu, P.; Havu, V.; Ren, X.; Reuter, K. ; Scheffler, M. *Comp. Phys. Comm.*, **2009**, *180*, 2175–2196.

[135] Reyes, A.; Fomina, L.; Rumsh, L.; Fomine, S. *Int. J. Quant. Chem.*, **2007**, *104*, 335–341.

[136] Cabaleiro-Lago, E. M.; Carrazana-García, J. A.; Rodríguez-Otero, J. and . *J. Chem. Phys.*, **2009**, *130*, 234307.

[137] Huff, E. M. and Pulay, P. *Mol. Phys.*, **2009**, *107*, 1197–1207.

[138] Heßelmann, A. and Jansen, G. *Phys. Chem. Chem. Phys.*, **2003**, *5*, 5010–5014.

[139] Tekin, A. and Jansen, G. *Phys. Chem. Chem. Phys.*, **2007**, *9*, 1680–1687.

[140] Goedecker, S.; Teter, M.; Hutter, J. *Phys. Rev. B*, **1996**, *54*, 1703–1710.

[141] Peverati, R. and Baldridge, K. K. *J. Chem. Theory Comp.*, **2008**, *4*, 2030–2048.

[142] Perdew, J. P.; Burke, K.; Ernzerhof, M. *Phys. Rev. Lett.*, **1996**, *77*, 3865–3868.

[143] Becke, A. D. *Phys. Rev. A*, **1988**, *38*, 3098–3100.

[144] Lee, C.; Yang, W.; Parr, R. G. *Phys. Rev. B*, **1988**, *37*, 785–789.

[145] Becke, A. D. *J. Chem. Phys.*, **1997**, *107*, 8554–8560.

[146] Hirshfeld, F. L. *Theo. Chim. Acta*, **1977**, *44*, 129–138.

[147] Havu, V.; Blum, V.; Havu, P.; Scheffler, M. *J. Comp. Phys.*, **2009**, *228*, 8367–8379.

[148] Applequist, J. *J. Phys. Chem.*, **1993**, *97*, 6016–6023.

[149] Dehez, F.; Soetens, J.-C.; Chipot, C.; Angyan, J. G.; Millot, C. *J. Phys. Chem. A*, **2000**, *104*, 1293–1303.

[150] Jenness, G.; Karalti, O.; Jordan, K. D. *Phys. Chem. Chem. Phys.*, **2010**, *12*, 6375–6381.

[151] Allen, M. J.; Tung, V. C.; Kaner, R. B. *Chem. Rev.*, **2010**, *110*, 132–145.

[152] Rubeš, M.; Kysilka, J.; Nachtigall, P.; Bludský, O. *Phys. Chem. Chem. Phys.*, **2010**, *12*, 6438–6444.

[153] Forte, G.; Grassi, A.; Lombardo, G. M.; Angilella, G. G. N.; March, N. H.; and Pucci, R. *Phys. Chem. Liq.*, **2009**, *47*, 599–606.

[154] Lin, C. S.; Zhang, R. Q.; Lee, S. T.; Elstner, M.; Frauenheim, T.; Wan, and L. J. *J. Phys. Chem. B*, **2005**, *109*, 14183–14188.

[155] Grimme, S.; Antony, J.; Ehrlich, S.; Krieg, H. *J. Chem. Phys.*, **2010**, *132*, 154104.

[156] Langreth, D. C.; Lundqvist, B. I.; Chakarova-Käck, S. D.; Cooper, V. R.; and Dion, M.; Hyldgaard, P.; Kelkkanen, A.; Kleis, J.; Kong, L.; Li, S.; and Moses, P. G.; Murray, E.; Puzder, A.; Rydberg, H.; Schrder, E.; and Thonhauser, T. *J. of Phys.*, **2009**, *21*, 084203.

[157] Lee, K.; Murray, E. D.; Kong, L.; Lundqvist, B. I.; Langreth, D. C. *Phys. Rev. B*, **2010**, *82*, 081101.

[158] Szabo, A. and Ostlund, N. S. *Modern Quantum Chemistry: Introduction to Advanced Electronic and Structure Theory*. Dover Publications, Inc., 1996.

[159] Hampel, C.; Peterson, K. A.; Werner, H.-J. *Chem. Phys. Lett.*, **1992**, *190*, 1–12.

[160] Deegan, M. J. O. and Knowles, P. J. *Chem. Phys. Lett.*, **1994**, *227*, 321–326.

[161] Rubeš, M.; Soldán, P.; Nachtigall, P.; Bludský, O. *O. Chem. Phys. J.*, **2008**, *1*, 1–11.

[162] Kresse, G. and Hafner, J. *Phys. Rev. B*, **1993**, *47*, 558–561.

[163] Kresse, G. and Hafner, J. *Phys. Rev. B*, **1994**, *49*, 14251–14269.

[164] Kresse, G. and Furthmller, J. *Comput. Mat. Sci.*, **1996**, *6*, 15.

[165] Kresse, G. and Furthmüller, J. *Phys. Rev. B*, **1996**, *54*, 11169–11186.

[166] Román-Pérez, G. and Soler, J. M. *Phys. Rev. Lett.*, **2009**, *103*, 096102.

[167] Thom H. Dunning, J. *J. Chem. Phys.*, **1989**, *90*, 1007–1023.

[168] Werner, H.-J.; Adler, T. B.; Manby, F. R. *J. Chem. Phys.*, **2007**, *126*, 164102.

[169] Adler, T. B.; Knizia, G.; Werner, H.-J. *J. Chem. Phys.*, **2007**, *127*, 221106.

[170] Knizia, G.; Adler, T. B.; Werner, H.-J. *J. Chem. Phys.*, **2009**, *130*, 054104.

[171] Riley, K. E.; Pitoňák, M.; Jurečka, P.; Hobza, P. *Chem. Rev.*, **2010**, 5023–5063.

[172] Heßelmann, A. *J. Chem. Phys.*, **2008**, *128*, 144112.

[173] Heßelmann, A. *Private Communication*, **2010**.

[174] Peterson, K. A.; Adler, T. B.; Werner, H.-J. *J. Chem. Phys.*, **2008**, *128*, 084102.

[175] Pople, J. A.; Head-Gordon, M.; Raghavachari, K. *J. Chem. Phys.*, **1987**, *87*, 5968–5975.

[176] Koopmans, T. *Physica*, **1934**, *1*, 104–113.

[177] Zhang, Y. and Yang, W. *Phys. Rev. Lett.*, **1998**, *80*, 890.

[178] Bludský, O.; Rubeš, M.; Soldán, P.; Nachtigall, P. *J. Chem. Phys.*, **2008**, *128*, 114102.

[179] Perdew, J. P. *Phys. Rev. B*, **1986**, *33*, 8822–8824.

[180] Murray, E. D.; Lee, K.; Langreth, D. C. *J. Chem. Theory Comput.*, **2009**, *5*, 2754–2762.

[181] Gell-Mann, M. and Brueckner, K. A. *Phys. Rev.*, **1957**, *106*, 364–368.

[182] Hehre, W. J.; Ditchfield, R.; Pople, J. A. *J. Chem. Phys.*, **1972**, *56*, 2257–2261.

[183] Francl, M. M.; Pietro, W. J.; Hehre, W. J.; Binkley, J. S.; Gordon, M. S.; and DeFrees, D. J.; Pople, J. A. *J. Chem. Phys.*, **1982**, *77*, 3654–3665.

[184] Falcetta, M. F. and Jordan, K. D. *J. Phys. Chem.*, **1990**, *94*, 5666–5669.

[185] Houk, K. N.; Lee, P. S.; Nendel, M. *J. of Org, Chem.*, **2001**, *66*, and 5517–5521.

[186] Hajgató, B.; Szieberth, D.; Geerlings, P.; Proft, F. D.; Deleuze, M. S. and . *J. Chem. Phys.*, **2009**, *131*, 224321.

[187] Kumar, R.; Wang, F.-F.; Jenness, G. R.; Jordan, K. D. *J. Chem. Phys.*, **2010**, *132*, 014309.

[188] Mulliken, R. S. *J. Chem. Phys.*, **1955**, *23*, 1833–1840.

[189] Karalti, O.; Jenness, G. R.; Al-Saidi, W.; Jordan, K. D. *in progress*, **2010**.

[190] Weigend, F. and Ahlrichs, R. *Phys. Chem. Chem. Phys.*, **2005**, *7*, 3297–3305.

[191] Scuseria, G. E.; Henderson, T. M.; Sorensen, D. C. *J. Chem. Phys.*, **2008**, *129*, 231101.

[192] Vydrov, O. A. and Van Voorhis, T. *Phys. Rev. A*, **2010**, *81*, 062708.

[193] Hohenberg, P. and Kohn, W. *Phys. Rev.*, **1964**, *136*, B864–B871.

[194] Kohn, W. and Sham, L. J. *Phys. Rev.*, **1965**, *140*, A1133–A1138.

[195] Kohn, W. *Rev. Mod. Phys.*, **1999**, *71*, 1253–1266.

[196] Kristyán, S. and Pulay, P. *Chem. Phys. Lett.*, **1994**, *229*, 175–180.

[197] Pérez-Jordá, J. M. and Becke, A. D. *Chem. Phys. Lett.*, **1995**, *233*, 134–137.

[198] Cerny, J. and Hobza, P. *Phys. Chem. Chem. Phys.*, **2007**, *9*, 5291–5303.

[199] Grimme, S.; Antony, J.; Schwabe, T.; Muck-Lichtenfeld, C. *Org. Biomol. Chem.*, **2007**, *5*, 741–758.

[200] Wu, Q. and Yang, W. *J. Chem. Phys.*, **2002**, *116*, 515–524.

[201] Santra, B.; Michaelides, A.; Fuchs, M.; Tkatchenko, A.; Filippi, C.; and Scheffler, M. *J. Chem. Phys.*, **2008**, *129*, 194111.

[202] Xu, X. and Goddard, W. A. *Proc. Natl. Acad. Sci.*, **2004**, *101*, 2673.

[203] Zhao, Y. and Truhlar, D. G. *J. Phys. Chem. A*, **2006**, *110*, 5121–5129.

[204] Zhang, Y.; Vela, A.; Salahub, D. *Theor. Chem. Acc.*, **2007**, *118*, 693.

[205] Vydrov, O. A. and Voorhis, T. V. *J. Chem. Phys.*, **2009**, *130*, 104105.

[206] Schwegler, E.; Grossman, J. C.; Gygi, F.; Galli, G. *J. Chem. Phys.*, **2004**, *121*, 5400–5409.

[207] Grossman, J. C.; Schwegler, E.; Draeger, E. W.; Gygi, F.; Galli, G. *J. Chem. Phys.*, **2004**, *120*, 300–311.

[208] Kuo, I.-F. W.; Mundy, C. J.; McGrath, M. J.; Siepmann, J. I.; VandeVondele, and J.; Sprik, M.; Hutter, J.; Chen, B.; Klein, M. L.; Mohamed, F.; Krack, and M.; Parrinello, M. *J. Phys. Chem. B*, **2004**, *108*, 12990–12998.

[209] Lee, H.-S. and Tuckerman, M. E. *J. Chem. Phys.*, **2006**, *125*, 154507.

[210] Allesch, M.; Schwegler, E.; Gygi, F.; Galli, G. *J. Chem. Phys.*, **2004**, *120*, 5192–5198.

[211] Lin, I.-C.; Seitsonen, A. P.; Coutinho-Neto, M. D.; Tavernelli, I.; and Rothlisberger, U. *J. Phys. Chem. B*, **2009**, *113*, 1127–1131.

[212] Bukowski, R.; Szalewicz, K.; Groenenboom, G. C.; v. d. Avoird, A. *Science*, **2007**, *315*, 1249.

[213] Dahlke, E. E.; Olson, R. M.; Leverentz, H. R.; Truhlar, D. G. *J. Phys. Chem. A*, **2008**, *112*, 3976–3984.

[214] Su, J. T.; Xu, X.; Goddard, W. A. *J. Phys. Chem. A*, **2004**, *108*, 10518–10526.

[215] Kelkkanen, A. K.; Lundqvist, B. I.; Nørskov, J. K. *J. Chem. Phys.*, **2009**, *131*, 046102.

[216] Bates, D. M. and Tschumper, G. S. *J. Phys. Chem. A*, **2009**, *113*, 3555–3559.

[217] Xantheas, S. S.; Burnham, C. J.; Harrison, R. J. *J. Chem. Phys.*, **2002**, *116*, 1493–1499.

[218] Möller, C. and Plesset, M. S. *Phys. Rev.*, **1934**, *46*, 618–622.

[219] Perdew, J. P. In Ziesche, P. and Eschrig, H. , editors, *Electronic Structure of and Solids*. Akademie Verlag, Berlin, 1991.

[220] Becke, A. D. *J. Chem. Phys.*, **1993**, *98*, 5648–5652.

[221] Vosko, S. H.; Wilk, L.; Nusair, M. *Can. J. Phys.*, **1980**, *58*, 1200.

[222] Stephens, P. J.; Devlin, F. J.; Chabalowski, C. F.; Frisch, M. J. *J. Phys. Chem.*, **1994**, *98*, 11623–11627.

[223] Ojamaee, L. and Hermansson, K. *J. Phys. Chem.*, **1994**, *98*, 4271–4282.

[224] Xantheas, S. S. *Chem. Phys.*, **2000**, *258*, 225–231.

[225] Xantheas, S. S. *J. Chem. Phys.*, **1994**, *100*, 7523–7534.

[226] Cui, J.; Liu, H.; Jordan, K. D. *J. Phys. Chem. B*, **2006**, *110*, 18872–18878.

[227] Christie, R. A. and Jordan, K. D. *J. Phys. Chem. A*, **2001**, *105*, 7551–7558.

[228] Pedulla, J. M.; Kim, K.; Jordan, K. D. *Chem. Phys. Lett.*, **1998**, *291*, 78–84.

[229] Woon, D. E. and Thom H. Dunning, J. *J. Chem. Phys.*, **1994**, *100*, 2975–2988.

[230] Langlet, J.; Bergés, J.; Reinhardt, P. *J. Mol. Struct. (THEOCHEM)*, **2004**, *685*, 43.

[231] Bukowski, R.; Cencek, W.; Jankowski, P.; Jeziorska, M.; Jeziorski, B.; and Kucharski, S. A.; Lotrich, V. F.; Misquitta, A. J.; Moszyński, R.; and Patkowski, K.; Podeszwa, R.; Rybak, S.; Szalewicz, K.; Williams, H. L.; and Wheatley, R. J.; Wormer, P. E. S.;; Zuchowski, P. S. Sapt2008: An Ab Initio Program for Many-Body Symmetry-Adapted and Perturbation Theory Calculations of Intermolecular Interaction Energies. University of Delaware and University of Warsaw.

[232] Lotrich, V. F. and Szalewicz, K. *J. Chem. Phys.*, **1997**, *106*, 9668–9687.

[233] Saunders, V. and Guest, M. Atmol program package.

[234] Reinhardt, P. and Piquemal, J.-P. *Int. J. Quant. Chem.*, **2009**, *109*, 3259.

[235] Santra, B.; Michaelides, A.; Scheffler, M. *J. Chem. Phys.*, **2007**, *127*, 184104.

[236] Piquemal, J.-P.; Marquez, A.; Parisel, O.; Giessner-Prettre, C. *J. Comput. Chem.*, **2005**, *26*, 1052.

[237] Perdew, J. P. and Zunger, A. *Phys. Rev. B*, **1981**, *23*, 5048–5079.

[238] Habitz, P.; Bagus, P.; Siegbahn, P.; Clementi, E. *Int. J. Quant. Chem.*, **1983**, *23*, 1803.

[239] Chałasiński, G.; Szcześniak, M. M.; Cieplak, P.; Scheiner, S. *J. Chem. Phys.*, **1991**, *94*, 2873–2883.

[240] Pedulla, J. M.; Vila, F.; Jordan, K. D. *J. Chem. Phys.*, **1996**, *105*, 11091–11099.

[241] Tkatchenko, A. and von Lilienfeld, O. A. *Phys. Rev. B*, **2008**, *78*, 045116.

[242] Klimes, J.; Bowler, D. R.; Michaelides, A. *J. Phys.: Condens Matter*, **2010**, *22*, 022201.

[243] Kanai, Y. and Grossman, J. C. *Phys. Rev. A*, **2009**, *80*, 032504.

[244] Cooper, V. R. *Phys. Rev. B*, **2010**, *81*, 161104.

[245] Johnson, E. R.; Becke, A. D.; Sherrill, C. D.; DiLabio, G. A. *J. Chem. Phys.*, **2009**, *131*, 034111.

[246] Al-Saidi, W. A.; Jenness, G. R.; Jordan, K. D. *Unpublished Results*, **2010**.

[247] Handy, N. C. and Cohen, A. J. *Mol. Phys.*, **2001**, *99*, 403.

[248] Becke, A. D. *J. Chem. Phys.*, **1996**, *104*, 1040–1046.

[249] Graäfenstein, J. and Cremer, D. *Theor. Chem. Acc.*, **2009**, *123*, 171.

[250] Cornell, W.; Cieplak, P.; Bayly, C.; Gould, I.; Merz, K.; Ferguson, D.; and Spellmeyer, D.; Fox, T.; Caldwell, J.; Kollman, P. *J. Am. Chem. Soc.*, **1996**, *117*, 5179–5197.

[251] Jorgensen, W. L.; Maxwell, D. S.; TiradoRives, J. *J. Am. Chem. Soc.*, **1996**, *118*, 11225–11236.

[252] Ren, P. and Ponder, J. *J. Comp. Chem.*, **2002**, *23*, 1497–1506.

[253] Brooks, B. R.; Brooks, C. L.; Mackerell, A. D.; Nilsson, L.; Petrella, and R. J.; Roux, B.; Won, Y.; Archontis, G.; Bartels, C.; Boresch, S.; and Caflisch, A.; Caves, L.; Cui, Q.; Dinner, A. R.; Feig, M.; Fischer, S.; and Gao, J.; Hodoscek, M.; Im, W.; Kuczera, K.; Lazaridis, T.; Ma, J.; and Ovchinnikov, V.; Paci, E.; Pastor, R. W.; Post, C. B.; Pu, J. Z.; and Schaefer, M.; Tidor, B.; Venable, R. M.; Woodcock, H. L.; Wu, X.; Yang, and W.; York, D. M.; Karplus, M. *J. Comp. Chem*, **2009**, *30*, 1545–1614.

[254] Gresh, N. *Curr. Pharm. Des.*, **2006**, *12*, and 2121–2158.

[255] Berendsen, H. J. C.; Postma, W. F.; van Gunsteren, W.; F..; J., H. *Intermolecular Forces*. Reidel, Dordrecht, 1981.

[256] Jorgensen, W. L.; Chandrasekhar, J.; Madura, J. D.; Impey, R. W.; Klein, and M. L. *J. Chem. Phys.*, **1983**, *79*, 926–935.

[257] Berendsen, H. J. C.; Grigera, J. R.; Straatsma, T. P. *J. Phys. Chem.*, **1987**, *91*, 6269.

[258] Rick, S.; Stuart, S.; Berne, B. *J .Chem. Phys.*, **1994**, *101*, 6141–6156.

[259] Mahoney, M. W. and Jorgensen, W. L. *J. Chem. Phys.*, **2001**, *114*, 363.

[260] Burnham, C. J. and Xantheas, S. S. *J. Chem. Phys.*, **2002**, *116*, 1500–1510.

[261] Horn, H. W.; Swope, W. C.; Pitera, J. W.; Madura, J. D.; Dick, T. J.; and Hura, G. L.; Head-Gordon, T. *J. Chem. Phys.*, **2004**, *120*, 9665–9678.

[262] Abascal, J. L. F. and Vega, C. *J. Chem. Phys.*, **2005**, *123*, 234505.

[263] Yang, L.; Tan, C.; Hsieh, M.; Wang, J.; Duan, Y.; Cieplak, P.; Caldwell, and J.; Kollman, P.; Luo, R. *J. Phys. Chem. B*, **2006**, *110*, 13166–13176.

[264] Lamoureux, G.; Harder, E.; Vorobyov, I.; Roux, B.; MacKerell, A. *Chem. Phys. Letts.*, **2006**, *418*, 245–249.

[265] Kumar, R. and Skinner, J. L. *J. Phys. Chem. B*, **2008**, *2008*, 8311–8318.

[266] Chen, B.; Xing, J.; Siepmann, J. *J. Phys. Chem. B*, **2000**, *104*, 2391–2401.

[267] Piquemal, J.-P.; Chevreau, H.; Gresh, N. *J. Phys. Chem. A*, **2003**, *107*, 10353–10359.

[268] Yu, H. and van Gunsteren, W. F. *Comput. Phys. Comm.*, **2005**, *172*, 69–85.

[269] Piquemal, J.-P.; Chevreau, H.; Gresh, N. *J. Chem. Theo. Comp.*, **2007**, *3*, 824–837.

[270] Stone, A. J. *Science*, **2008**, *321*, 787–789.

[271] Fellers, R.; Leforestier, C.; Braly, L.; Brown, M.; Saykally, R. *Science*, **1999**, *284*, 945–948.

[272] Yu, H. and van Gunsteren, W. *J. Chem. Phys.*, **2004**, *121*, 9549–9564.

[273] Mankoo, P. K. and Keyes, T. *J. Chem. Phys.*, **2008**, *129*.

[274] McBride, C.; Vega, C.; Noya, E. G.; Ramirez, R.; Sese, L. M. *J. Chem. Phys.*, **2009**, *131*.

[275] Stern, H.; Rittner, F.; Berne, B.; Friesner, R. *J. Chem. Phys.*, **2001**, *115*, 2237–2251.

[276] Burnham, C. J.; Anick, D. J.; Mankoo, P. K.; Reiter, G. F. *J. Chem. Phys.*, **2008**, *128*, 154519.

[277] Sommerfeld, T.; DeFusco, A.; Jordan, K. D. *J. Phys. Chem. A*, **2008**, *112*, 11021–11035.

[278] Choi, T. H. and Jordan, K. D. *Chem. Phys. Letts.*, **2009**, *475*, 293–297.

[279] Burnham, C. J. and Xantheas, S. S. *J. Chem. Phys.*, **2002**, *116*, 5115–5124.

[280] Fanourgakis, G. and Xantheas, S. *J. Phys. Chem. A*, **2006**, *110*, 4100–4106.

[281] Thole, B. T. *Chem. Phys.*, **1981**, *59*, 341–350.

[282] Hodges, M. P.; Stone, A. J.; Xantheas, S. S. *J. Phys. Chem. A*, **1997**, *101*, 9163–9168.

[283] Mas, E.; Bukowski, R.; Szalewicz, K. *J. Chem. Phys.*, **2003**, *118*, 4404–4413.

[284] Cisneros, G. A.; Tholander, S. N.-I.; Parisel, O.; Darden, T. A.; Elking, and D.; Perera, L.; Piquemal, J.-P. *Int. J. Quat. Chem.*, **2008**, *108*, 1905–1912.

[285] Piquemal, J.-P.; Cisneros, G. A.; Reinhardt, P.; Gresh, N.; Darden, T. A. *J. Chem. Phys.*, **2006**, *124*, 104101–104112.

[286] Freitag, M. A.; Gordon, M. S.; Jensen, J. H.; Stevens, W. J. *J. Chem. Phys.*, **2000**, *112*, 7300–7306.

[287] Smith, B. J.; Swanton, D. J.; Pople, J. A.; III, H. F. S.; Radom, L. *J. Chem. Phys.*, **1990**, *92*, 1240–1247.

[288] Stone, A. J. and Alderton, M. *Mol. Phys.*, **1985**, *56*, 1047.

[289] Murphy, W. F. *J. Chem. Phys.*, **1977**, *67*, 5877–5882.

[290] Tang, K. T. and Toennies, J. P. *J. Chem. Phys.*, **1984**, *80*, 3726–3741.

[291] Patkowski, K.; Szalewicz, K.; Jeziorski, B. *J. Chem. Phys.*, **2006**, *125*, 154107.

[292] Weigend, F.; Häser, M.; Patzelt, H.; Alrichs, R. *Chem. Phys. Lett.*, **1998**, *294*, 143.

[293] Cui, J.; Liu, H.; Jordan, K. D. *J. Phys. Chem. B*, **2006**, *110*, 18872–18878.

[294] Stanton, J.; Gauss, J.; Perera, S.; Watts, J.; Yau, A.; Nooijen, M.; and Oliphant, N.; Szalay, P.; Lauderdale, W.; Gwaltney, S.; Beck, S.; and Balkova, A.; Bernholdt, D.; Baeck, K.; Rozyczko, P.; Sekino, H.; and C.Huber.; Pittner, J.; Cencek, W.; Taylor, D.; Bartlett, R. Aces II, A program product of the Quantum Theory Project, University of Florida

[295] Jeziorski, B.; Moszyński, R.; Szalewicz, K. *Chem. Rev.*, **1994**, *94*, 1887–1930.

[296] Ewald, P. P. *Ann. Phys.*, **1921**, *369*, 253.

[297] Yonetani, Y. *J. Chem. Phys.*, **2006**, *124*, 204501.

[298] Fanourgakis, G. S. and Xantheas, S. S. *J. Chem. Phys.*, **2008**, *128*, 074506.

[299] Soper, A. K. *Chem. Phys.*, **2000**, *258*, 121–137.

[300] Habershon, S.; Markland, T. E.; Manolopoulos, D. E. *J. Chem. Phys.*, **2009**, *131*, 024501.

[301] Cheng, B. M.; Grover, J. R.; Walters, E. A. *Chem. Phys. Lett.*, **1995**, *232*, 364–369.

[302] Suzuki, S.; Green, P. G.; Bumgarner, R. E.; Dasgupta, S.; Goddard, I.; and Blake, G. A. *Science*, **1992**, *257*, 942–945.

[303] Jeziorska, M.; Jeziorski, B.; Čížek, J. *Int. J. Quant. Chem.*, **1987**, *32*, 149–164.

[304] Moszynski, R.; Jeziorski, B.; Rybak, S.; Szalewicz, K.; Williams, H. L. *J. Chem. Phys.*, **1994**, *100*, 5080–5092.

[305] Dreizler, R. M. and Gross, E. *Density Functional Theory*. Springer, Berlin, 1990.

[306] Jansen, G. and Heßelmann, A. *J. Phys. Chem. A*, **2001**, *105*, 11156–11157.

[307] Gross, E.; Dobson, J.; Petersilka, M. **1996**, *181*, 81–172.

[308] Casimir, H. B. G. and Polder, D. *Phys. Rev.*, **1948**, *73*, 360–372.

[309] Hohenstein, E. G. and Sherrill, C. D. *J. Chem. Phys.*, **2010**, *132*, 184111.

[310] Hohenstein, E. G. and Sherrill, C. D. *J. Chem. Phys.*, **2010**, *133*, 014101.

[311] Hohenstein, E. G. and Sherrill, C. D. *J. Chem. Phys.*, **2010**, *133*, 104107.